Université de Montréal

Towards Understanding the Nature and Diversity of Small Planets in the Universe: Discovery and Initial Characterization of Wolf 503 b and LP 791-18 d

par

Merrin Peterson

Département de physique
Faculté des arts et des sciences

Mémoire présenté en vue de l'obtention du grade de
Maître ès sciences (M.Sc.)
en Astrophysique

May 7, 2021

Université de Montréal

Faculté des études supérieures et postdoctorales

Ce mémoire intitulé

Towards Understanding the Nature and Diversity of Small Planets in the Universe: Discovery and Initial Characterization of Wolf 503 b and LP 791-18 d

présenté par

Merrin Peterson

a été évalué par un jury composé des personnes suivantes :

Paul Charbonneau
(président-rapporteur)

Björn Benneke
(directeur de recherche)

René Doyon
(membre du jury)

Résumé

Avec la découverte de milliers de nouvelles planètes au cours des vingt dernières années, une nouvelle population complexe de planètes plus petites que Neptune et plus grandes que la Terre a été découverte. Ces planètes se divisent en deux groupes : les plus grandes sub-Neptunes avec des atmosphères étendues dominées par H, et les plus petites super-Terres qui ont tout au plus des atmosphères minces. Cette division peut être expliquée par une variété de mécanismes, y compris la photoévaporation, la perte de masse alimentée par le noyau, et la formation de gaz pauvres et vides : la population de petites planètes est probablement façonnée par une combinaison de ces mécanismes qui peut dépendre du type stellaire. Dans ce travail, nous décrivons la découverte de deux nouvelles planètes qui sont bien adaptées à l'étude de la nature de la population des petites planètes : Wolf 503 b et LP 791-18 d. Wolf 503 b est une planète de $2.03^{+0.08}_{-0.07}$ $R_\oplus$ orbitant autour de l'étoile brillante ($J = 8.32$ mag), proche ($D = 44.5$ pc) à mouvement propre élevé K3.5V Wolf 503 (EPIC 212779563). Nous confirmons que la signature du transit *K2* est planétaire en utilisant à la fois des images d'archives et des images d'optique adaptative à haut contraste de l'observatoire Palomar. Son rayon place Wolf 503b directement entre les populations de super-Terre et de sub-Neptune, un rayon auquel les planètes sont rarement trouvées et la composition de masse attendue est ambiguë, et la luminosité de l'étoile hôte fait de Wolf 503b une cible de choix pour le suivi des vitesses radiales et la spectroscopie de transit. La deuxième planète que nous présentons est une planète de taille terrestre orbitant autour de la naine froide M6 LP 791-18. La nouvelle planète d rejoint un système bien aligné avec au moins deux autres planètes, la plus externe étant une sous-Neptune, offrant une occasion unique à ce jour d'étudier un système avec une planète de taille terrestre tempérée et une sous-Neptune qui a conservé son enveloppe gazeuse ou volatile. La découverte de LP 791-18d permet de mesurer la masse du système grâce aux variations du temps de transit, et nous trouvons une masse de $9.3^{+1.5}_{-1.4}\,M_\oplus$ pour la sub-Neptune LP 791-18c et une masse de $0.8^{+0.5}_{-0.4}\,M_\oplus$ pour l'exo-Terre LP 791-18d ($< 2.3\ M_\oplus$ à 3σ). La planète est également soumise à un fort réchauffement continu par les marées, ce qui peut entraîner une activité géologique et un dégazage volcanique. Pour l'avenir, LP 791-18d et Wolf 503b offrent des opportunités uniques d'étudier les origines et la conservation des atmosphères des petites planètes. **Mots clés:** méthodes: observationnelles — planètes

et satellites: atmosphères — planètes et satellites: individuels (Wolf 503b) — planètes et satellites: individuels (LP 791-18d) — planètes et satellites: évolution physique - - planètes et satellites: planètes gazeuses

Abstract

With the discovery of thousands of new planets in the past twenty years, a new and complex population of planets has been discovered which are smaller than Neptune and larger than the Earth. These planets are split into two groups: the larger sub-Neptunes with extended H-dominated atmospheres, and the smaller super-Earths which have at most thin atmospheres. This division can be explained by a variety of mechanisms, including photoevaporation, core-powered mass-loss, and gas-poor and gas-empty formation: the small-planet population is likely shaped by a combination of these which may depend on stellar type. In this work we describe the discovery of two new planets which are well-suited to investigating the nature of the small planet population: Wolf 503b and LP 791-18d. Wolf 503 b is a $2.03^{+0.08}_{-0.07}$ $R_\oplus$ planet orbiting the bright ($J = 8.32$ mag), nearby ($D = 44.5$ pc) high proper motion K3.5V star Wolf 503 (EPIC 212779563). We confirm that the *K2* transit signature is planetary using both archival images and high-contrast adaptive optics images from the Palomar observatory. Its radius places Wolf 503 b directly between the populations of super-Earths and sub-Neptunes, a radius at which planets are rarely found and the expected bulk composition is ambiguous, and the brightness of the host star makes Wolf 503b a prime target for radial velocity follow-up and transit spectroscopy. The second planet we introduce is an Earth-sized planet orbiting the cool M6 dwarf LP 791-18. The new planet d joins a well-aligned system with at least two more planets, the outermost being a sub-Neptune, providing a to-date unique opportunity to investigate a system with a temperate Earth-sized planet and a sub-Neptune that retained its gas or volatile envelope. The discovery of LP 791-18d makes the system amenable to mass measurements via transit timing variations, and we find a mass of $9.3^{+1.5}_{-1.4}\,M_\oplus$ for the sub-Neptune LP 791-18c and a mass of $0.8^{+0.5}_{-0.4}\,M_\oplus$ for the exo-Earth LP 791-18d ($< 2.3\ M_\oplus$ at 3σ). The planet is also subject to strong continued tidal heating, which may result in geological activity and volcanic outgassing. Looking forward, LP 791-18d and Wolf 503b offer unique opportunities to study the origins and retention of small-planet atmospheres.

Keywords: methods: observational — planets and satellites: atmospheres — planets and satellites: individual (Wolf 503b) — planets and satellites: individual (LP 791-18d) — planets and satellites: physical evolution — planets and satellites: gaseous planets

Contents

List of tables

List of figures

List of Acronyms and Abbreviations

TESS	Transiting Exoplanet Survey Satellite
JWST	James Webb Space Telescope
ExoTEP	EXOplanet Transits Eclipses and Phasecurves
HST	Hubble Space Telescope
JWST	James Webb Space Telescope
RV	Radial Velocity
SNR	Signal to Noise Ratio

Remerciements

Thank you Björn for giving me every opportunity I could possibly handle and for taking control of the things that I couldn't. Your understanding has been instrumental and I'm lucky to have had the chance to experience research in your group. Thanks to my family for believing in me and frequently providing phone support. I wouldn't be here or anywhere else without the merrin-help-line.

Introduction

1. The brief history of exoplanet science

Until the late 20th century, planetary studies were limited to observations of the Earth and its seven neighbors. With no other option, we've historically made the assumption that the solar system, with its small inner terrestrial planets and large, outer gaseous planets, is an adequate example of the average planetary system and have used it exclusively to model planet formation. Even when the concept of extra-solar life has been approached as likely very exotic and unique, it's usually assumed that this life will occur on planets, or at least in systems, similar to our own. In 1992, the first exoplanets (TRES 2b and 3b) were discovered orbiting a pulsar, followed quickly in 1995 by 51 Pegasi b, the first exoplanet orbiting a sun-like star, a planet heavier than Saturn and orbiting closer to its host than mercury to the Sun. These initial exo-worlds gave the first evidence that our solar system is not only one among many, but that it is one among a very wide variety.

With experimental methods and instruments developed specifically for planet hunting, and with the Kepler satellite in particular, we now realize that our system is atypical, and that previously unknown classes of planets are in fact the most common in the galaxy. Our understanding of planet formation is grounded in the most common planets as these are the most likely result of the formation process. And so our understanding of this process has changed radically in the past decade with the discovery that the most likely class of planet is a body larger in radius than the Earth, but smaller than Neptune, for which there is no solar system analogue. The importance of these planets is exaggerated by the discovery that, in this range of radii, there appears to be a sharp transition between planets which maintain significant atmospheres, and planets which have almost no atmosphere at all. An understanding of the creation, maintenance and loss of atmospheres leads to an understanding of planet habitability, and to a more accurate picture of the Earth's history and that of the full solar system.

Our catalogue of exoplanets has expanded to over 4'000 since 1992, and with this, our vision of a habitable planet has expanded as well. If such a planet is to be found by Earth-bound observers, it will likely be one in a system entirely different from our own, one with

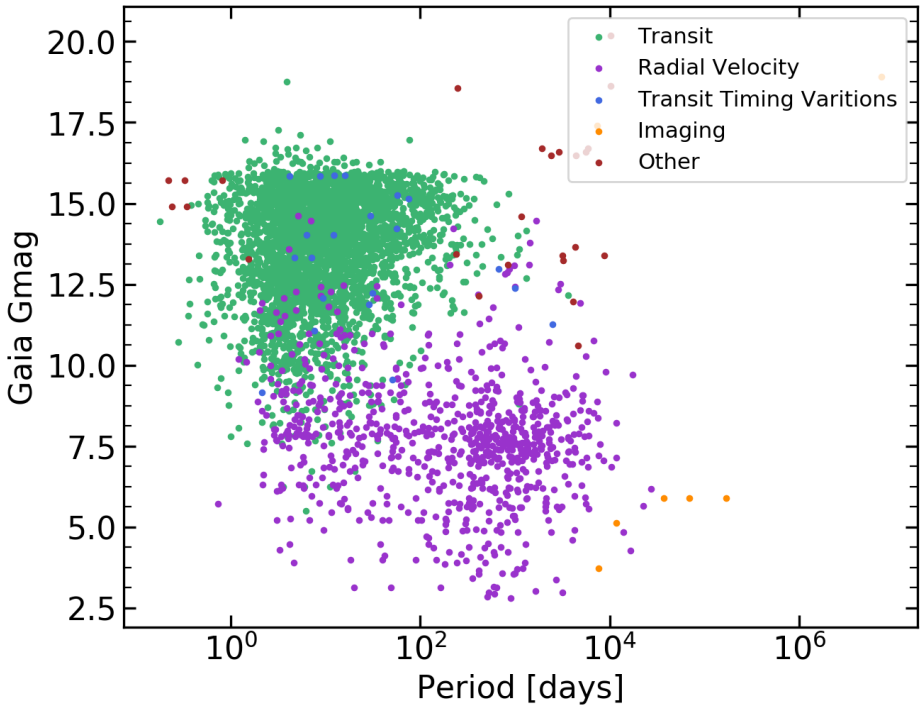

Fig. 1.1. Confirmed planets of the NASA Exoplanet Archive plotted by period and host star magnitude. Radial velocity tends to require a brighter host star than the transit method whereas the transit method strongly favours short period planets. Transiting planets were found primarily by Kepler. Planets discovered through transit timing variations can be found around dimmer stars than the radial velocity method.

a much smaller host star and a unique configuration of planets. To build an understanding of exoplanets and their habitability, we need to find those rare, nearby systems which can be studied in detail, particularly for planets which are unlike those found in our solar system and cannot be studied in any other way. This thesis describes the discovery and initial characterization of two exoplanets, Wolf 503 b and LP 791-18 d which will be instrumental in piecing together the formation and evolution pathways of small planets.

2. Technical Background

There are a variety of techniques used to first discover exoplanets, and to further take their most important measurements, including mass, radius and temperature. The planet detection techniques introduced here rely on the effects of planets on the light of their host stars. Fig. 1.1 illustrates the main methods for planet identification and the regimes for which they are most effective.

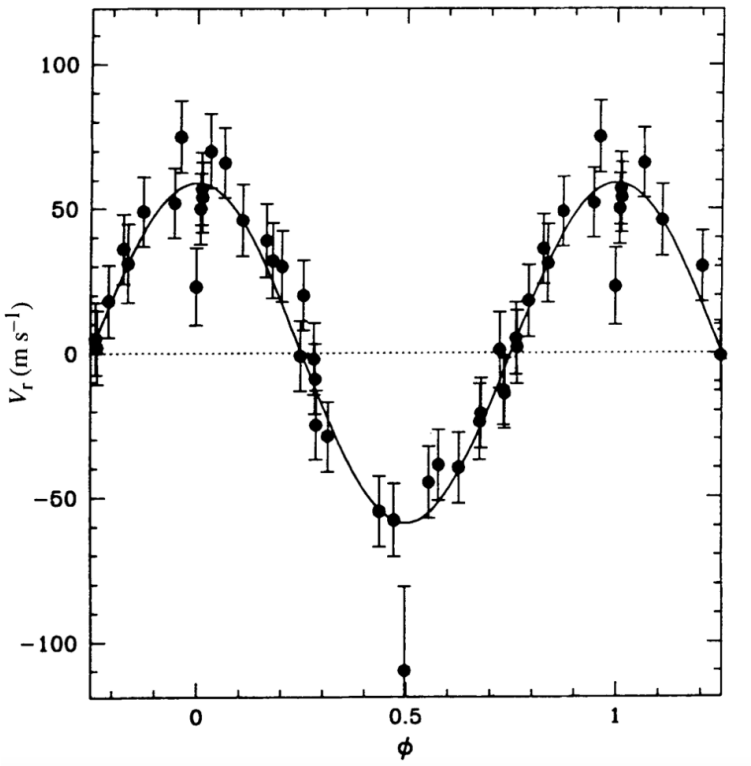

Fig. 1.2. Radial velocity measurements of 51 Pegasi shown over the phase of the planet 51 Pegasi b taken from [32]. These observations were used to find the first exoplanet around a Sun-like star. Modern instruments like HARPS-N -S, SPIRou, HIRES, allow us to detect radial velocity patterns of much smaller amplitude, on the order of 1-2m/s, and determine the masses of much smaller planets on longer orbits.

2.1. Radial Velocity

Radial velocity measurements allow the detection and mass estimation of exoplanets from the gravitational effects they have on their host stars. A star's radial velocity is its speed directly towards or away from the Earth which induces a Doppler effect on the light received from the star and shifts the lines of the stellar spectrum. This movement can be measured by high-resolution spectrographs to determine the star's radial velocity. Since planet and star both orbit a common center of gravity, a planet-hosting star moves toward and away from the Earth with its velocity changing in a periodic fashion, and a maximum speed determined in part by the mass of the planet relative to the star. 51 Pegasi b was the first planet to be discovered through radial velocity[32], and its sinusoidal impact on 51 Pegasi is shown in Fig. 1.2.

With enough measurements of the stellar velocity to show the periodic impact of the planet, many key orbital elements of the planet can be calculated from this pattern. The planet's phase and period P are the same as that of the pattern, giving the approximate

semi-major axis a through Kepler's third law. The planet's eccentricity e (the degree to which the orbit is circular) can be modelled from the shape of the pattern, as it will be sinusoidal only for circular orbits ($e = 0$) and become more peaked for eccentric ones ($0 < e < 1$). Unfortunately the inclination i of the planet's orbit relative to its line of sight with the Earth is degenerate in the radial velocity pattern with the planet mass: a small planet on a nearly edge-on orbit ($i = 90°$) can produce the same effect as a large planet on a nearly face-on orbit ($i = 0°$). As such, this method is biased towards large, short-period planets with nearly edge-on orbits, and if the inclination is unknown, the radial velocity semi-amplitude can only be used to determine the value $M_p \sin i$. The inclination can be estimated from the rotation of the star itself, assuming the planet's orbit is aligned with the star's rotation, but i can only be precisely determined if the planet is also transiting: that is, when the inclination is nearly 90° and the planet crosses the Earth's line of sight to the star, blocking some of the star's light, and providing a wealth of additional information about the planet.

2.2. Transit

The transit method is a very efficient way to search for planets and is also the only way to measure a planet's radius. In this method, planets are identified through continuous photometric monitoring of their host stars, by the periodic dimming caused when a planet crossing in front of the star blocks a small amount of light from the Earth, as illustrated in Fig. 1.3. Though extremely slight for most planets, the periodicity and specific shape of this dimming allows us to separate planetary transits from stellar activity.

The shape of a transit is determined by several planetary and orbital properties. The fraction by which the star dims is the fraction of the star's surface area blocked by the planet, and so the depth of a transit is equal to $(R_p/R_s)^2$, the planet/star radius ratio, which gives the planet radius when that of the star is estimated through spectroscopy and stellar relations (as well as its mass). The planet's period and phase are determined by the timing of the transits, and the inclination can be determined from the transit shape and duration. If the inclination is very nearly 90°, the planet crosses the full radius of the star, and the transit has a longer duration and will change in brightness more quickly, making the transit more box-shaped than v-shaped. The transit is also shaped by the stellar limb darkening, the changing brightness of the stellar disk as seen by an observer on Earth: as the planet blocks the brighter center of the star, the transit is deepest. In most cases, the inclination must be so nearly edge-on to produce a transit that it can be assumed to be 90°, and so for a planet with radial velocity measurements that also transits, the true mass can be determined as $M_p \sin i = M_p$. A target for which both transit and radial velocity measurements are available has a mass and radius, and therefore density, measurement, and we may hypothesize about its composition and the presence of its atmosphere.

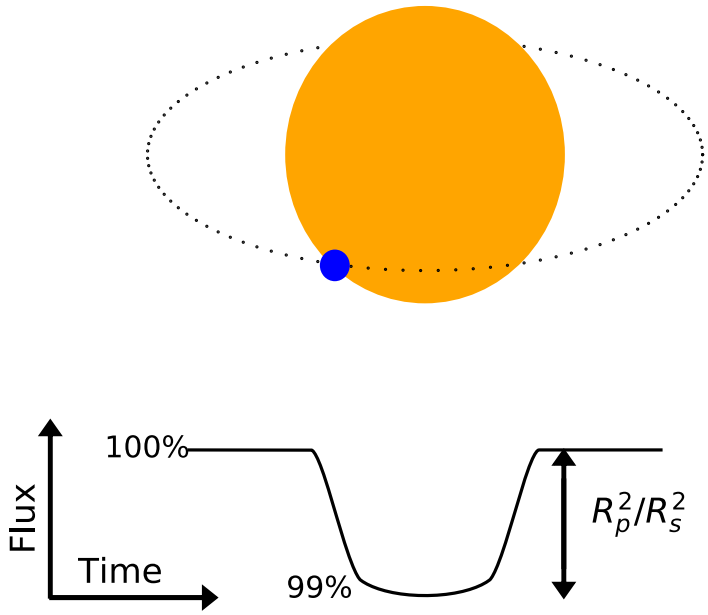

Fig. 1.3. Visualization of the transit of a very large planet, with a radius 10% that of its host star, orbiting at an inclination of 87° and a distance 15 times the radius of the star. The brightness of the star decreases by 1% during the transit, which is shaped partly by the inclination and duration of the orbit as well as the stellar limb darkening.

Similar to radial velocity measurements, this method is most sensitive to large, short-period planets, as these have a stronger and more easily detected transit, although the planet must also be precisely aligned to transit. However, transits are an ideal way to survey large amounts of stars for planets. The radial velocity method may sometimes require hours of observations on expensive and competitive high-resolution spectrographs for a single observation of a single target with no guarantee that it may host planets, whereas with the transit method an instrument with a large enough field of view can monitor tens of thousands of stars simultaneously, compensating for the low likelihood that any single planetary system will transit. And by monitoring thousands of stars for planets in precisely the same way, transit surveys allow us to estimate the fraction of stars which host planets, as discussed further in section 3. Transiting planets are also the only planets for which transit photometry is possible, in which the spectrum of a planet's atmosphere is taken from the changes in stellar light during transit, an essential technique for exoplanet characterization. Although radial velocity surveillance continues, the most productive planet-hunting missions to this day (such as Kepler/K2 and TESS) use the transit method, with radial velocity being most useful as a follow-up measurement to confirm photometric signals which resemble planet transits and determine their masses.

2.3. Transit Timing Variations

Although the transit method relies on the periodicity of planetary transits, these are not always perfectly periodic, particularly for multi-planet systems in specific configurations. As a planet in such a multiple system moves in its orbit, it is gravitationally affected by its companions. For planets in resonant systems, for which the orbital period of one planet is nearly an integer ratio of the period of another planet, this effect is amplified and changes the motion of the planets, and thus the timing of their transits, in a periodic fashion.

The degree to which a planet's timing is affected depends on the mass of the other planet(s) which are disturbing it, and not on the mass of the planet itself. In this way, a non-transiting planet can be discovered and its mass measured even without radial velocity measurements, if it induces transit timing variations on a transiting planet in its system.

While much more complex than the radial velocity method, and limited to resonant systems, transit timing variations are essential in measuring the masses of the smallest planets. Planets of similar size and on similar orbits to that of the Earth, for example, would be impossible to detect through radial velocity measurements with current instrumentation. For these small planets, transit timing variations is the most effective, and in some cases the only, method available to determine the planet's mass and density.

3. The Kepler Satellite

As the first satellite designed specifically for planet hunting, the results of the Kepler satellite shaped, and largely created, the field of exoplanets as it exists today. Kepler was designed to photometrically monitor over 160'000 stars in a single 115 square degree field of view, with the goal of achieving the precision required to detect Earth-like planets orbiting Sun-like stars [2, 21]. Although the mission did not attain this precision due to failures in the satellite pointing, the satellite discovered over 2'000 planets, tripling our sample size in under 8 years, as can be seen in Fig. 1.4.

This influx of planets allowed for the first uniform, statistical studies of small exoplanet demographics, and the results were revolutionizing. Most importantly, it was shown that planets are found across a wide range of stellar types and at frequencies suggesting that most stars host at least one planet [16, 6]. This suggests that planet formation is a natural consequence of star formation and that planets are ubiquitous in the Universe. Furthermore, on orbital periods shorter than about 100 days, small planets are far more common than large ones [37, 7], as can be seen in Fig. 1.5, the distribution of planet sizes found by Kepler.

In Fig. 1.5, it can also be seen that, specifically, planets larger than Earth, but smaller than 4 $R_\oplus$ (the approximate radius of Neptune), are most common, even when no such planet exists in the solar system. Furthermore, this mountain in the planet population appears to be split into two peaks, with large populations of planets at 1.3 and 2.4 $R_\oplus$, and with very

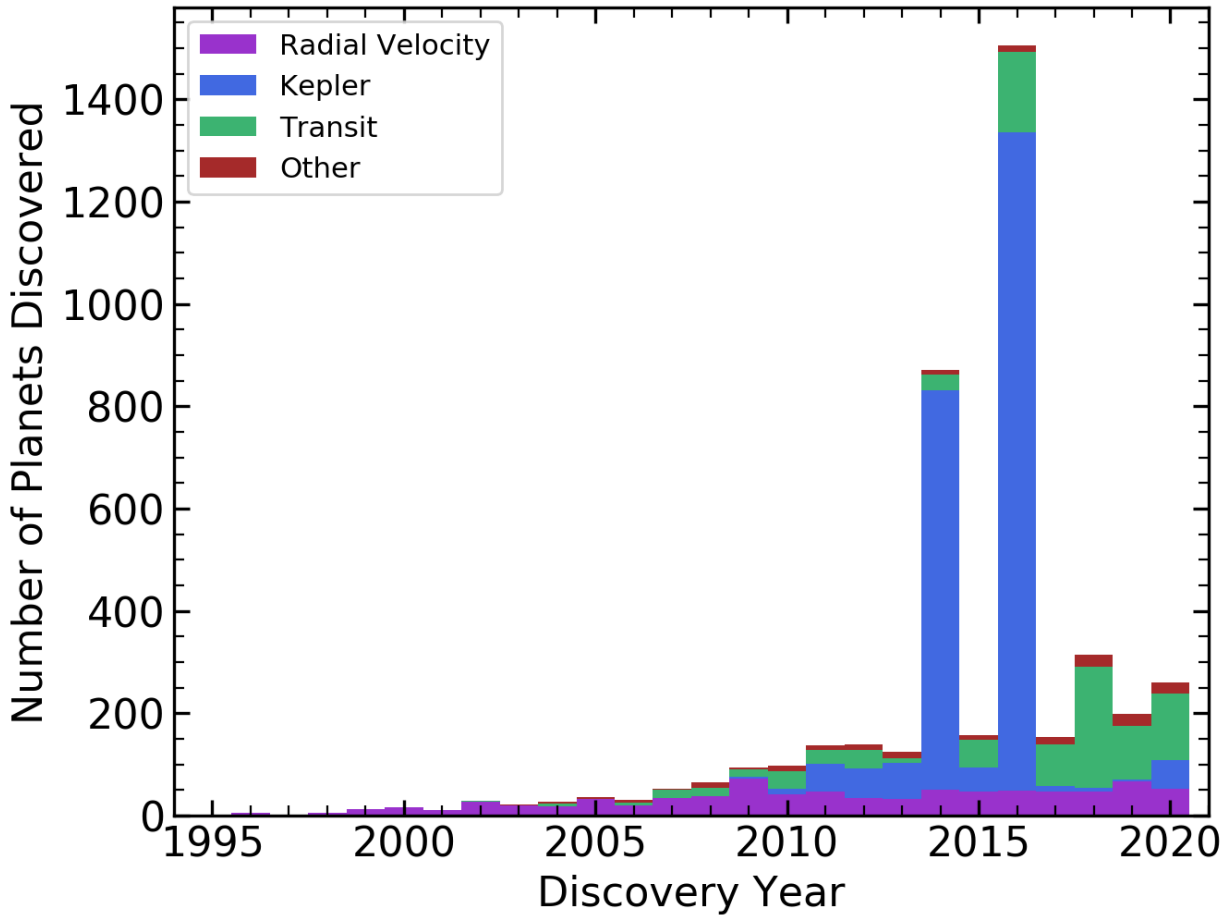

Fig. 1.4. Histogram of planet discovery dates, with colored groups indicating planets which were found by radial velocity, by Kepler, by transiting missions other than Kepler, and by other methods (such as transit timing variations, direct imaging and microlensing). The Kepler satellite is responsible for the majority of known exoplanets.

few planets in between. This structure is deeply meaningful as it must be a result either of planet formation or evolution, and the cause for the radius valley is widely disputed, making it one of the most impactful questions in exoplanet science today.

4. The Radius Valley, Super-Earths and Sub-Neptunes

4.1. Basic Planet Formation

The distinction between these two populations of small planets is believed to be that the larger planets have thick primordial atmospheres while the population of planets more similar in size to Earth does not, and planets in the radius valley have atmospheres of intermediate size and are more rare. The planets near 1.3 $R_\oplus$, being more similar in size to Earth, are referred to as the "super-Earths", which are dense rocky cores, while the planets larger than 2 $R_\oplus$ are termed the "sub-Neptunes" and have extended H/He envelopes and lower densities.

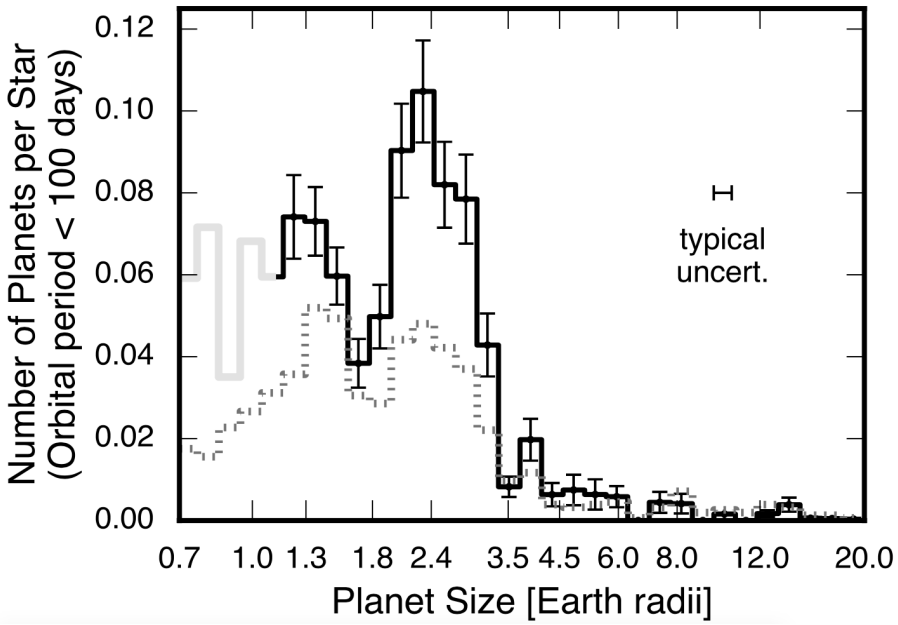

Fig. 1.5. Period and radius distribution of the Kepler planets[7]. Small planets are far more common than large planets on orbital periods shorter than 100 days. There are two separate populations of small planets at 1.3 and 2.5 Earth radii with a relative lack of intermediate planets, the radius gap. The dashed line shows the number distribution of planets before completeness-correction is applied. The light gray region of the histogram indicates that the pipeline completeness at P = 100 days is less than 25% for radii smaller than 1.14 $R_\oplus$.

Density measurements of planets across the radius gap support this theory [45, 42], and a variety of mechanisms have been shown to reproduce this result.

The fundamental idea of planet formation is that planets form in the protoplanetary disk which surrounds a young star through the initial development of dense, rocky or icy cores created by colliding disk material, which in some cases may accrete gas from the disk to form an atmosphere [27]. A gas giant is formed if the planet reaches a critical amount of gas and undergoes runaway accretion [38, 39]. The timeline for the formation of these cores and their mass distribution, the gas and dust content and temperature of the disk, the location of planets within it, and the evolution of all these things over time, are uncertain and affect the resulting planet population. Fortunately, the period-radius distribution of planets revealed by Kepler provides a strong constraint on planet formation theories as they must now reproduce the observed populations of super-Earths and sub-Neptunes. There are two basic pathways for the creation of these populations: either the super-Earths never had thick H/He atmospheres, or both populations are born with thick atmospheres only for the super-Earths to be evaporated. These scenarios require different conditions for the protoplanetary disk, which dissipates completely over roughly 6 million years after the star is formed [14]. The ability for planets to accrete gas from the disk depends on the mass of

the planetary cores as well as whether or not the disk is still gas-rich, gas-poor or gas-empty once this core has been formed, and these different scenarios carve out a different valley in period-radius space.

4.2. Gas-poor vs. Gas-rich formation

For the scenario of a primordial radius gap, in which super-Earths never accrete substantial atmospheres, the super-Earths must finish forming when the protoplanetary disk has little to no gas. This is expected to have been the formation pathway for the Earth [40, 33]. Sub-Neptunes would need to form as a separate population, generating massive cores more quickly in order to accrete an atmosphere before the disk is dissipated. If the super-Earths form when the disk is completely dissipated, the transitional radius between rocky and gaseous planets should theoretically increase at longer periods as the radii of rocky cores increases at longer periods, following the relation $R_{trans} \propto P^{0.11}$ [30], giving a positive slope in log-period log-radius space. However, for super-Earths simulated in a gas-poor, rather than completely gas-empty environment, in which they are able to accrete some amount of gases, the opposite slope is expected ($R_{trans} \propto P^{-0.08}$ to $P^{-0.15}$) [25]. Gas-poor conditions have also been shown to reproduce the observed radius gap with no strong dependence on the required core masses [25].

For the gas-rich scenario, in which the radius valley is sculpted by the loss of the primordial atmospheres of super-Earths, the super-Earths must form in a gas-rich environment and subsequently lose their atmospheres through thermal mass-loss such as photoevaporation or core-powered mass loss (or through more exotic methods such as impact erosion). Simulations of photoevaporation on the expected Kepler planet yield predicted the existence of a radius gap before it was observed [36], although producing this gap at the correct radii tends to require core masses for the super-Earths which are slightly higher than those observed in order to accrete these atmospheres [41]. As photoevaoration becomes less efficient for longer-period planets, the transition radius should decrease with increasing period following $R_{trans} \propto P^{-0.15}$ [30]. Core-powered mass loss is a similar evaporative mechanism in which the luminosity of young planets themselves drives mass-loss as the planets cool, creating the super-Earths [10, 11]. Core-powered mass-loss reproduces a radius valley of very similar slope and location in period-radius space, and with a similar core mass distribution, to that of photoevaporation [12], making it difficult to differentiate between the two effects, as they are both likely occurring simultaneously. However, core-powered mass loss has a much longer timescale of roughly 500 Myr while that of photoevaporation is only 100 Myr, and an increase in the population of super-Earths for stars older than 100-200 Myr would be indicative of core-powered mass loss over photoevaporation [13].

4.3. Observed Trends in the Planet Population

The radius valley is most likely shaped by a combination of mechanisms which is dependent upon stellar type. Photoevaporation has been shown to shape the observed radii of known exoplanets to some extent as there is a clear threshold in terms of gravitational binding energy and irradiation after which no planets maintain thick atmospheres known as the cosmic shoreline [29, 28, 46], and core-powered mass loss is also expected to be an important process for young, cooling planets with extended gaseous envelopes [10, 11]. Unfortunately, the efficiency of photoevaporation depends strongly on the early XUV output of the host star, which isn't a well-constrained property for stable older systems. Because of this it's not often possible to test whether or not individual planets are consistent with the theory and we can instead test for consistency by comparing pairs of evaporated and non-evaporated planets in the same system, which have been subjected to the same stellar XUV history [35]. A similar method can be applied for core-powered mass-loss to leverage that planets in the same system have been subjected to a similar disk evolution [3]. No compelling inconsistent systems have yet been identified in this manner, although this is not a confirmation of either theory [35, 3].

The radius valley has been shown to have a negative slope in radius-period space for Sun-like stars [8, 43, 31], as shown in Fig. 1.6, consistent with thermal mass-loss predictions as well as gas-poor formation. However, for low-mass stars (that is, cool stars with $T < 4700$ K), the location of this valley appears to have a positive slope in period-radius space in strong agreement with gas-empty formation [2]. The location of the radius valley has also been shown to increase with stellar mass [7], a feature predicted for each formation pathway [7, 30, 13]. It is possible that the radius valley is shaped by gas-empty formation for low-mass stars, with gas-poor formation like that of the Earth becoming more dominant with increasing stellar masses, possibly due to changes in the stellar disk, and with thermal mass loss further evolving the radii of most planets to some extent through both core-powered mass-loss and photoevaporation. The exact processes shaping the planet distribution and the regimes in which they act will best be determined by finding more planets near the radius valley orbiting a variety of stellar types, and more high-quality planets for which the density can be determined such that their rocky or gaseous state is unambiguous.

5. Venus analogues and Secondary Atmospheres

While the densities of the super-Earths preclude them from having thick atmospheres, thin Earth-like atmospheres have little effect on planet mass and radius and could be present and undetected on many known terrestrial exoplanets. Primary atmospheres contain mostly H_2 and are accreted from the protoplanetary disk during planet formation, and can make up the majority of a planet's mass and radius. Secondary atmospheres like those of Earth and

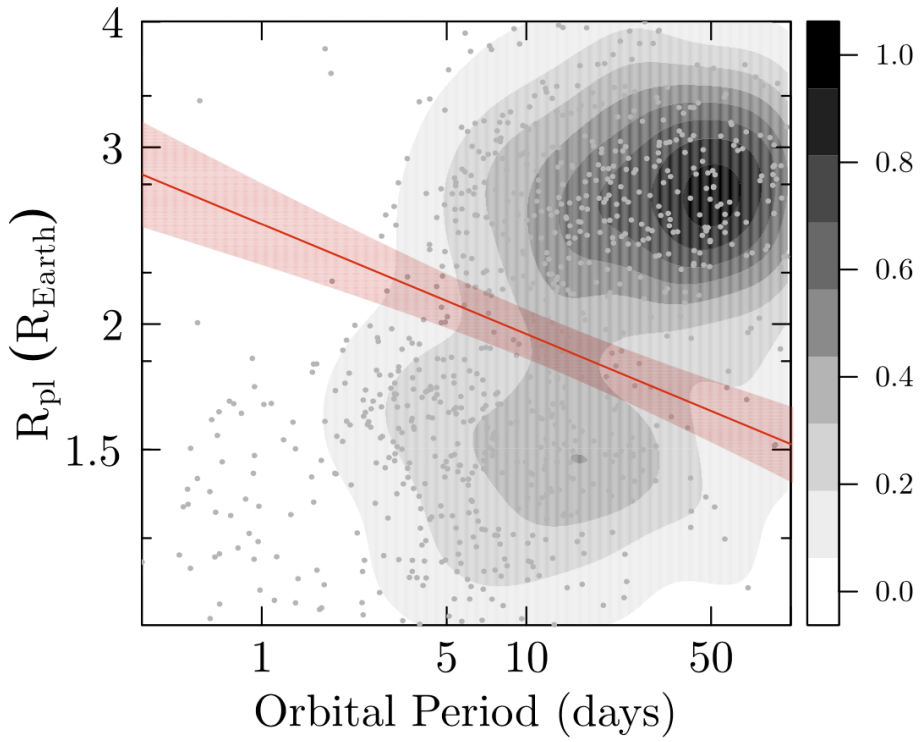

Fig. 1.6. Planet radius as a function of orbital period for small planets ($R < 4.0R_{\oplus}$) [31]. The radius valley is shown to have a negative slope, with smaller sub-Neptunes able to exist at longer radii and larger super-Earths on short radii. The shades of gray represent the normalized population density of exoplanets on the plot.

Venus have a higher mean molecular weight, due to a variety of molecules such as N_2, O_2 and CO_2, develop after the planetary cores themselves, and usually make up $\leq 1\%$ of the planet's mass, thus not measurably effect the planet's radius [28]. These atmospheres could either be formed through accretion at a later stage when the composition of the disk is evolved [22] or through degassing from the planet's solid materials, which may occur during planet formation or afterward through tectonics and volcanic activity [20]. Degassing is believed to be primarily responsible for the Earth's atmosphere [5], but the efficiency of these processes and subsequent atmospheric evolution are not well understood.

One of the most intriguing aspects of the small planet population is that these are the planets which may be most similar to Earth and to being potentially habitable, and will help us to investigate the boundaries in terms of radius and insolation at which planets become uninhabitable [17]. In our own solar system, it appears that such a boundary is present between the Earth and Venus. While the two planets are very similar in radius and bulk composition, Venus is believed to have undergone a runaway greenhouse effect [44] in which incoming radiation exceeded the planet's maximum outgoing thermal radiation, leading to the evaporation of its oceans and accumulation of greenhouse gases [18] and ultimately

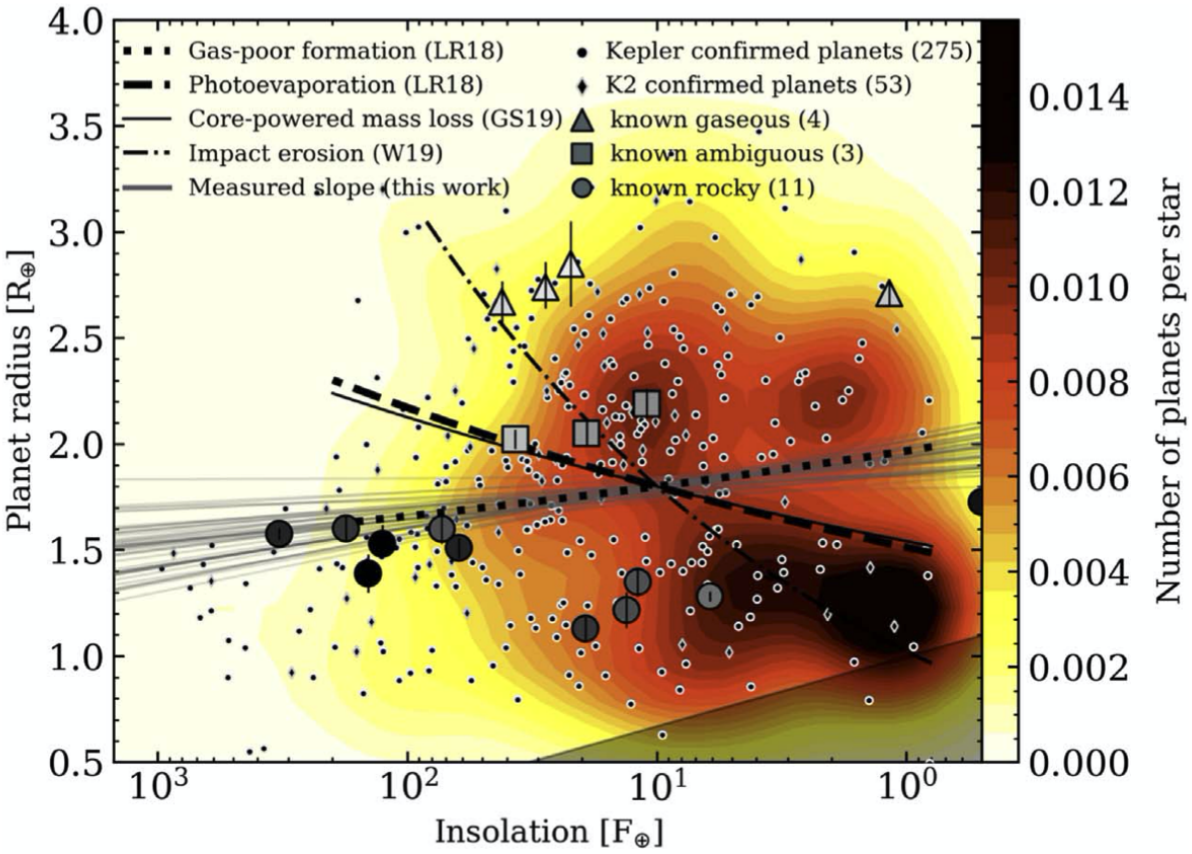

Fig. 1.7. Planet radius as a function of orbital period for planets orbiting low-mass stars ($T < 4700$ K, M dwarfs) in the Kepler sample [2]. The radius valley is shown to have a positive slope (gray lines) in contrast to the results found for Sun-like stars, shown in Fig. 1.6.

resulting in its thick and uninhabitable CO_2-dominated secondary atmosphere. It is unclear whether Venus may have at some point transitioned through a habitable phase or could have remained habitable on a slightly different orbit. Exoplanets offer an opportunity to test for the conditions which result in a runaway greenhouse effect by finding many exoplanets with a variety of insolations and sizes and determine which are Earth-like and which are Venus-like.

Unfortunately, the composition and size of these atmospheres which makes them conducive to habitability also makes them difficult to detect. Small planets which are not still in the process of forming are not nearly luminous enough for their own spectra to be observed, so these atmospheres can only be detected through transit spectroscopy. In this method, the stellar spectrum is observed both in and out of transit to determine how the star's light is affected as it filters through the planet's atmosphere, revealing the absorption spectrum of the planet so that its chemical composition and temperature-pressure profile can be modelled. A thin secondary atmosphere will affect only a very small amount of the

total light from the star, likely having an imperceptible effect on the stellar spectrum, unless the star and planet are not so different in size.

6. Planet Observability and the M Dwarf Opportunity

If our goal is to determine the atmospheric composition of ever-smaller planets in ever-greater detail, we must search for these planets around stars that are both small and nearby. Our ability to detect a planet's absorption spectrum depends on its signal to noise ratio, S/N, the expected depth of transmission features relative to the noise in the stellar spectrum. While the expected S/N depends on the atmospheric composition and scale height, these are generally unknown prior to observations; one way to compare the expected S/N for different planets regardless of atmospheric composition is with the transmission spectroscopy metric or TSM [19].

$$TSM = (\text{Scale factor}) \times \frac{\mathrm{R_p^3 T_{eq}}}{\mathrm{M_p R_*^2}} \times 10^{-\mathrm{m_J}/5} \tag{6.1}$$

The S/N scales as R_p^3/R_*^2, meaning it is much more difficult to detect spectral effects of smaller planets, but this difficulty is reduced if the star is also small. This effect is illustrated in Fig. 1.8. However, a small star is also less luminous, and the apparent magnitude of the host star effects the transmission S/N exponentially, making it similarly important that the star be nearby in order to reduce noise in the stellar spectrum. A closer, brighter star with a cleaner spectrum is also advantageous for follow-up radial velocity observations to determine the planet's mass.

For this reason, nearby M dwarfs, and smaller K dwarfs, are the best environments for atmospheric studies on small planets. Transmission spectroscopy has demonstrated that the super-Earth GJ 1214 b has a cloudy atmosphere [23]; water vapour has been detected in the cloudy H_2-dominated atmosphere of the sub-Neptune K2-18 b [1], and the eclipse of LHS 3844 b has shown that the hot super-Earth has no thick atmosphere [24]. All of these planets orbit red (M) dwarfs, and these discoveries would not have been possible were the planets orbiting large sun-like stars. TRAPPIST-1 is the smallest known planet-hosting star, and at a distance of only 12 pc, its seven transiting planets are the most favourable Earth-sized planets for JWST observations by a wide margin [9].

M dwarfs offer further advantages for planet-hunting in having a larger average number of planets per star and with these planets more likely to be habitable. Planet population studies for varying stellar types have shown that the frequency of planets smaller than about 4 $\mathrm{R_\oplus}$, and on orbital periods shorter than about 50 days, increases significantly with decreasing stellar temperature, with M dwarfs being at least twice as likely to host such a planet than a Sun-like star [16, 34]. For cooler stars, the 'habitable zone', the range in semi-major axis through which a planet could be the correct temperature to support liquid water, is much

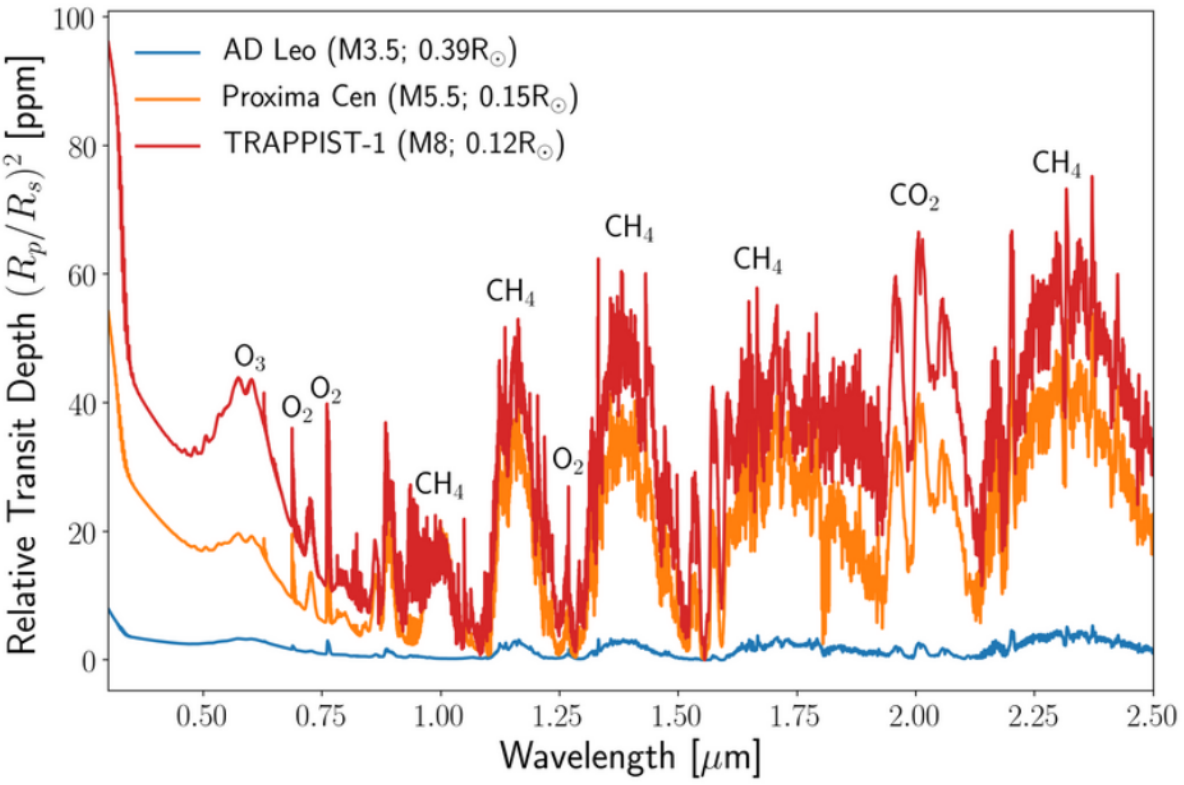

Fig. 1.8. Simulated transmission spectra for the same Earth-like planet orbiting M dwarfs of different radii [9]. The planet's spectral features are exaggerated for the mid and late M dwarfs.

closer to the star, making the close-in planets favoured by Kepler, and all transit missions, much more likely to be at habitable temperatures around M dwarfs than Sun-like stars.

It's also possible that the occurrence rates of these small, close-in planets increases dramatically for the coolest M dwarfs, given that TRAPPIST-1 is the smallest planet-hosting star discovered to date and also hosts seven such planets. Unfortunately, there are few known systems around late M dwarfs and population studies for these stellar types are imprecise, although there is some indication that late M dwarfs (M5) host more planets than larger M dwarfs (M3) [15]. Data from the SPECULOOS survey suggests that at least 10% of M dwarfs later than M7 host close-in terrestrial planets analogous to TRAPPIST-1 b [26]. There are few known late M dwarf planetary systems even though they may be most likely to host planets in part because the smallest M dwarfs are not luminous enough to be seen from Earth unless they're very nearby, and the Kepler satellite responsible for finding the majority of known small planets searched only a small area of the sky and thus a limited number of nearby cool dwarfs. Current planet-hunting missions such as TESS have been adapted to prioritize M dwarfs.

7. K2 and TESS

Given the significant observational and scientific advantages M dwarfs provide, the largest planet-hunting missions launched since Kepler have been tailored to better find planets around these stars. With the malfunction of Kepler's pointing system, the satellite could no longer observe its intended field of view continuously and was re-purposed for the K2 mission, in which the satellite observed 19 different fields around the ecliptic for roughly 90 days each. This method of searching a larger area for a shorter period of time is better suited to finding those nearby late M dwarfs which are unlikely to be found in any single small field of view. These pointing limitations also reduced the satellite's precision, making it more difficult to find planets around dimmer stars, also increasing the average signal to noise of resulting targets. Fig. 1.10 shows the confirmed planets found by Kepler and K2 as well as the unconfirmed planet candidates TESS has found thus far and demonstrates that the modified observing strategy of K2 yielded planets of a higher average signal to noise.

TESS, the Transiting Exoplanet Survey Satellite is NASA's current planet-hunting mission succeeding Kepler/K2. Where Kepler was designed to monitor a single patch of the sky for several years in the hopes of finding an Earth analogue around a Sun-like star, TESS is designed to search almost the entire sky for planets orbiting nearby, bright stars which will be most amenable to spectroscopic follow-up. The satellite's field of view is 20 times larger than that of Kepler, and in its initial two-year mission the satellite surveyed over 75% of the sky nearly continuously, producing 27-day lightcurves for most of this area, but with some sectors overlapping to produce longer series of observations. These relatively short lightcurves result in planet detections with fairly short orbital periods, but for M dwarfs these orbits can still be habitable. The wavelength response of TESS is also shifted to the red relative to Kepler to increase sensitivity to M dwarf spectra which peak at these wavelengths, where Kepler was similarly designed to cater to Sun-like (F, G and K) stars, as shown in Fig. 1.9. Spectroscopic instruments such as SPIRou are also being pushed into the infrared as these are similarly advantageous for follow-up mass measurements and transmission spectroscopy for planets around small, cool stars. These strategic changes are producing the expected results; as shown in Fig. 1.10, the TESS planet candidates have a systematically higher signal to noise ratio than the Kepler or K2 planets despite many of them having smaller radii, because these planets orbit cooler stars.

Even with the instrumentation of JWST, transmission spectroscopy of planets similar in size and temperature to Earth will only be remotely possible for a handful of targets in the night sky [9]. As these observations require small host stars to be feasible, and these small stars must also be very nearby to be observable, there are most likely only a few hundred such stars in the night sky, only a fraction of which would be aligned to host transiting planets. TRAPPIST-1 may be the best system that exists to be found [9]. As TESS continues to

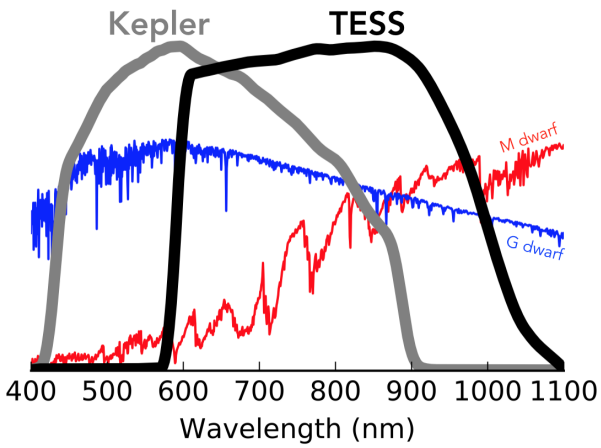

Fig. 1.9. TESS and Kepler satellite wavelength response functions. TESS observes further to red wavelengths than Kepler, to better observe M dwarfs which are brightest at these wavelengths, whereas Kepler was designed to prioritize Sun-like stars. (image credit: nasa.gov)

observe beyond its two year mission and covers the entire sky, nearly all of these small, observable planets will be revealed, and with these planets belonging to unique systems and having unique compositions, each will play a crucial role in our modeling and understanding of small planet formation. In the following work, two such planets are identified using the transit method and their scientific advantages are expounded.

8. Contributions

My contributions to each article are described in their corresponding sections. The remainder of this thesis is my work.

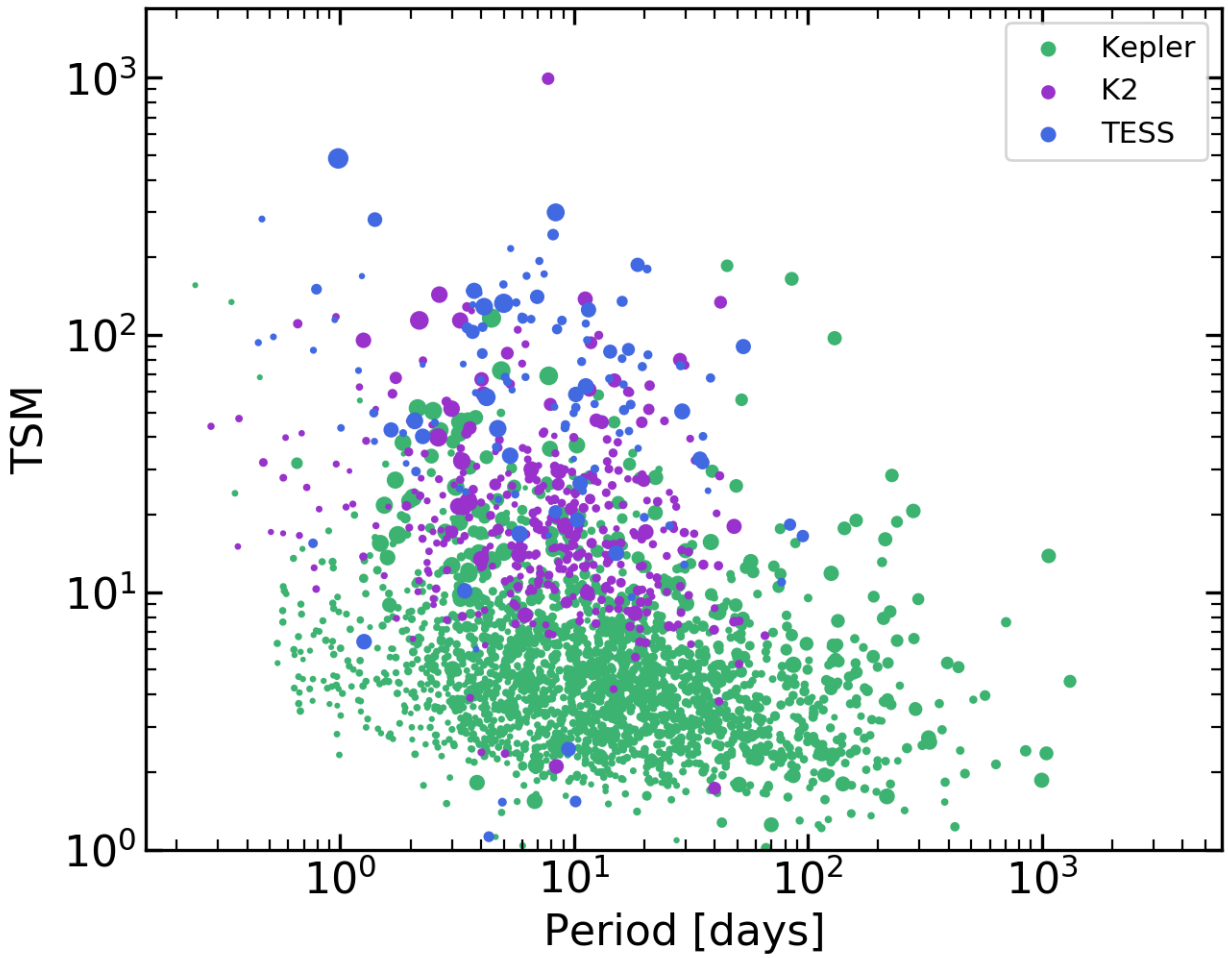

Fig. 1.10. Kepler and K2 confirmed planet populations contrasted with the TESS planet candidates, with the y-axis representing the TSM and point size representing planet radius. The TESS planet candidates and the K2 planets have a systematically higher signal to noise than the Kepler planets due to the modified observing strategies of these missions, which search larger areas and produce shorter lightcurves.

References

[1] Björn Benneke, Ian Wong, Caroline Piaulet, Heather A. Knutson, Joshua Lothringer, Caroline V. Morley, Ian J. M. Crossfield, Peter Gao, Thomas P. Greene, Courtney Dressing, Diana Dragomir, Andrew W. Howard, Peter R. McCullough, Eliza M. R. Kempton, Jonathan J. Fortney, and Jonathan Fraine. Water Vapor and Clouds on the Habitable-zone Sub-Neptune Exoplanet K2-18b. ApJ, 887(1):L14, December 2019.

[2] William J. Borucki, David Koch, Gibor Basri, Natalie Batalha, Timothy Brown, Douglas Caldwell, John Caldwell, Jørgen Christensen-Dalsgaard, William D. Cochran, Edna DeVore, Edward W. Dunham, Andrea K. Dupree, Thomas N. Gautier, John C. Geary, Ronald Gilliland, Alan Gould, Steve B. Howell, Jon M. Jenkins, Yoji Kondo, David W. Latham, Geoffrey W. Marcy, Søren Meibom, Hans Kjeldsen, Jack J. Lissauer, David G. Monet, David Morrison, Dimitar Sasselov, Jill Tarter, Alan Boss, Don Brownlee, Toby Owen, Derek Buzasi, David Charbonneau, Laurance Doyle, Jonathan Fortney, Eric B. Ford, Matthew J. Holman, Sara Seager, Jason H. Steffen, William F. Welsh, Jason Rowe, Howard Anderson, Lars Buchhave, David Ciardi, Lucianne Walkowicz, William Sherry, Elliott Horch, Howard Isaacson, Mark E. Everett, Debra Fischer, Guillermo Torres, John Asher Johnson, Michael Endl, Phillip MacQueen, Stephen T. Bryson, Jessie Dotson, Michael Haas, Jeffrey Kolodziejczak, Jeffrey Van Cleve, Hema Chandrasekaran, Joseph D. Twicken, Elisa V. Quintana, Bruce D. Clarke, Christopher Allen, Jie Li, Haley Wu, Peter Tenenbaum, Ekaterina Verner, Frederick Bruhweiler, Jason Barnes, and Andrej Prsa. Kepler Planet-Detection Mission: Introduction and First Results. *Science*, 327(5968):977, February 2010.

[3] Ryan Cloutier, Jason D. Eastman, Joseph E. Rodriguez, Nicola Astudillo-Defru, Xavier Bonfils, Annelies Mortier, Christopher A. Watson, Manu Stalport, Matteo Pinamonti, Florian Lienhard, Avet Harutyunyan, Mario Damasso, David W. Latham, Karen A. Collins, Robert Massey, Jonathan Irwin, Jennifer G. Winters, David Charbonneau, Carl Ziegler, Elisabeth Matthews, Ian J. M. Crossfield, Laura Kreidberg, Samuel N. Quinn, George Ricker, Roland Vanderspek, Sara Seager, Joshua Winn, Jon M. Jenkins, Michael Vezie, Stéphane Udry, Joseph D. Twicken, Peter Tenenbaum, Alessandro Sozzetti, Damien Ségransan, Joshua E. Schlieder, Dimitar Sasselov, Nuno C. Santos, Ken Rice, Benjamin V. Rackham, Ennio Poretti, Giampaolo Piotto, David Phillips, Francesco Pepe, Emilio Molinari, Lucile Mignon, Giuseppina Micela, Claudio Melo, José R. de Medeiros, Michel Mayor, Rachel A. Matson, Aldo F. Martinez Fiorenzano, Andrew W. Mann, Antonio Magazzú, Christophe Lovis, Mercedes López-Morales, Eric Lopez, Jack J. Lissauer, Sébastien Lépine, Nicholas Law, John F. Kielkopf, John A. Johnson, Eric L. N. Jensen, Steve B. Howell, Erica Gonzales, Adriano Ghedina, Thierry

Forveille, Pedro Figueira, Xavier Dumusque, Courtney D. Dressing, René Doyon, Rodrigo F. Díaz, Luca Di Fabrizio, Xavier Delfosse, Rosario Cosentino, Dennis M. Conti, Kevin I. Collins, Andrew Collier Cameron, David Ciardi, Douglas A. Caldwell, Christopher Burke, Lars Buchhave, César Briceño, Patricia Boyd, François Bouchy, Charles Beichman, Étienne Artigau, and Jose M. Almenara. A Pair of TESS Planets Spanning the Radius Valley around the Nearby Mid-M Dwarf LTT 3780. AJ, 160(1):3, July 2020.

[4] Ryan Cloutier and Kristen Menou. Evolution of the radius valley around low-mass stars from kepler and k2. *The Astronomical Journal*, 159(5):211, apr 2020.

[5] Nicolas Dauphas and Alessandro Morbidelli. Geochemical and planetary dynamical views on the origin of Earth's atmosphere and oceans. *arXiv e-prints*, page arXiv:1312.1202, December 2013.

[6] Courtney D. Dressing and David Charbonneau. The Occurrence of Potentially Habitable Planets Orbiting M Dwarfs Estimated from the Full Kepler Dataset and an Empirical Measurement of the Detection Sensitivity. ApJ, 807(1):45, July 2015.

[7] Benjamin J. Fulton and Erik A. Petigura. The California-Kepler Survey. VII. Precise Planet Radii Leveraging Gaia DR2 Reveal the Stellar Mass Dependence of the Planet Radius Gap. AJ, 156(6):264, December 2018.

[8] Benjamin J. Fulton, Erik A. Petigura, Andrew W. Howard, Howard Isaacson, Geoffrey W. Marcy, Phillip A. Cargile, Leslie Hebb, Lauren M. Weiss, John Asher Johnson, Timothy D. Morton, Evan Sinukoff, Ian J. M. Crossfield, and Lea A. Hirsch. The California-Kepler Survey. III. A Gap in the Radius Distribution of Small Planets. AJ, 154(3):109, September 2017.

[9] Michaël Gillon, Victoria Meadows, Eric Agol, Adam J. Burgasser, Drake Deming, René Doyon, Jonathan Fortney, Laura Kreidberg, James Owen, Franck Selsis, Julien de Wit, Jacob Lustig-Yaeger, and Benjamin V. Rackham. The TRAPPIST-1 JWST Community Initiative. *arXiv e-prints*, page arXiv:2002.04798, February 2020.

[10] Sivan Ginzburg, Hilke E. Schlichting, and Re'em Sari. Super-Earth Atmospheres: Self-consistent Gas Accretion and Retention. ApJ, 825(1):29, July 2016.

[11] Sivan Ginzburg, Hilke E. Schlichting, and Re'em Sari. Core-powered mass-loss and the radius distribution of small exoplanets. MNRAS, 476(1):759–765, May 2018.

[12] Akash Gupta and Hilke E. Schlichting. Sculpting the valley in the radius distribution of small exoplanets as a by-product of planet formation: the core-powered mass-loss mechanism. MNRAS, 487(1):24–33, July 2019.

[13] Akash Gupta and Hilke E. Schlichting. Signatures of the core-powered mass-loss mechanism in the exoplanet population: dependence on stellar properties and observational predictions. MNRAS, 493(1):792–806, March 2020.

[14] Jr. Haisch, Karl E., Elizabeth A. Lada, and Charles J. Lada. Disk Frequencies and Lifetimes in Young Clusters. ApJ, 553(2):L153–L156, June 2001.

[15] Kevin K. Hardegree-Ullman, Michael C. Cushing, Philip S. Muirhead, and Jessie L. Christiansen. Kepler Planet Occurrence Rates for Mid-type M Dwarfs as a Function of Spectral Type. AJ, 158(2):75, August 2019.

[16] Andrew W. Howard, Geoffrey W. Marcy, Stephen T. Bryson, Jon M. Jenkins, Jason F. Rowe, Natalie M. Batalha, William J. Borucki, David G. Koch, Edward W. Dunham, III Gautier, Thomas N., Jeffrey Van Cleve, William D. Cochran, David W. Latham, Jack J. Lissauer, Guillermo Torres, Timothy M. Brown, Ronald L. Gilliland, Lars A. Buchhave, Douglas A. Caldwell, Jørgen Christensen-Dalsgaard, David Ciardi, Francois Fressin, Michael R. Haas, Steve B. Howell, Hans Kjeldsen, Sara Seager, Leslie Rogers, Dimitar D. Sasselov, Jason H. Steffen, Gibor S. Basri, David Charbonneau, Jessie Christiansen, Bruce Clarke, Andrea Dupree, Daniel C. Fabrycky, Debra A. Fischer, Eric B. Ford, Jonathan J. Fortney, Jill Tarter, Forrest R. Girouard, Matthew J. Holman, John Asher Johnson, Todd C. Klaus, Pavel Machalek, Althea V. Moorhead, Robert C. Morehead, Darin Ragozzine, Peter Tenenbaum, Joseph D. Twicken, Samuel N. Quinn, Howard Isaacson, Avi Shporer, Philip W. Lucas, Lucianne M. Walkowicz, William F. Welsh, Alan Boss, Edna Devore, Alan Gould, Jeffrey C. Smith, Robert L. Morris, Andrej Prsa, Timothy D. Morton, Martin Still, Susan E. Thompson, Fergal Mullally, Michael Endl, and Phillip J. MacQueen. Planet Occurrence within 0.25 AU of Solar-type Stars from Kepler. ApJS, 201(2):15, August 2012.

[17] Stephen R. Kane, Giada Arney, David Crisp, Shawn Domagal-Goldman, Lori S. Glaze, Colin Goldblatt, David Grinspoon, James W. Head, Adrian Lenardic, Cayman Unterborn, Michael J. Way, and Kevin J. Zahnle. Venus as a Laboratory for Exoplanetary Science. *Journal of Geophysical Research (Planets)*, 124(8):2015–2028, August 2019.

[18] J. F. Kasting. Runaway and moist greenhouse atmospheres and the evolution of Earth and Venus. Icarus, 74(3):472–494, June 1988.

[19] Eliza M. R. Kempton, Jacob L. Bean, Dana R. Louie, Drake Deming, Daniel D. B. Koll, Megan Mansfield, Jessie L. Christiansen, Mercedes López-Morales, Mark R. Swain, Robert T. Zellem, Sarah Ballard, Thomas Barclay, Joanna K. Barstow, Natasha E. Batalha, Thomas G. Beatty, Zach Berta-Thompson, Jayne Birkby, Lars A. Buchhave, David Charbonneau, Nicolas B. Cowan, Ian Crossfield, Miguel de Val-Borro, René Doyon, Diana Dragomir, Eric Gaidos, Kevin Heng, Renyu Hu, Stephen R. Kane, Laura Kreidberg, Matthias Mallonn, Caroline V. Morley, Norio Narita, Valerio Nascimbeni, Enric Pallé, Elisa V. Quintana, Emily Rauscher, Sara Seager, Evgenya L. Shkolnik, David K. Sing, Alessandro Sozzetti, Keivan G. Stassun, Jeff A. Valenti, and Carolina von Essen. A Framework for Prioritizing the TESS Planetary Candidates Most Amenable to Atmospheric Characterization. PASP, 130(993):114401, November 2018.

[20] Edwin S. Kite and Megan N. Barnett. Exoplanet secondary atmosphere loss and revival. *Proceedings of the National Academy of Science*, 117:18264–18271, July 2020.

[21] David G. Koch, William J. Borucki, Gibor Basri, Natalie M. Batalha, Timothy M. Brown, Douglas Caldwell, Jørgen Christensen-Dalsgaard, William D. Cochran, Edna DeVore, Edward W. Dunham, III Gautier, Thomas N., John C. Geary, Ronald L. Gilliland, Alan Gould, Jon Jenkins, Yoji Kondo, David W. Latham, Jack J. Lissauer, Geoffrey Marcy, David Monet, Dimitar Sasselov, Alan Boss, Donald Brownlee, John Caldwell, Andrea K. Dupree, Steve B. Howell, Hans Kjeldsen, Søren Meibom, David Morrison, Tobias Owen, Harold Reitsema, Jill Tarter, Stephen T. Bryson, Jessie L. Dotson, Paul Gazis, Michael R. Haas, Jeffrey Kolodziejczak, Jason F. Rowe, Jeffrey E. Van Cleve, Christopher Allen, Hema Chandrasekaran, Bruce D. Clarke, Jie Li, Elisa V. Quintana, Peter Tenenbaum, Joseph D. Twicken, and Hayley Wu. Kepler Mission Design, Realized Photometric Performance, and Early Science. ApJ, 713(2):L79–L86, April 2010.

[22] Quentin Kral, Jeanne Davoult, and Benjamin Charnay. Formation of secondary atmospheres on terrestrial planets by late disk accretion. *Nature Astronomy*, 4:769–775, April 2020.

[23] Laura Kreidberg, Jacob L. Bean, Jean-Michel Désert, Björn Benneke, Drake Deming, Kevin B. Stevenson, Sara Seager, Zachory Berta-Thompson, Andreas Seifahrt, and Derek Homeier. Clouds in the atmosphere of the super-Earth exoplanet GJ1214b. Nature, 505(7481):69–72, January 2014.

[24] Laura Kreidberg, Daniel D. B. Koll, Caroline Morley, Renyu Hu, Laura Schaefer, Drake Deming, Kevin B. Stevenson, Jason Dittmann, Andrew Vanderburg, David Berardo, Xueying Guo, Keivan Stassun, Ian Crossfield, David Charbonneau, David W. Latham, Abraham Loeb, George Ricker, Sara Seager, and Roland Vanderspek. Absence of a thick atmosphere on the terrestrial exoplanet LHS 3844b. Nature, 573(7772):87–90, August 2019.

[25] Eve J. Lee and Nicholas J. Connors. Primordial Radius Gap and Potentially Broad Core Mass Distributions of Super-Earths and Sub-Neptunes. ApJ, 908(1):32, February 2021.

[26] F. Lienhard, D. Queloz, M. Gillon, A. Burdanov, L. Delrez, E. Ducrot, W. Handley, E. Jehin, C. A. Murray, A. H. M. J. Triaud, E. Gillen, A. Mortier, and B. V. Rackham. Global analysis of the TRAPPIST Ultra-Cool Dwarf Transit Survey. MNRAS, 497(3):3790–3808, September 2020.

[27] Jack J. Lissauer. Planet formation. *Annual Review of Astronomy and Astrophysics*, 31(1):129–172, 1993.

[28] Eric D. Lopez and Jonathan J. Fortney. UNDERSTANDING THE MASS-RADIUS RELATION FOR SUB-NEPTUNES: RADIUS AS a PROXY FOR COMPOSITION. *The Astrophysical Journal*, 792(1):1, aug 2014.

[29] Eric D. Lopez, Jonathan J. Fortney, and Neil Miller. HOW THERMAL EVOLUTION AND MASS-LOSS SCULPT POPULATIONS OF SUPER-EARTHS AND SUB-NEPTUNES: APPLICATION TO THE KEPLER-11 SYSTEM AND BEYOND. *The Astrophysical Journal*, 761(1):59, nov 2012.

[30] Eric D Lopez and Ken Rice. How formation time-scales affect the period dependence of the transition between rocky super-Earths and gaseous sub-Neptunes and implications for eta Earth. *Monthly Notices of the Royal Astronomical Society*, 479(4):5303–5311, 07 2018.

[31] Cintia F. Martinez, Katia Cunha, Luan Ghezzi, and Verne V. Smith. A spectroscopic analysis of the california-kepler survey sample. i. stellar parameters, planetary radii, and a slope in the radius gap. *The Astrophysical Journal*, 875(1):29, apr 2019.

[32] Michel Mayor and Didier Queloz. A Jupiter-mass companion to a solar-type star. Nature, 378(6555):355–359, November 1995.

[33] A. Morbidelli, J. I. Lunine, D. P. O'Brien, S. N. Raymond, and K. J. Walsh. Building Terrestrial Planets. *Annual Review of Earth and Planetary Sciences*, 40(1):251–275, May 2012.

[34] Gijs D. Mulders, Ilaria Pascucci, and Dániel Apai. A Stellar-mass-dependent Drop in Planet Occurrence Rates. ApJ, 798(2):112, January 2015.

[35] James E. Owen and Beatriz Campos Estrada. Testing exoplanet evaporation with multitransiting systems. MNRAS, 491(4):5287–5297, February 2020.

[36] James E. Owen and Yanqin Wu. Kepler Planets: A Tale of Evaporation. ApJ, 775(2):105, October 2013.

[37] Erik A. Petigura, Geoffrey W. Marcy, and Andrew W. Howard. A Plateau in the Planet Population below Twice the Size of Earth. ApJ, 770(1):69, June 2013.

[38] James B. Pollack, Olenka Hubickyj, Peter Bodenheimer, Jack J. Lissauer, Morris Podolak, and Yuval Greenzweig. Formation of the Giant Planets by Concurrent Accretion of Solids and Gas. Icarus, 124(1):62–85, November 1996.

[39] Roman R. Rafikov. Atmospheres of Protoplanetary Cores: Critical Mass for Nucleated Instability. ApJ, 648(1):666–682, September 2006.

[40] Sean N. Raymond, David P. O'Brien, Alessandro Morbidelli, and Nathan A. Kaib. Building the terrestrial planets: Constrained accretion in the inner Solar System. Icarus, 203(2):644–662, October 2009.

[41] James G. Rogers and James E. Owen. Unveiling the planet population at birth. MNRAS, 503(1):1526–1542, May 2021.

[42] Leslie A. Rogers. MOST1.6 EARTH-RADIUS PLANETS ARE NOT ROCKY. *The Astrophysical Journal*, 801(1):41, mar 2015.

[43] V. Van Eylen, Camilla Agentoft, M. S. Lundkvist, H. Kjeldsen, J. E. Owen, B. J. Fulton, E. Petigura, and I. Snellen. An asteroseismic view of the radius valley: stripped cores,

not born rocky. MNRAS, 479(4):4786–4795, October 2018.

[44] J. C. G. Walker. Evolution of the atmosphere of Venus. *Journal of Atmospheric Sciences*, 32:1248–1256, June 1975.

[45] Lauren M. Weiss and Geoffrey W. Marcy. THE MASS-RADIUS RELATION FOR 65 EXOPLANETS SMALLER THAN 4 EARTH RADII. *The Astrophysical Journal*, 783(1):L6, feb 2014.

[46] Kevin J. Zahnle and David C. Catling. The Cosmic Shoreline: The Evidence that Escape Determines which Planets Have Atmospheres, and what this May Mean for Proxima Centauri B. ApJ, 843(2):122, July 2017.

First Article.

A 2 Earth Radius Planet Orbiting the Bright Nearby K Dwarf Wolf 503

by

Merrin Peterson[1], Björn Benneke[1], Trevor J. David[2], Courtney D. Dressing[3], David Ciardi[4], Ian J. M. Crossfield[5], Joshua E. Schlieder[6], Erik A. Petigura[7,8], Eric E. Mamajek[2], Jessie L. Christiansen[4], Sam N. Quinn[9], Benjamin J. Fulton[4], Andrew W. Howard[7], Evan Sinukoff[7], Charles Beichman[4], David W. Latham[10], Liang Yu[5], Nicole Arango[11], Avi Shporer[5], Thomas Henning[12], Chelsea X.Huang[5], Molly R. Kosiarek[13,14], Jason Dittmann[5], and Howard Isaacson[3]

([1]) Department of Physics and Institute for Research on Exoplanets, Université de Montréal, Montreal, QC, Canada

([2]) Jet Propulsion Laboratory, California Institute of Technology, 4800 Oak Grove Drive, Pasadena, CA 91109, USA

([3]) Department of Astronomy, University of California, Berkeley, CA 94720

([4]) Caltech/IPAC-NASA Exoplanet Science Institute, 770 S. Wilson Ave, Pasadena, CA 91106, USA

([5]) Department of Physics, and Kavli Institute for Astrophysics and Space Research, Massachusetts Institute of Technology, Cambridge, MA 02139, USA

([6]) NASA Goddard Space Flight Center, 8800 Greenbelt Road, Greenbelt, MD 20771, USA

([7]) Department of Astronomy, California Institute of Technology, Pasadena, CA 91125, USA

([8]) NASA Hubble Fellow

([9]) Harvard-Smithsonian Center for Astrophysics, 60 Garden Street, Cambridge, MA 02138, USA

([10]) Center for Astrophysics, 60 Garden Street, Cambridge, MA 02138, USA

([11]) College of the Canyons, Valencia, CA 91355, USA

([12]) Max Planck Institute for Astronomy, 69117 Heidelberg, Germany

([13]) NSF Graduate Student Fellow

([14]) Department of Astronomy and Astrophysics, University of California, Santa Cruz, CA 95064, USA

This article is published in *The Astronomical Journal*.

The main contributions of Merrin Peterson for this article are presented.

- Vetting of candidate planet signals with coauthors
- K2 lightcurve analysis and fitting
- Archival Imagery analysis
- Wrote the introduction, discussion and abstract with comments provided by coauthors

ABSTRACT. Since its launch in 2009, the *Kepler* telescope has found thousands of planets with radii between that of Earth and Neptune. Recent studies of the distribution of these planets have revealed a gap in the population near 1.5–2.0 $R_\oplus$, informally dividing these planets into “super-Earths" and “sub-Neptunes". The origin of this division is difficult to investigate directly because the majority of planets found by Kepler orbit distant, dim stars and are not amenable to radial velocity follow-up or transit spectroscopy, making bulk density and atmospheric measurements difficult. Here, we present the discovery and validation of a newly found $2.03^{+0.08}_{-0.07}$ $R_\oplus$ planet in direct proximity to the radius gap, orbiting the bright (J = 8.32 mag), nearby (D = 44.5 pc) high proper motion K3.5V star Wolf 503 (EPIC 212779563). We determine the possibility of a companion star and false positive detection to be extremely low using both archival images and high-contrast adaptive optics images from the Palomar observatory. The brightness of the host star makes Wolf 503b a prime target for prompt radial velocity follow-up, and with the small stellar radius (0.690 ± 0.025 $R_\odot$), it is also an excellent target for *HST* transit spectroscopy and detailed atmospheric characterization with *JWST*. With its measured radius near the gap in the planet radius and occurrence rate distribution, Wolf 503b offers a key opportunity to better understand the origin of this radius gap as well as the nature of the intriguing populations of “super-Earths" and “sub-Neptunes" as a whole.

Keywords: methods: observational — planets and satellites: atmospheres — planets and satellites: individual (Wolf 503b) — planets and satellites: physical evolution — planets and satellites: gaseous planets

1. Introduction

The majority of close-in planets found by NASA's *Kepler* satellite throughout the past decade are smaller than Neptune, but larger than Earth [2, 39, 24]. The *Kepler* and *K2* missions have shown that, of the planets to which *Kepler* is most sensitive ($P < 100$ days, $R_p > 1.0 R_\oplus$), these smaller planets are by far the most common in the galaxy [17, 23], though there is no analog in the solar system from which this could have been predicted.

A gap in the population of planets at radii larger than 4.0 $R_\oplus$ (i.e., larger than Neptune) is satisfactorily explained by runaway gas accretion [43, 26, 38]. Larger planets are massive enough to accrete H and He from the protoplanetary disc, becoming puffy and increasing in radius. However, refined studies of the distribution of planets within the $1-4$ $R_\oplus$ range have revealed a significant drop in the population, or "Fulton gap" (shown in Fig. 2.1) between $1.5-2.0$ $R_\oplus$ [23, 40, 18], which is not yet well-understood.

Photoevaporation presents a possible explanation for the gap, and is a particularly important factor for the close-in planets preferentially detected by *Kepler*. Planets with radii between 1.5 and 2.0 $R_\oplus$ could represent a relatively rare group of planets retaining thin atmospheres, while super-Earths are photoevaporated rocky bodies and the sub-Neptunes are massive enough to retain thick atmospheres [30]. Jin and Mordasini [27] find support for this theory using planetary formation and evolution models. They observe that planets of increasing radius are more volatile-rich, with an anti-correlation between density and orbital distance. Furthermore, Fulton and Petigura [18] find observational evidence for the photoevaporation theory in their discovery that the populations of sub-Neptunes shifts to higher levels of incident flux for higher mass stars. Since stellar activity driven by rotation and convection is generally stronger and longer lived in lower-mass stars, the atmospheres of planets orbiting smaller stars experience prolonged exposure to high-energy X-ray and UV photons and energetic particle fluxes. The atmospheres of sub-Neptunes orbiting lower-mass stars therefore suffer increased photoevaporation while receiving comparable levels of incident flux as similar planets orbiting higher-mass stars. The shift of this population to higher incident flux for higher-mass stars indicates that the gap is a result of photoevaporation.

It has also been postulated that the sub-Neptunes form earlier in the evolution of the protoplanetary disc than super-Earths, when there is still more gas in the disc, giving them thicker atmospheres and larger radii [29]. The gap would then represent an intermediate stage in disc evolution in which planets are not likely to form.

Explanations for the bimodal distribution of planets which invoke composition should be tested with mass (i.e., bulk density) measurements and transit spectroscopy to determine the composition and atmospheric mass fraction of planets on both sides of the rift. However, planets favorable for these detailed follow-up characterizations are missing. Although *Kepler*

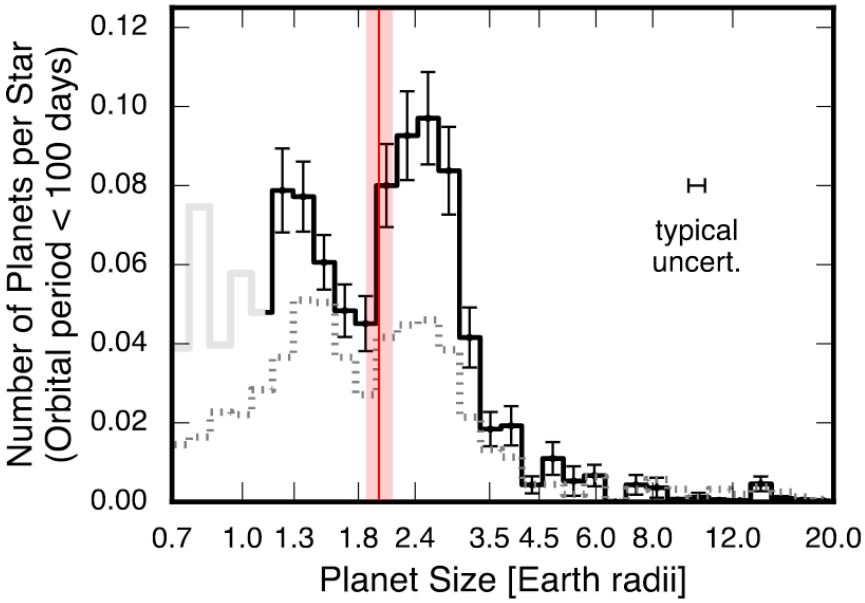

Fig. 2.1. Observed planet radius distribution adapted from Fulton and Petigura [18]. There is a significant decrease in the planet population from 1.5–2.0 $R_\oplus$. The 1σ radius limits for Wolf 503b are overplotted in red and lie directly adjacent to the radius gap, potentially indicating the planet is in the process of photoevaporation.

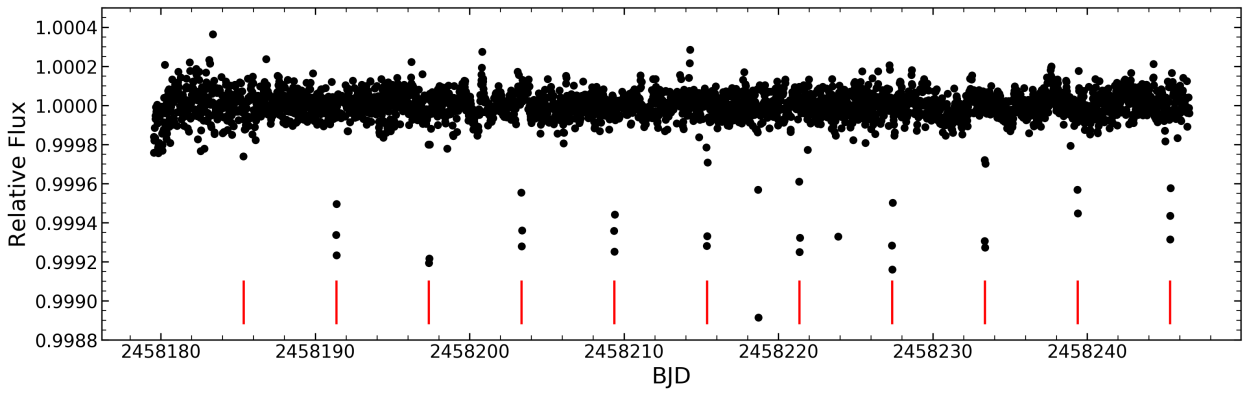

Fig. 2.2. Extracted light curve for Wolf 503 (EPIC 212779563). Transit times according to our fit are indicated with a red line. The first observed transit is not easily visible in this plot because the transit coincided with a thruster burn during which two data points were flagged and removed (see Fig. 2.6).

has found thousands of bona fide $1-4\ R_\oplus$ planets, due to the satellite's 100 sq. deg. field-of-view, relatively few bright stars were targeted and most Kepler planet hosts are distant and dim. For this reason, the detailed spectra required from these stars to make quality mass and atmospheric composition measurements are often unattainable. Although there has been

much effort to constrain the density of planets in this region [15, 53, 46], the parameter space near the Fulton gap remains relatively unexplored.

In this work, we present the detection and validation of a newly found ~2.0 $R_\oplus$ planet from *K2*, Wolf 503b, which represents one of the best opportunities to date to conduct a detailed radial velocity and atmospheric study of a planet in the 1-4$R_\oplus$ range. In Sec. 2.1 we describe the collection and calibration of the *K2* photometry, as well as our detection pipeline. In Sec. 2.2 we discuss the research history of the host star and its galactic origins. We obtain our own spectrum of Wolf 503, classify the star and determine stellar parameters in Sec. 2.3. Our methods of target validation are described in Sec. 2.4 and the final light curve fitting and results are found in Sec. 2.5. These results are summarized and discussed in Sec. 3.

2. Observations and Analysis

Identified as a planet candidate from C17 of *K2* (see Crossfield et al. [12]), Wolf 503 was recognized as an excellent host for follow-up study, being both bright ($K_p = 9.9$) and nearby (45pc). Here we present the treatment of the photometry used to detect Wolf 503b, as well as our planet validation techniques, and derive both planetary and stellar parameters.

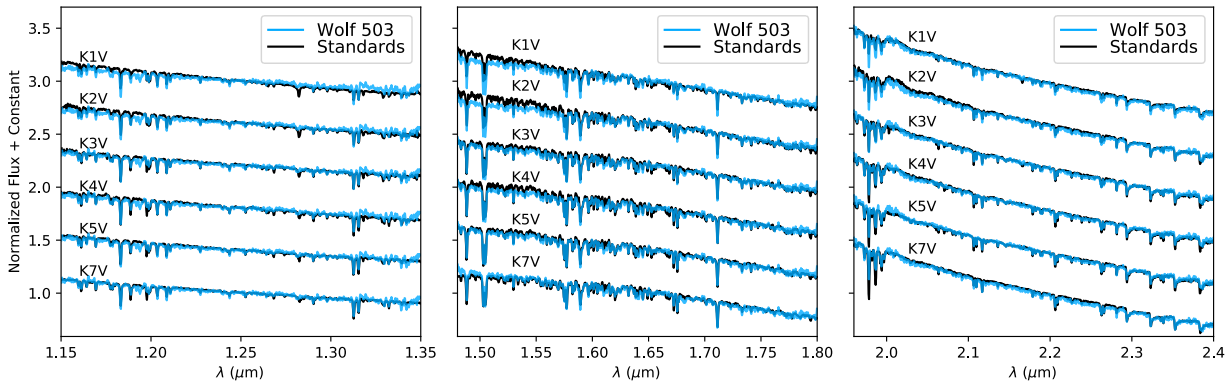

Fig. 2.3. Final, calibrated SpeX spectra for Wolf 503 shown compared to spectral standards. We find the best visual match for Wolf 503 indicates a K3.5V±0.5 spectral type, consistent with previous classifications (see Sec. 2.2).

2.1. Photometry Extraction and Transit Detection

The photometric extraction and transit detection methods used to identify Wolf 503b are the same as those applied by our team to all light curves in C17 and are described in our corresponding C17 summary paper, Crossfield et al. [12]. As *K2* operates using only two of *Kepler*'s four initial reaction wheels, the telescope drifts along its roll axis by a few pixels every several days, and thruster firings are used to maintain the telescope's pointing.

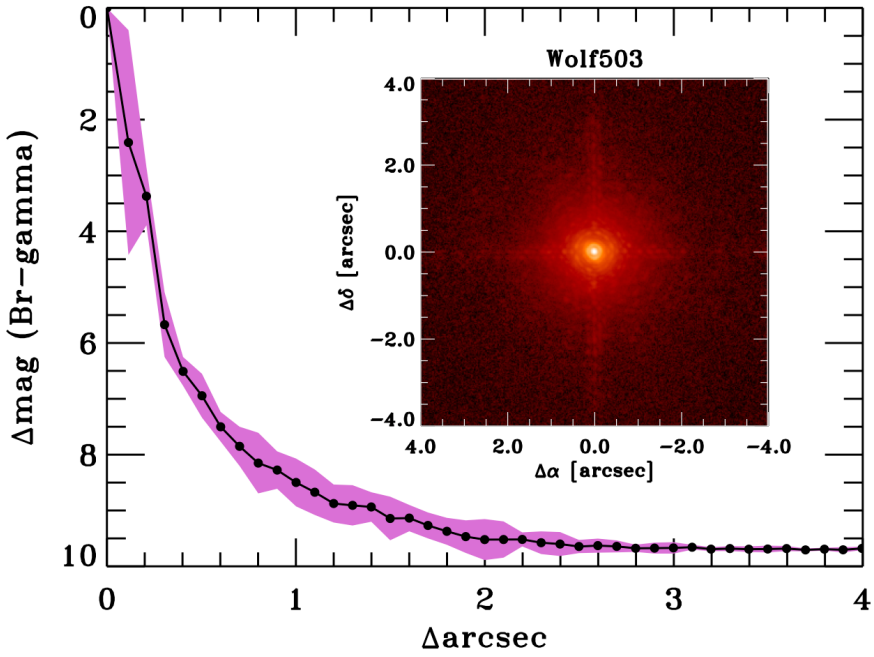

Fig. 2.4. Contrast sensitivity and inset image of Wolf 503 in Br-γ as observed with the Palomar Observatory Hale Telescope adaptive optics system, The 5σ contrast limit is plotted against angular separation in arcseconds (fill circles). The shaded region represents the dispersion in the sensitivity caused by the azimuthal structure in the image (inset).

The change in flux resulting from this drift is removed by fitting the flux as a function of position along the drift path, which is highly similar between thruster firings. However, data acquired during these thruster burns is not reliable and is masked out, as in the first transit of the light curve for Wolf 503, shown in Fig. 2.2.

With the extracted light curve, we detected a candidate at $P = 6.0$ days with $S/N = 38$ having 11 transits throughout the time of observation. The candidate was marked as a particularly intriguing KOI its favorable host star following the manual vetting procedure of the C17 candidates.

2.2. Previous work on Wolf 503

Wolf 503 (BD-05 3763, MCC 147, LHS 2799, G 64-24, HIP 67285, TYC 4973-1501-1, 2MASS J13472346-0608121) has been a sparsely studied nearby cool star since its discovery a century ago as a high proper motion star by Wolf [55]. The star subsequently appeared in several high proper motion catalogues over the past century, as Ci 20 806 in Porter et al.

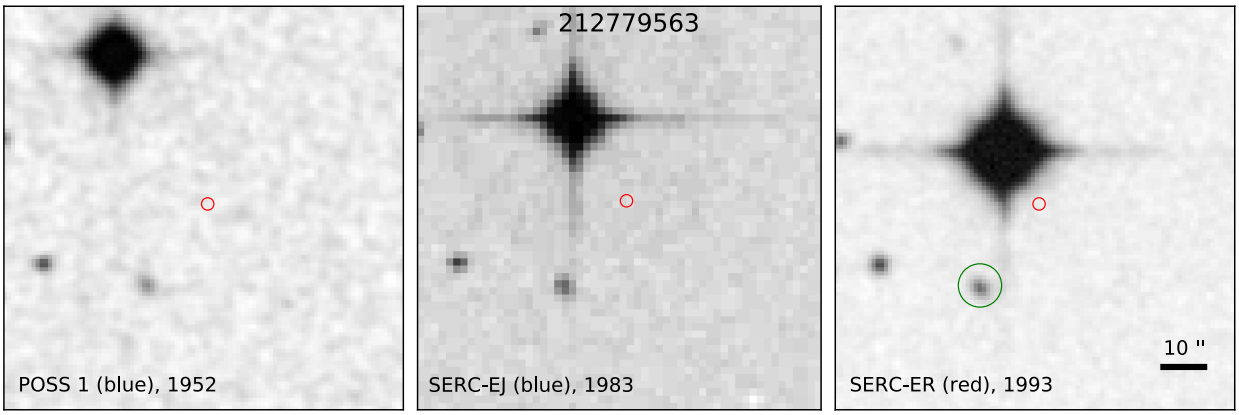

Fig. 2.5. Archival images from the blue plate of the POSS I sky survey (with a limiting magnitude of 21.0, taken May 23, 1952), from the blue SERC-EJ survey taken at the UK Schmidt Telescope (with a limiting magnitude of 23.0 taken May 7, 1983) and the red SERC-ER survey also taken at UKST (with a limiting magnitude of 22.0, taken May 27, 1993). Wolf 503's significant high proper motion is clear in the sequence of images, and there are no background sources detected at its 2018 location marked in red (R.A.=13h47h23.031s, Dec=-06d08m23.047s, calculated using the Gaia DR2 proper motion measurements). The nearest source is the faint galaxy LCRS B134447.1-055347, circled in green in the right panel, which is both 10 magnitudes fainter than Wolf 503 and found outside our extraction aperture.

[44], as G 64-24 in Giclas et al. [20], and with Wilhelm Luyten designating the star no fewer than six times in his proper motion catalogs.[1]

The star was classified in numerous spectral surveys: as a K5V by Upgren et al. [50, identified as UPG 336], and Bidelman [9] published Kuiper's posthumous classification for the star as K4 from his 1937-1944 survey. Pickles and Depagne [42] found that the best fit template for the $B_T V_T J H K_S$ photometry was that for a K4V star.

2.2.1. *Distance, Kinematics and Stellar Population*

Recently Gaia DR2 has provided an ultra-precise trigonometric parallax (ϖ = 22.430 ± 0.048 mas; corresponding to d = 44.583 ± 0.096 pc), as well as precise proper motion and radial velocity measurements, which are listed in Table 2.1. Gaia itself measured a radial velocity of -46.64 ± 0.50 km s^{-1} (2 observations), and independently, Sperauskas et al. [49] reported a radial velocity of -47.4 ± 0.7km s^{-1} based on 2 CORAVEL measurements over 98 days. Combining the Gaia DR2 position, proper motion, and parallax, and the mean Gaia DR2 ground-based radial velocity (from HARPS), we estimate a barycentric space velocity of U, V, W = -25.21, -116.86, -88.44 (±0.18, 0.21, 0.13) km s^{-1} (total velocity 148.71 ± 0.18 km s^{-1}), where U is towards the Galactic center, V is in the direction of Galactic rotation, and W is towards the north Galactic pole [41]. Using the

[1]Entry #402 in Luyten [31] (stars with motions exceeding 0″.5/yr), as LPM 492 in Luyten [32], LFT 1037 in Luyten [35], LHS 2799 in Luyten [33], and as NLTT 35228 and LTT 5351 in Luyten [34].

velocity moments and local stellar population densities from Bensby et al. [7], this UVW velocity is consistent with the following membership probabilities: $<10^{-5}$%, 81%, 19%, for the thin disk, thick disk, and halo, respectively, highly indicative of kinematic membership to the thick disc population.

Mikolaitis et al. [37] analyzed high resolution high S/N HARPS spectra and found the star to be fairly metal poor ([Fe/H] $\simeq$ -0.37 based on two pairs of [Fe I/H] and [Fe II/H] abundances). Its combination of low metallicity, supersolar [Mg I/Fe] ($\sim$0.28) and [Zn I/Fe] (0.19), and subsolar [Mn I/Fe] ($\sim$-0.16), led Mikolaitis et al. [37] to chemically classify the and chemical abundance data for Wolf 503 are consistent with membership to the thick disk. The thick disk shows a metallicity-age gradient [e.g. 8], and given Wolf 503's combination of [Fe/H] and [Mg/Fe] compared to age-dated thick disk members [23], it is likely in the age range $\sim$9-13 Gyr. Hence we adopt an age of 11 ± 2 Gyr for Wolf 503.

2.3. Spectroscopy and Stellar Parameters

We obtained an $R \approx 2000$ infrared spectrum of Wolf 503 covering the spectral range between $0.7 - 2.55\mu m$ at the NASA Infrared Telescope Facility (IRTF). We use the SpeX spectrograph in SXD mode with the 0.3" x 15" slit. The spectrum was taken UT 2018 June 03, on a partly cloudy night with an average seeing of $0.6''$. Reduction of the spectrum was performed with the *SpeXTool* [13] and *xtellcor* [51] software packages as in Dressing et al. [14]. The sky subtraction was performed using a nearby A star, HD 122749, observed immediately after Wolf 503b. The final JHK band IRTF spectra of Wolf 503 are shown in Fig. 2.3 and compared to those of spectral standards. The best visual match indicates a spectral type of K3.5V$\pm$0.5, suggesting an effective temperature of approximately $4750 \pm 100\,K$ from the SpeX spectrum.

During the vetting of candidates from C17 of $K2$ described in Crossfield et al. [12], a spectrum was also obtained from the Tillinghast Reflector Echelle Spectrograph [TRES; 16] mounted on the 1.5-m Tillinghast Reflector at Fred Lawrence Whipple Observatory on Mount Hopkins on UT 2018 May 23. TRES is a fiber-fed, cross-dispersed echelle spectrograph with a resolving power of $R\sim$44,000, a wavelength coverage of 3850–9100 Å, and radial-velocity stability of 10 to $15\,\mathrm{m\,s^{-1}}$. The spectrum was reduced and optimally extracted, and wavelength calibrated according to the procedure described in Buchhave et al. [10], and we derived stellar atmospheric parameters using the Stellar Parameter Classification code [SPC; 11]. We find $T_{\rm eff} = 4640 \pm 50\,\mathrm{K}$, $\log g = 4.68 \pm 0.10$, [Fe/H] $= -0.47 \pm 0.08$, and $v \sin i_\star = 0.8 \pm 0.5$. We note that SPC determines the stellar parameters using synthetic spectra with a fixed macroturbulence of $1\,\mathrm{km\,s^{-1}}$, which may bias $v \sin i_\star$ measurements of slow rotators like this one. Regardless, Wolf 503 has a low projected rotational velocity, as is expected for an old K dwarf, which bolsters its status as a good candidate for precise radial velocity observations. We derive a barycentric radial velocity of $-46.629 \pm 0.075\,\mathrm{km\,s^{-1}}$.

Table 2.1. Stellar Parameters

Parameter	Value	Source
Identifying Information		
α R.A. (hh:mm:ss) J2000	13:47:23.4439	
δ Dec. (dd:mm:ss) J2000	-06:08:12.731	
EPIC ID	212779563	
Photometric Properties		
B (mag).....	11.30 ± 0.01	[36]
V (mag).....	10.28 ± 0.01	[36]
G (mag).....	9.808 ± 0.001	Gaia DR1
J (mag).....	8.324 ± 0.019	2MASS
H (mag).....	7.774 ± 0.051	2MASS
K (mag).....	7.617 ± 0.023	2MASS
Spectroscopic and Derived Properties		
μ_α (mas yr^{-1})	-342.833 ± 0.073	Gaia DR2
μ_δ (mas yr^{-1})	-573.134 ± 0.073	Gaia DR2
Barycentric rv (km s$^-$1)	-46.826 ± 0.015	Gaia DR2
Distance (pc)	44.583 ± 0.096	Gaia DR2
Age (Gyr)	11 ± 2	This Paper
Spectral Type	K3.5V$\pm$0.5	This Paper
$[Fe/H]$	-0.47 ± 0.08	This Paper
log g	$4.62^{+0.02}_{-0.01}$	This Paper
$T_{\rm eff}$ (K)	4716 ± 60	This Paper
M_* ($M_\odot$)	$0.688^{+0.023}_{-0.016}$	This Paper
R_* ($R_\odot$)	$0.690^{+0.025}_{-0.024}$	This Paper
L_* ($L_\odot$)	$0.227^{+0.009}_{-0.010}$	This Paper

We conclude that the SpeX spectrum and the TRES spectrum result in consistent estimates of the stellar temperature. These values are also consistent with the value from the PASTEL catalogue of 4759 K [47] as well as Wolf 503's colors ($B-V = 1.02$, $V-K = 2.66$), leading us to adopt the K3.5V$\pm$0.5 subtype.

Finally, we adopt $T_{\rm eff} = 4716 \pm 60$ K, the average and scatter of the three spectroscopic values, as our final value for the stellar temperature. We then calculate the stellar parameters using Isoclassify [25]. Isoclassify uses measured stellar parameters in comparison to a sample of 2200 *Kepler* stars with combined Gaia and asteroseismic data in order to determine stellar parameters such as mass and radius with reliable uncertainty based on MIST models. We adopt the $\log g$ and [Fe/H] from the TRES spectrum, as well as the K magnitude, which is least affected by extinction. We determine the best stellar radius estimate using the direct method in Isoclassify [25], which uses bolometric corrections and direct physical relations to derive stellar properties, but does not return a mass. We obtain the stellar mass using the

grid mode, which places the star on stellar evolutionary tracks to determine its properties. The two modes returned consistent stellar radii. The resulting stellar parameters are listed in Table 2.1.

2.4. Target Validation

By far the most pernicious false positives detected in *K2* data are eclipsing binaries, which may closely resemble exoplanet transits at grazing incidence, or when the binary system is found in the background of a brighter star [1]. We used archival and adaptive optics images to investigate the possibility of a false positive detection due to a companion star or background sources, and find no source in the vicinity of Wolf 503 which could have contaminated our detection.

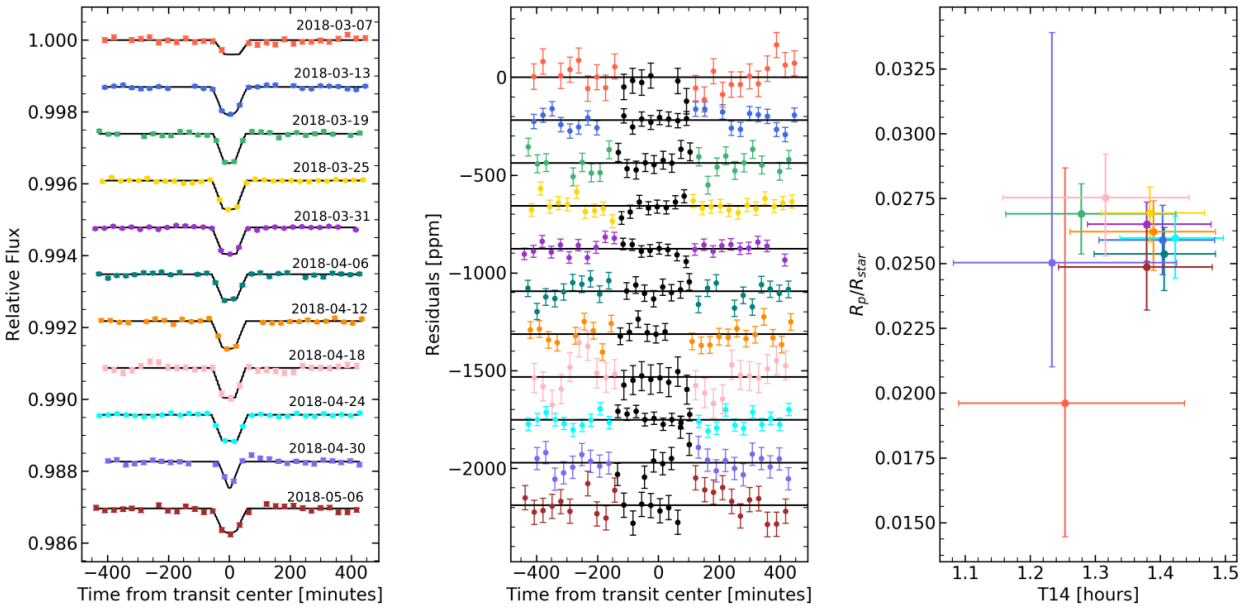

Fig. 2.6. Individual *K2* transit fits of Wolf 503b. The left panel shows each individual transit with its corresponding best fit model. The residuals are shown in the center panel, with the residuals in the range $T_0 \pm T_{14}$ marked in black. The right plot shows the best guess and 1σ, or 68% confidence limits on the R_p/R_* and T_{14} parameters, which are consistent for all transits, further support that the signal best matches that of a transiting planet. Uncertainties on the first and tenth transits (red and violet) are higher due to masked data points coinciding with a thruster burn near the time of the transit.

2.4.1. *Adaptive Optics*

Wolf 503 was observed on the night of UT 2018 June 01 UT at Palomar Observatory with the 200″ Hale Telescope using the near-infrared adaptive optics (AO) system P3K and the infrared camera PHARO [22]. PHARO has a pixel scale of 0.025″ per pixel with a full field of view of approximately 25″. The data were obtained with a narrow-band Br-γ filter

($\lambda_o = 2.18;\ \Delta_\lambda = 0.03\ \mu m$). The narrowness of the filter enables integration on the primary target without saturation, and the central wavelength of the filter is sufficiently close to the central wavelength of the 2MASS K_{short} filter ($\lambda_o = 2.15; \Delta\lambda = 0.31$) enabling the deblending of the 2MASS magnitude of the primary star based on the observed magnitude difference of any detected companions.

The AO data were obtained in a five-point quincunx dither pattern with each dither position separated by $4''$. Each dither position is observed three times, each offset from the previous image by $0.5''$ for a total of 15 frames; the integration time per frame was 4.428 s for a total of 66 s on-source integration time. We use the dithered images to remove sky background and dark current, and then align, flatfield, and stack the individual images. The final PHARO AO data have a FWHM of $0.099''$.

The sensitivities of the final combined AO image were determined by injecting simulated sources azimuthally around Wolf 503 every 45° at separations of integer multiples of the FWHM of the central source. The brightness of each injected source was scaled until standard aperture photometry detected it with 5σ significance. The resulting brightness of the injected sources relative to Wolf 503 set the contrast limits at that injection location. The average 5σ limits and associated rms dispersion caused by azimuthal asymmetries from residual speckles as a function of distance from the primary target are shown in Fig. 2.4.

The AO imaging revealed no additional stars within $0.099''$. For a system at a distance of 44.58 pc, this limits the separation of a possible binary to less than 4.4 AU.

2.4.2. *Archival Images*

Even in the absence of a nearby contaminant, adaptive optics cannot eliminate the possibility of a background source directly behind the target, which could be responsible for the signal itself, or could otherwise decrease the apparent transit depth. To address this, we exploit archival imaging from the Palomar Observatory Sky Survey I, and the SERC-EJ and SERC-ER surveys taken on the UK Schmidt telescope. Fig. 2.5 shows the present-day location of Wolf 503 in each of the 3 surveys. The blue plate from POSS I (taken May 23, 1952) and the red SERC-ER survey image (taken March 29, 1993 with the UK Schmidt Telescope) have a $1''$pixel scale, and the blue SERC-EJ image (taken May 7, 1983) has a $0''.59$ pixel scale.

The high proper motion of Wolf 503 reveals clearly that there is no background source at the star's 2018 location. The nearest object detected to Wolf 503's present-day location is the galaxy LCRS B134447.1-055347, which is located $\approx 25.1''$ from the target, placing it outside the aperture used in our extraction. Moreover, the galaxy has a Gaia magnitude of 19.6: being both 10 magnitudes fainter and outside the aperture, we find no background sources which may influence our photometry, indicating that any possible stellar contaminant must be bound within the limit of 4.4 AU given by our adaptive optics.

Table 2.2. Planet Parameters

Parameter	Units	Value
T_0	BJD_{TBD} - 2457000	$1185.36087^{+0.00053}_{-0.00038}$
P	day	$6.00118^{+0.00008}_{-0.00011}$
R_p/R_*	%	$2.694^{+0.026}_{-0.026}$
T_{14}	hr	$1.321^{+0.051}_{-0.039}$
b	-	$0.387^{+0.067}_{-0.061}$
R_p	$R_\oplus$	$2.030^{+0.076}_{-0.073}$
a	AU	0.0571 ± 0.0020
S	$S_\oplus$	69.6 ± 3
$T_{\mathrm{eq,A=0}}$	K	805 ± 9

As discussed in Sec. 2.5, the light curve is consistent either with a transiting planet or a highly specific multiple star system, and we therefore find the likelihood of a false positive due to a bound eclipsing binary companion to be extremely low.

One scenario which remains plausible is the case of a bound companion orbiting within 4.4 AU which does not transit Wolf 503, but contributes to the total flux and dilutes the planet's transit depth. According to the distribution of binary star systems found in Raghavan et al. [45], fewer than 12% of stars belong to such close systems. Additionally, Kraus et al. [28] find that binary systems with separations smaller than 50 AU are not likely to host planets, and that planets in binary systems orbiting closer than 5 AU are extremely rare, suggesting that this scenario is also not likely.

Such a companion would also induce a significant radial velocity of which there is no indication throughout measurements from Gaia, CORAVEL and our team. Each of these measurements are consistent within 2σ and differ by less than 0.8 $\mathrm{km\,s^{-1}}$. Even a 0.1 $M_\odot$ companion orbiting at 4.4 AU would induce a radial velocity of 1.6 $\mathrm{km\,s^{-1}}$, and according to the modelled mass-luminosity relations in Spada et al. [48], such a star would be roughly 4 mag dimmer in the K band and 9 mag dimmer in V and would not significantly affect the transit depth. The possibility of such a companion could conclusively be eliminated with high-resolution spectroscopy.

2.5. Light Curve Fitting

We fit the light curve of Wolf 503 using *ExoTEP*, a modular light curve analysis tool developed for the joint analysis of data from *Kepler*, *Spitzer*, and *HST*. *ExoTEP* jointly or individually fits transits and explores the parameter space using the Affine Invariant Markov Chain Monte Carlo (AI-MCMC) Ensemble sampler available through the emcee package in Python. Details can be found in Benneke et al. [4].

We performed individual transit fits in addition to fitting the transits simultaneously. For all fits, we initialize the MCMC chains with uniform priors using the best fit values from the initial detection pipeline (see Sec. 2.1), and fit the transit start time T_0, duration T_{14},

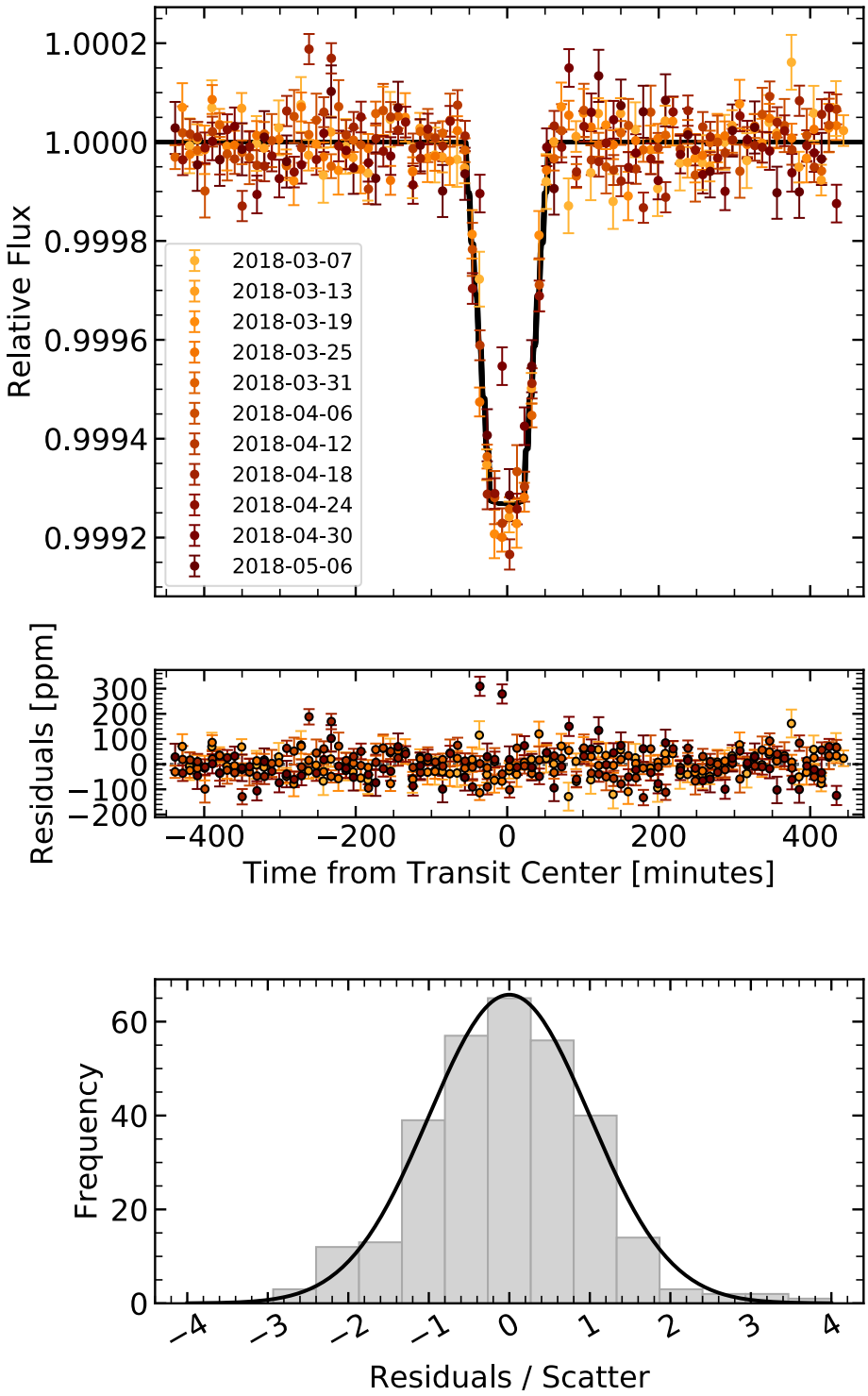

Fig. 2.7. Final light curve fit from *ExoTEP* for the combined 11 transits. In the top panel, the best fit is shown in black with the detrended light curves for each transit. Accounting for the 30 minute cadence of the *K2* data gives the best fit its trapezoidal shape. The residuals are plotted in the middle panel, and are binned in the bottom panel histogram by the number of σ from the best fit, where they follow a standard normal distribution of the same area.

depth R_p/R_*, impact parameter b, limb darkening coefficient, as well as a linear background for each transit and scatter term. For the joint fit, we also fit the period P. In each fit, we assign 6 walkers for each parameter and find good convergence after 3000 steps, taking the initial 60% as burn-in.

The transits were first fit individually, and the resulting fits are shown in Fig. 2.6. Of the 11 transits observed, all are consistent in R_p/R_* and T_{14}. We obtain our best fitting planet parameters from a joint fit of the 11 transits using the initialization as previously described. The parameters resulting from this fit are summarized in Table 2.2, where the error in R_p and a are dominated by the stellar parameters. The best fit light curve is shown in Fig. 2.7, where the combined residuals are well-behaved.

The best fit is distinctly flat-bottomed, inconsistent with the V-shaped light curves characteristic of eclipsing binaries, unless Wolf 503 were to belong to a trinary system with two smaller stars orbiting on a 12-day period, within 4.4AU, aligned to be completely eclipsing. In addition to being far more contrived than a single transiting planet, the depth and duration of the transits in Fig. 2.6 are highly regular, and show no even-odd variation which would be expected of such an eclipsing binary. As discussed in Sec. 2.4, such a companion would also induce a significant radial velocity which has not been detected and would be easily revealed using high-resolution spectroscopy.

3. Discussion

From our combined imaging, photometric and spectral analyses, we establish Wolf 503b as a $2.03^{+0.08}_{-0.07}\,R_\oplus$ planet orbiting its K3.5V$\pm$0.5 dwarf host star with a period of 6.0012 days. Wolf 503b is truly distinguished as its size places it directly at the edge of the radius gap near 1.5–2.0 $R_\oplus$, while its bright host star (H=7.77 mag, V=10.28 mag) makes it one of the best targets for radial velocity follow-up and transit spectroscopy at its size (Fig. 2.8).

Radial velocity measurements of Wolf 503b present an excellent opportunity to probe the bulk density of a planet just outside the radius gap. The amplitude of the expected RV signal depends strongly on the planet composition and amount of gas accreted. As Wolf 503b is similar in size to 55 Cnc e, though at a lower temperature, we investigate its composition using the mass-radius relationships for rocky compositions found in Valencia et al. [52] and Gillon et al. [21]. For the gas-poor scenario, the minimum mass required for a rocky composition (with no iron), is roughly $10\,M_\oplus$, with an Earth-like composition corresponding to $14\,M_\oplus$. These masses would result in RV amplitudes of roughly 4.5 and 6.3 m/s. For a volatile planet with a 0.01% H/He envelope, we would expect a mass of roughly $8\,M_\oplus$, whereas a 20% water envelope would suggest $6\,M_\oplus$, and the empirical mass-radius relation by Weiss et al. [54] would suggest $5.3\,M_\oplus$, giving RV amplitudes of 3.6, 2.7, and 2.4 m/s. These amplitudes are detectable with existing precision radial velocity spectrographs, particularly for a bright target such as Wolf 503. As the gas-rich scenario produces much

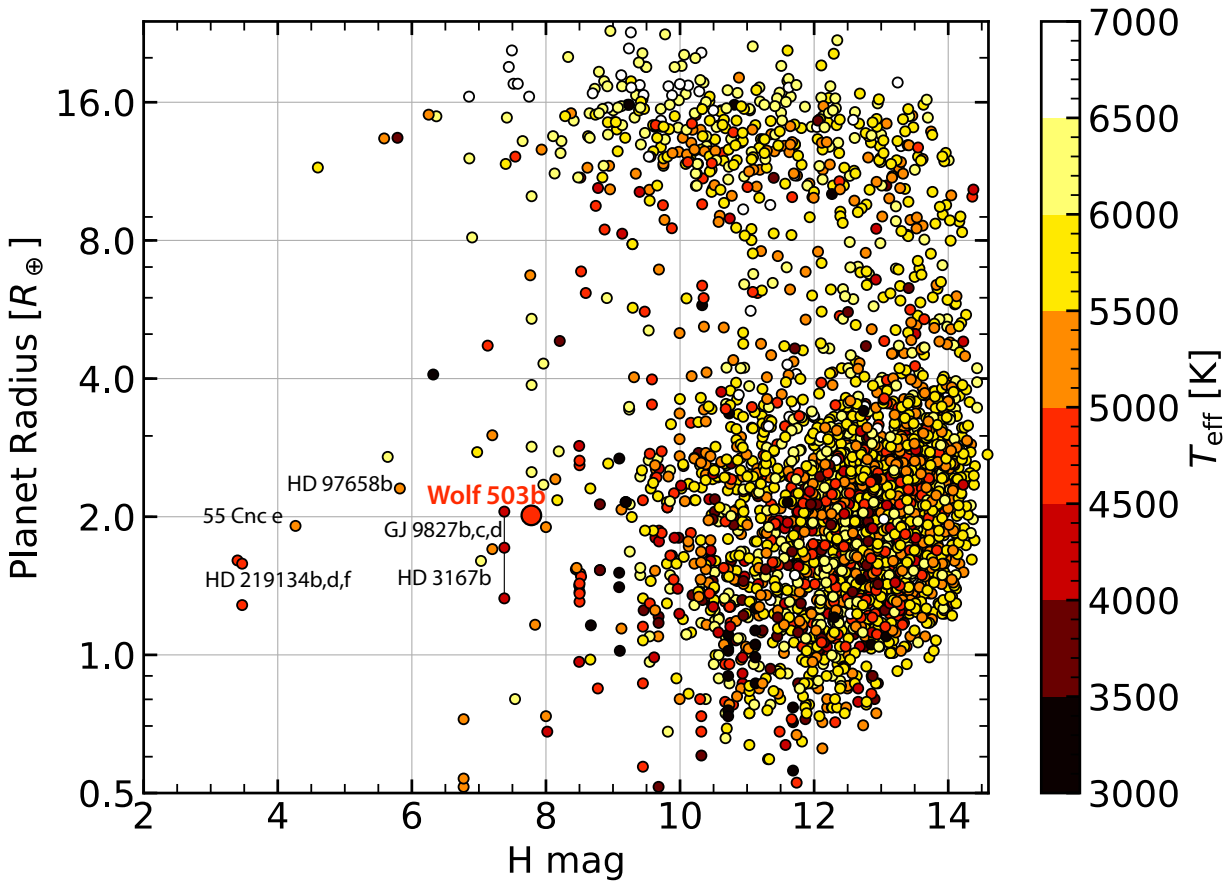

Fig. 2.8. Planet radius and stellar host magnitude of Wolf 503b (larger circle) in comparison to all planets at the NASA Exoplanet Archive (colored points). The color of the points indicates the stellar temperature. Planets in a similar size range orbiting bright stars are labeled. Wolf 503 is among the brightest systems with a planet near 2 $R_\oplus$ detected to date.

smaller RV amplitudes, these measurements will provide critical constraints on the bulk composition of the planet.

Wolf 503b is also an ideal target for detailed characterization with *HST* and *JWST*. The signal to noise for future HST transit spectroscopy was estimated in comparison to other confirmed planets near the radius gap, assuming a volatile-rich H/He envelope for each planet. Using the same estimated planet mass of $5.3M_\oplus$, Wolf 503b is expected to be the second best candidate, behind only 55 Cnc e, for studying a planet in the 1.8-2.1 $R_\oplus$ range where planets may be transitioning into the radius gap through photoevaporation. The planet is also approximately 1000K cooler than 55 Cnc e, making it much more likely to have a significant H_2 fraction in its atmosphere, but may also be in the process of photoevaporation. With $J = 8.32$ mag, it is just below the saturation levels of $J > 7$ mag and $J > 6$ mag on the *NIRISS* and *NIRSpec* grisms. If Wolf 503b indeed harbours a thick atmosphere, it is one of the best known targets to date for transmission spectroscopy at its size. Fig. 2.9 shows two

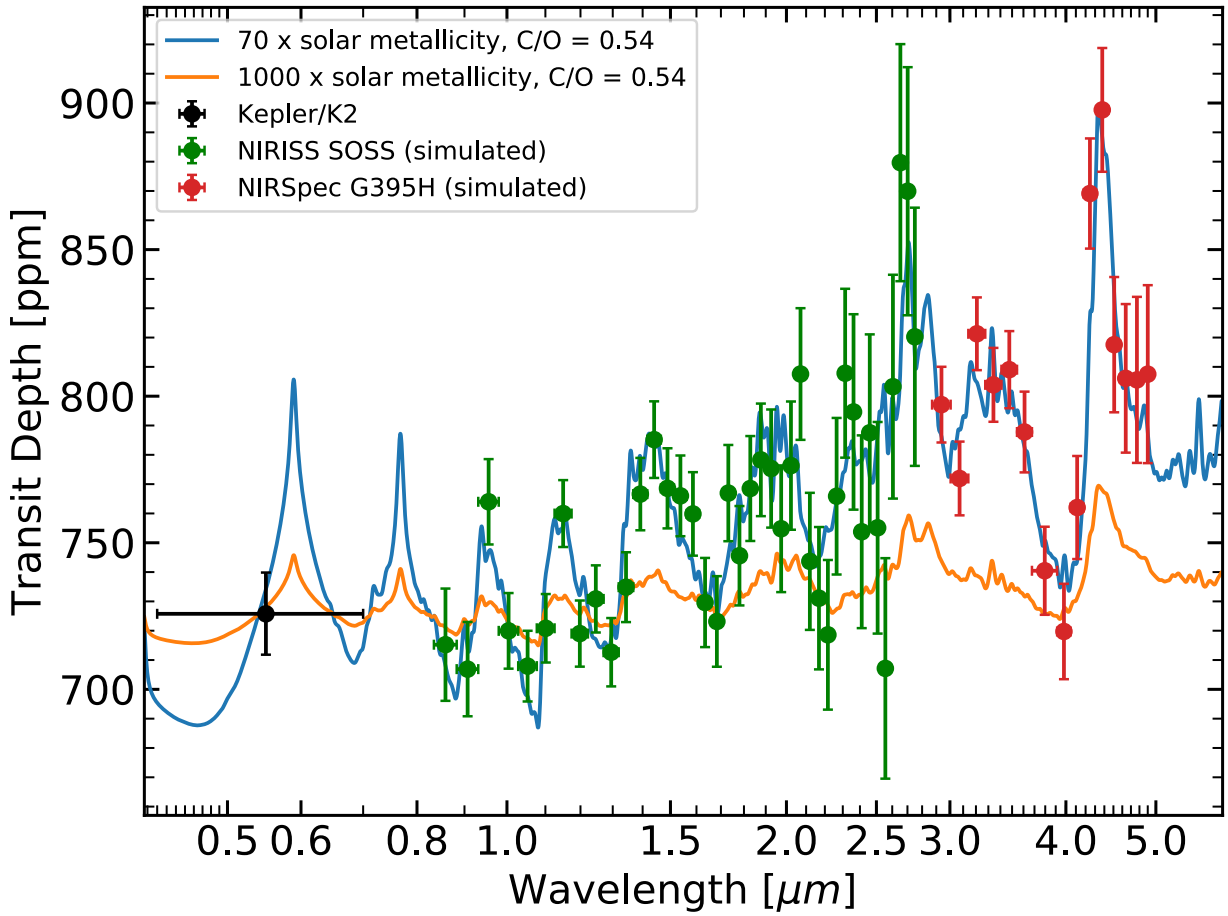

Fig. 2.9. Model transit spectra and simulated *JWST* observations for Wolf 503b. Observations of a single transit with JWST/NIRISS (green) or JWST/NIRSpec (red) could readily detect molecular absorption for hydrogen-dominated, cloud free atmospheres (blue). The planetary mass assumed in the models is $5.3\,M_{\oplus}$. Models are computed as described in Benneke and Seager [5] and Benneke [6]. Simulated observational uncertainties are from PandExo [3].

simulated transit spectra for Wolf 503b, the blue corresponding to a hydrogen-rich, Neptune-like atmosphere and the orange corresponding to an atmosphere rich in water. Simulated *NIRISS* and *NIRSpec* data for the Neptune-like atmosphere is overplotted, demonstrating the high-confidence with which we will be able to constrain the structure and abundances of atmospheric molecules on Wolf 503b.

Both radial velocity measurements and atmospheric characterization with *HST* would be valuable short-term follow-up to this work. Wolf 503b is among only a handful of planets in its size range for which this follow-up can be done efficiently today. As such, we expect Wolf 503b to play a critical role in providing near-term insights into the distribution of core masses, the envelope fraction, and the role of photoevaporation for planets near the Fulton

gap. It can also serve as an archetype for this class of small planets orbiting nearby stars in preparation for future characterization of similarly bright *TESS* systems.

4. Acknowledgments

We acknowledge support from NASA through K2GO grant 80NSSC18K0308 and from NSF through grant AST-1824644. This paper includes data collected by the Kepler mission. Funding for the Kepler mission is provided by the NASA Science Mission directorate. Some of the data presented in this paper were obtained from the Mikulski Archive for Space Telescopes (MAST). STScI is operated by the Association of Universities for Research in Astronomy, Inc., under NASA contract NAS5–26555. Support for MAST for non–HST data is provided by the NASA Office of Space Science via grant NNX13AC07G and by other grants and contracts. This research has made use of the Exoplanet Follow-up Observing Program (ExoFOP), which is operated by the California Institute of Technology, under contract with the National Aeronautics and Space Administration. Part of this research was carried out at the Jet Propulsion Laboratory, California Institute of Technology, under a contract with the National Aeronautics and Space Administration. EEM and TJD acknowledge support from the JPL Exoplanet Science Initiative. EEM acknowledges support from the NASA NExSS program.

Facilities: Kepler, K2, Palomar, IRTF, FLWO:1.5m (TRES)

References

[1] M. Abdul-Masih, A. Prša, K. Conroy, S. Bloemen, T. Boyajian, L. R. Doyle, C. Johnston, V. Kostov, D. W. Latham, G. Matijevič, A. Shporer, and J. Southworth. Kepler Eclipsing Binary Stars. VIII. Identification of False Positive Eclipsing Binaries and Re-extraction of New Light Curves. AJ, 151:101, April 2016. doi: 10.3847/0004-6256/151/4/101.

[2] N. M. Batalha, J. F. Rowe, S. T. Bryson, T. Barclay, C. J. Burke, D. A. Caldwell, J. L. Christiansen, F. Mullally, S. E. Thompson, T. M. Brown, A. K. Dupree, D. C. Fabrycky, E. B. Ford, J. J. Fortney, R. L. Gilliland, H. Isaacson, D. W. Latham, G. W. Marcy, S. N. Quinn, D. Ragozzine, A. Shporer, W. J. Borucki, D. R. Ciardi, T. N. Gautier, III, M. R. Haas, J. M. Jenkins, D. G. Koch, J. J. Lissauer, W. Rapin, G. S. Basri, A. P. Boss, L. A. Buchhave, J. A. Carter, D. Charbonneau, J. Christensen-Dalsgaard, B. D. Clarke, W. D. Cochran, B.-O. Demory, J.-M. Desert, E. Devore, L. R. Doyle, G. A. Esquerdo, M. Everett, F. Fressin, J. C. Geary, F. R. Girouard, A. Gould, J. R. Hall, M. J. Holman, A. W. Howard, S. B. Howell, K. A. Ibrahim, K. Kinemuchi, H. Kjeldsen, T. C. Klaus, J. Li, P. W. Lucas, S. Meibom, R. L. Morris, A. Prša, E. Quintana, D. T. Sanderfer, D. Sasselov, S. E. Seader, J. C. Smith, J. H. Steffen, M. Still, M. C. Stumpe, J. C. Tarter, P. Tenenbaum, G. Torres, J. D. Twicken, K. Uddin, J. Van Cleve, L. Walkowicz, and W. F. Welsh. Planetary Candidates Observed by Kepler. III. Analysis of the First 16 Months of Data. ApJS, 204:24, February 2013. doi: 10.1088/0067-0049/204/2/24.

[3] Natasha E. Batalha, Avi Mandell, Klaus Pontoppidan, Kevin B. Stevenson, Nikole K. Lewis, Jason Kalirai, Nick Earl, Thomas Greene, Loïc Albert, and Louise D. Nielsen. PandExo: A Community Tool for Transiting Exoplanet Science with JWST & HST. *PASP*, 129(976):064501, 2017. ISSN 1538-3873. doi: 10.1088/1538-3873/aa65b0.

[4] B. Benneke, M. Werner, E. Petigura, H. Knutson, C. Dressing, I. J. M. Crossfield, J. E. Schlieder, J. Livingston, C. Beichman, J. Christiansen, J. Krick, V. Gorjian, A. W. Howard, E. Sinukoff, D. R. Ciardi, and R. L. Akeson. Spitzer Observations Confirm and Rescue the Habitable-zone Super-Earth K2-18b for Future Characterization. ApJ, 834:187, January 2017. doi: 10.3847/1538-4357/834/2/187.

[5] Bjoern Benneke and Sara Seager. Atmospheric Retrieval for Super-Earths: Uniquely Constraining the Atmospheric Composition with Transmission Spectroscopy. *The Astrophysical Journal*, 753(2):100, July 2012. ISSN 0004-637X, 1538-4357. doi: 10.1088/0004-637X/753/2/100.

[6] Björn Benneke. Strict Upper Limits on the Carbon-to-Oxygen Ratios of Eight Hot Jupiters from Self-Consistent Atmospheric Retrieval. *arXiv:1504.07655 [astro-ph]*, April 2015. arXiv: 1504.07655.

[7] T. Bensby, S. Feltzing, and I. Lundström. Elemental abundance trends in the Galactic thin and thick disks as traced by nearby F and G dwarf stars. A&A, 410:527–551, November 2003. doi: 10.1051/0004-6361:20031213.

[8] T. Bensby, S. Feltzing, and I. Lundström. A possible age-metallicity relation in the Galactic thick disk? A&A, 421:969–976, July 2004. doi: 10.1051/0004-6361:20035957.

[9] W. P. Bidelman. G. P. Kuiper's spectral classifications of proper-motion stars. ApJS, 59:197–227, October 1985. doi: 10.1086/191069.

[10] L. A. Buchhave, G. Á. Bakos, J. D. Hartman, G. Torres, G. Kovács, D. W. Latham, R. W. Noyes, G. A. Esquerdo, M. Everett, A. W. Howard, G. W. Marcy, D. A. Fischer, J. A. Johnson, J. Andersen, G. Fűrész, G. Perumpilly, D. D. Sasselov, R. P. Stefanik, B. Béky, J. Lázár, I. Papp, and P. Sári. HAT-P-16b: A 4 M $_J$ Planet Transiting a Bright Star on an Eccentric Orbit. ApJ, 720:1118–1125, September 2010. doi: 10.1088/0004-637X/720/2/1118.

[11] L. A. Buchhave, D. W. Latham, A. Johansen, M. Bizzarro, G. Torres, J. F. Rowe, N. M. Batalha, W. J. Borucki, E. Brugamyer, C. Caldwell, S. T. Bryson, D. R. Ciardi, W. D. Cochran, M. Endl, G. A. Esquerdo, E. B. Ford, J. C. Geary, R. L. Gilliland, T. Hansen, H. Isaacson, J. B. Laird, P. W. Lucas, G. W. Marcy, J. A. Morse, P. Robertson, A. Shporer, R. P. Stefanik, M. Still, and S. N. Quinn. An abundance of small exoplanets around stars with a wide range of metallicities. Nature, 486:375–377, June 2012. doi: 10.1038/nature11121.

[12] I. J. M. Crossfield, N. Guerrero, T. David, S. N. Quinn, A. D. Feinstein, C. Huang, L. Yu, K. A. Collins, B. J. Fulton, B. Benneke, M. Peterson, A. Bieryla, J. E. Schlieder, M. R. Kosiarek, M. Bristow, E. Newton, M. Bedell, D. W. Latham, J. L. Christiansen, G. A. Esquerdo, P. Berlind, M. L. Calkins, A. Shporer, J. Burt, S. Ballard, J. E. Rodriguez, N. Mehrle, S. Seager, J. Dittmann, D. Berardo, L. Sha, Z. Essack, Z. Zhan, M. Owens, I. Kain, J. H. Livingston, E. A. Petigura, C. D. Dressing, E. J. Gonzales, H. Isaacson, and A. W. Howard. A TESS Dress Rehearsal: Planetary Candidates and Variables from K2 Campaign 17. *ArXiv e-prints*, June 2018.

[13] M. C. Cushing, J. T. Rayner, and W. D. Vacca. An Infrared Spectroscopic Sequence of M, L, and T Dwarfs. ApJ, 623:1115–1140, April 2005. doi: 10.1086/428040.

[14] C. D. Dressing, A. Vanderburg, J. E. Schlieder, I. J. M. Crossfield, H. A. Knutson, E. R. Newton, D. R. Ciardi, B. J. Fulton, E. J. Gonzales, A. W. Howard, H. Isaacson, J. Livingston, E. A. Petigura, E. Sinukoff, M. Everett, E. Horch, and S. B. Howell. Characterizing K2 Candidate Planetary Systems Orbiting Low-mass Stars. II. Planetary Systems Observed During Campaigns 1–7. AJ, 154:207, November 2017. doi: 10.3847/1538-3881/aa89f2.

[15] X. Dumusque, A. S. Bonomo, R. D. Haywood, L. Malavolta, D. Ségransan, L. A. Buchhave, A. Collier Cameron, D. W. Latham, E. Molinari, F. Pepe, S. Udry, D. Charbonneau, R. Cosentino, C. D. Dressing, P. Figueira, A. F. M. Fiorenzano, S. Gettel, A. Harutyunyan, K. Horne, M. Lopez-Morales, C. Lovis, M. Mayor, G. Micela, F. Motalebi, V. Nascimbeni, D. F. Phillips, G. Piotto, D. Pollacco, D. Queloz, K. Rice, D. Sasselov, A. Sozzetti, A. Szentgyorgyi, and C. Watson. The Kepler-10 Planetary System Revisited by HARPS-N: A Hot Rocky World and a Solid Neptune-Mass Planet. ApJ, 789:154, July 2014. doi: 10.1088/0004-637X/789/2/154.

[16] G. Fűrész. "tres". *PhD thesis, University of Szeged, Hungary*, 2008.

[17] F. Fressin, G. Torres, D. Charbonneau, S. T. Bryson, J. Christiansen, C. D. Dressing, J. M. Jenkins, L. M. Walkowicz, and N. M. Batalha. The False Positive Rate of Kepler and the Occurrence of Planets. ApJ, 766:81, April 2013. doi: 10.1088/0004-637X/766/2/81.

[18] B. J. Fulton and E. A. Petigura. The California Kepler Survey VII. Precise Planet Radii Leveraging Gaia DR2 Reveal the Stellar Mass Dependence of the Planet Radius Gap. *ArXiv e-prints*, May 2018.

[23] B. J. Fulton, E. A. Petigura, A. W. Howard, H. Isaacson, G. W. Marcy, P. A. Cargile, L. Hebb, L. M. Weiss, J. A. Johnson, T. D. Morton, E. Sinukoff, I. J. M. Crossfield, and L. A. Hirsch. The California-Kepler Survey. III. A Gap in the Radius Distribution of Small Planets. AJ, 154:109, September 2017. doi: 10.3847/1538-3881/aa80eb.

[20] H. L. Giclas, R. Burnham, and N. G. Thomas. Lowell proper motions III : proper motion survey of the Northern Hemisphere with the 13-inch photographic telescope of the Lowell Observatory. *Lowell Observatory Bulletin*, 5:61–132, 1961.

[21] M. Gillon, B.-O. Demory, B. Benneke, D. Valencia, D. Deming, S. Seager, C. Lovis, M. Mayor, F. Pepe, D. Queloz, D. Ségransan, and S. Udry. Improved precision on the radius of the nearby super-Earth 55 Cnc e. A&A, 539:A28, March 2012. doi: 10.1051/0004-6361/201118309.

[22] T. L. Hayward, B. Brandl, B. Pirger, C. Blacken, G. E. Gull, J. Schoenwald, and J. R. Houck. PHARO: A Near-Infrared Camera for the Palomar Adaptive Optics System. PASP, 113:105–118, January 2001. doi: 10.1086/317969.

[23] M. Haywood, P. Di Matteo, M. D. Lehnert, D. Katz, and A. Gómez. The age structure of stellar populations in the solar vicinity. Clues of a two-phase formation history of the Milky Way disk. A&A, 560:A109, December 2013. doi: 10.1051/0004-6361/201321397.

[24] A. W. Howard. Observed Properties of Extrasolar Planets. *Science*, 340:572–576, May 2013. doi: 10.1126/science.1233545.

[25] Daniel Huber, Joel Zinn, Mathias Bojsen-Hansen, Marc Pinsonneault, Christian Sahlholdt, Aldo Serenelli, Victor Silva Aguirre, Keivan Stassun, Dennis Stello, Jamie Tayar, Fabienne Bastien, Timothy R. Bedding, Lars A. Buchhave, William J. Chaplin,

Guy R. Davies, Rafael A. García, David W. Latham, Savita Mathur, Benoit Mosser, and Sanjib Sharma. Asteroseismology and Gaia: Testing Scaling Relations Using 2200 Kepler Stars with TGAS Parallaxes. *The Astrophysical Journal*, 844:102, August 2017. ISSN 0004-637X. doi: 10.3847/1538-4357/aa75ca.

[26] S. Ida and D. N. C. Lin. Toward a Deterministic Model of Planetary Formation. I. A Desert in the Mass and Semimajor Axis Distributions of Extrasolar Planets. ApJ, 604: 388–413, March 2004. doi: 10.1086/381724.

[27] S. Jin and C. Mordasini. Compositional Imprints in Density–Distance–Time: A Rocky Composition for Close-in Low-mass Exoplanets from the Location of the Valley of Evaporation. ApJ, 853:163, February 2018. doi: 10.3847/1538-4357/aa9f1e.

[28] A. L. Kraus, M. J. Ireland, D. Huber, A. W. Mann, and T. J. Dupuy. The Impact of Stellar Multiplicity on Planetary Systems. I. The Ruinous Influence of Close Binary Companions. AJ, 152:8, July 2016. doi: 10.3847/0004-6256/152/1/8.

[29] E. J. Lee, E. Chiang, and C. W. Ormel. Make Super-Earths, Not Jupiters: Accreting Nebular Gas onto Solid Cores at 0.1 AU and Beyond. ApJ, 797:95, December 2014. doi: 10.1088/0004-637X/797/2/95.

[30] E. D. Lopez and K. Rice. Predictions for the Period Dependence of the Transition Between Rocky Super-Earths and Gaseous Sub-Neptunes and Implications for eta Earth. *ArXiv e-prints*, October 2016.

[31] W. J. Luyten. Bulletin Number 344 - A study of stars with large proper motions. *Lick Observatory Bulletin*, 11:1–32, 1923. doi: 10.5479/ADS/bib/1923LicOB.11.1L.

[32] W. J. Luyten. Bruce proper motion survey. *Publications of the Astronomical Observatory University of Minnesota*, 3:1–22, 1941.

[33] W. J. Luyten. *LHS catalogue. A catalogue of stars with proper motions exceeding 0“5 annually*. University of Minnesota, 1979.

[34] W. J. Luyten. *NLTT Catalogue. Volume_III. 0___to -30_*. University of Minnesota, 1980.

[35] W. J. Luyten. VizieR Online Data Catalog: LFT Catalogue (Luyten, 1955). *VizieR Online Data Catalog*, 1054, February 1995.

[36] J. C. Mermilliod. UBV Photoelectric Photometry Catalogue (1986). III Errors and Problems on DM and HD Stars. *Bulletin d'Information du Centre de Donnees Stellaires*, 32:37, May 1987.

[37] Š. Mikolaitis, P. de Laverny, A. Recio-Blanco, V. Hill, C. C. Worley, and M. de Pascale. The AMBRE project: Iron-peak elements in the solar neighbourhood. A&A, 600:A22, April 2017. doi: 10.1051/0004-6361/201629629.

[38] C. Mordasini, Y. Alibert, and W. Benz. Extrasolar planet population synthesis. I. Method, formation tracks, and mass-distance distribution. A&A, 501:1139–1160, July 2009. doi: 10.1051/0004-6361/200810301.

[39] F. Mullally, J. L. Coughlin, S. E. Thompson, J. Rowe, C. Burke, D. W. Latham, N. M. Batalha, S. T. Bryson, J. Christiansen, C. E. Henze, A. Ofir, B. Quarles, A. Shporer, V. Van Eylen, C. Van Laerhoven, Y. Shah, A. Wolfgang, W. J. Chaplin, J.-W. Xie, R. Akeson, V. Argabright, E. Bachtell, T. Barclay, W. J. Borucki, D. A. Caldwell, J. R. Campbell, J. H. Catanzarite, W. D. Cochran, R. M. Duren, S. W. Fleming, D. Fraquelli, F. R. Girouard, M. R. Haas, K. G. Hełminiak, S. B. Howell, D. Huber, K. Larson, T. N. Gautier, III, J. M. Jenkins, J. Li, J. J. Lissauer, S. McArthur, C. Miller, R. L. Morris, A. Patil-Sabale, P. Plavchan, D. Putnam, E. V. Quintana, S. Ramirez, V. Silva Aguirre, S. Seader, J. C. Smith, J. H. Steffen, C. Stewart, J. Stober, M. Still, P. Tenenbaum, J. Troeltzsch, J. D. Twicken, and K. A. Zamudio. Planetary Candidates Observed by Kepler. VI. Planet Sample from Q1–Q16 (47 Months). ApJS, 217:31, April 2015. doi: 10.1088/0067-0049/217/2/31.

[40] J. E. Owen and Y. Wu. Kepler Planets: A Tale of Evaporation. ApJ, 775:105, October 2013. doi: 10.1088/0004-637X/775/2/105.

[41] M. A. C. Perryman, L. Lindegren, J. Kovalevsky, E. Hoeg, U. Bastian, P. L. Bernacca, M. Crézé, F. Donati, M. Grenon, M. Grewing, F. van Leeuwen, H. van der Marel, F. Mignard, C. A. Murray, R. S. Le Poole, H. Schrijver, C. Turon, F. Arenou, M. Froeschlé, and C. S. Petersen. The HIPPARCOS Catalogue. A&A, 323:L49–L52, July 1997.

[42] A. Pickles and É. Depagne. All-Sky Spectrally Matched UBVRI - ZY and u' g' r' i' z' Magnitudes for Stars in the Tycho2 Catalog. PASP, 122:1437, December 2010. doi: 10.1086/657947.

[43] James B. Pollack, Olenka Hubickyj, Peter Bodenheimer, Jack J. Lissauer, Morris Podolak, and Yuval Greenzweig. Formation of the giant planets by concurrent accretion of solids and gas. *Icarus*, 124(1):62 – 85, 1996. ISSN 0019-1035. doi: https://doi.org/10.1006/icar.1996.0190. URL `http://www.sciencedirect.com/science/article/pii/S0019103596901906`.

[44] J. G. Porter, E. J. Yowell, and E. S. Smith. A catalogue of 1474 stars with proper motion exceeding four-tenths year. *Publications of the Cincinnati Observatory*, 20:1–32, 1930.

[45] D. Raghavan, H. A. McAlister, T. J. Henry, D. W. Latham, G. W. Marcy, B. D. Mason, D. R. Gies, R. J. White, and T. A. ten Brummelaar. A Survey of Stellar Families: Multiplicity of Solar-type Stars. ApJS, 190:1–42, September 2010. doi: 10.1088/0067-0049/190/1/1.

[46] L. A. Rogers. Most 1.6 Earth-radius Planets are Not Rocky. ApJ, 801:41, March 2015. doi: 10.1088/0004-637X/801/1/41.

[47] C. Soubiran, J.-F. Le Campion, G. Cayrel de Strobel, and A. Caillo. The PASTEL catalogue of stellar parameters. *A&A*, 515:A111, June 2010. ISSN 0004-6361, 1432-0746. doi: 10.1051/0004-6361/201014247.

[48] F. Spada, P. Demarque, Y. C. Kim, and A. Sills. The radius discrepancy in low-mass stars: Single versus binaries. *The Astrophysical Journal*, 776(2):87, 2013. URL `http://stacks.iop.org/0004-637X/776/i=2/a=87`.

[49] J. Sperauskas, L. Začs, W. J. Schuster, and V. Deveikis. The Binary Nature of CH-Like Stars. ApJ, 826:85, July 2016. doi: 10.3847/0004-637X/826/1/85.

[50] A. R. Upgren, R. Grossenbacher, W. S. Penhallow, D. J. MacConnell, and R. L. Frye. Dwarf K and M stars in the southern hemisphere. AJ, 77:486–499, August 1972. doi: 10.1086/111308.

[51] W. D. Vacca, M. C. Cushing, and J. T. Rayner. A Method of Correcting Near-Infrared Spectra for Telluric Absorption. PASP, 115:389–409, March 2003. doi: 10.1086/346193.

[52] D. Valencia, M. Ikoma, T. Guillot, and N. Nettelmann. Composition and fate of short-period super-Earths - The case of CoRoT-7b. *Astronomy and Astrophysics*, 516:11, 2010. doi: 10.1051/0004-6361/200912839.

[53] L. M. Weiss and G. W. Marcy. The Mass-Radius Relation for 65 Exoplanets Smaller than 4 Earth Radii. ApJ, 783:L6, March 2014. doi: 10.1088/2041-8205/783/1/L6.

[54] Lauren M. Weiss, Geoffrey W. Marcy, Jason F. Rowe, Andrew W. Howard, Howard Isaacson, Jonathan J. Fortney, Neil Miller, Brice-Olivier Demory, Debra A. Fischer, Elisabeth R. Adams, Andrea K. Dupree, Steve B. Howell, Rea Kolbl, John Asher Johnson, Elliott P. Horch, Mark E. Everett, Daniel C. Fabrycky, and Sara Seager. THE MASS OF KOI-94d AND A RELATION FOR PLANET RADIUS, MASS, AND INCIDENT FLUXBased in part on observations obtained at the W. M. Keck Observatory, which is operated by the University of California and the California Institute of Technology. *ApJ*, 768(1):14, April 2013. ISSN 0004-637X. doi: 10.1088/0004-637X/768/1/14.

[55] M. Wolf. Katalog von 1053 staerker bewegten Fixsternen. *Veroeffentlichungen der Badischen Sternwarte zu Heidelberg*, 7, 1919.

Second Article.

A temperate Earth-sized planet with strongly tidally-heated interior transiting the M6 dwarf LP 791-18

by

Merrin Peterson[1], Björn Benneke[1], Karen Collins[2], Ian J. M. Crossfield[3], Caroline Piaulet[1], Mohamad Ali-Dib[1], Jessie L. Christiansen[4], Jonathan Gagné[5], Jackie Faherty[6], Courtney Dressing[7], David Charbonneau[2], Felipe Murgas[8], Marion Cointepas[9], Jose Manuel Almenara[9], Xavier Bonfils[9], Stephen Kane[10], Michael W Werner[11], Varoujan Gorjian[11], Avi Shporer[12], Francisco J. Pozuelos Romero[13], Quentin Jay Socia[14], Ryan Cloutier[2,15], Jeremy Dietrich[2], Jonathan Irwin[2], Lauren Weiss[16], William Waalkes[17], Zach Berta-Thomson[17], Thomas Evans[12], Daniel Apai[14,18], Hannu Parviainen[8], Enric Pallé[8], Norio Narita[19], Andrew W. Howard[20], Diana Dragomir[21], Khalid Barkaoui[22], Micheal Gillon[23], Emmanuel Jehin[24], George Ricker[12], David W. Latham[2], Joshua N. Winn[25], Sara Seager[12,26,27], Howard Isaacson[7], Alex Bixel[14], Aidan Gibbs[28], Jon M. Jenkins[29], Jeffrey C. Smith[30], Jose Perez Chavez[31], Benjamin V. Rackham[12], Thomas Henning[32], Paul Gabor[33], Wen-Ping Chen[34], Nestor Espinoza[35], Eric L. N. Jensen[36], Kevin I. Collins[37], Richard P. Schwarz[38], Dennis M. Conti[39], Gavin Wang[40], John F. Kielkopf[41], Shude Mao[42], Keith Horne[43], Ramotholo Sefako[44], Samuel N. Quinn[2], Dan Moldovan[45], Michael Fausnaugh[12], Gábor Fűűrész[12], and Thomas Barclay[46,47]

([1]) Department of Physics and Institute for Research on Exoplanets, Université de Montréal, Montreal, QC, Canada

([2]) Center for Astrophysics | Harvard & Smithsonian, 60 Garden St., Cambridge, MA 02138, USA

([3]) Department of Physics and Astronomy, University of Kansas, Lawrence, KS, USA

([4]) Caltech/IPAC-NASA Exoplanet Science Institute, 770 S. Wilson Ave, Pasadena, CA 91106, USA

([5]) Planétarium Rio Tinto Alcan and Institute for Research on Exoplanets, Université de Montréal, Montreal, QC, Canada

([6]) American Museum for National History, New York, NY, USA

([7]) Department of Astronomy, University of California - Berkeley, Berkeley, CA, 94720, USA

([8]) Instituto de Astrofisica de Canarias. Via Lactea s/n 38200, La Laguna. Canary Islands. Spain.

([9]) Institut de Planétologie et d'Astrophysique de Grenoble, Grenoble, France

([10]) Department of Earth and Planetary Sciences, University of California, Riverside, CA 92521, USA

([11]) Jet Propulsion Laboratory, California Institute of Technology, 4800 Oak Grove Drive, Pasadena, CA 91109, USA

([12]) Department of Physics and Kavli Institute of Astronomy, Massachusetts Institute of Technology, Cambridge, MA, 02139, USA

([13]) Origenes Cosmologiques et Astrophysiques, University of Liège, Belgium

([14]) Steward Observatory, 933 N Cherry Avenue, Tucson, AZ 85721, USA

([15]) Banting Fellow

([16]) University of Hawaii, Honolulu, Hawaii, USA

([17]) Department of Astrophysical and Planetary Sciences, University of Colorado, Boulder, CO, USA

([18]) Department of Astronomy, The University of Arizona, 933 N. Cherry Avenue, Tucson, AZ 85721, USA

([19]) The University of Tokyo, Tokyo, Japan

([20]) Department of Astronomy, California Institute of Technology, Pasadena, CA 91125, USA

([21]) Department of Physics and Astronomy, University of New Mexico, Albuquerque, NM, USA

([22]) Oukaimeden Observatory, High Energy Physics and Astrophysics Laboratory, Cadi Ayyad University, Marrakech, Morocco

([23]) Astrobiology Research Unit, Université de Liège, 19C Allée du 6 Août, 4000 Liège, Belgium

([24]) Space Sciences, Technologies and Astrophysics Research (STAR), Institute, Université de Liège, 19C Allée du 6 Août, 4000 Liège, Belgium

([25]) Department of Astrophysical Sciences, Princeton University, 4 Ivy Ln, Princeton, NJ 08544, USA

([26]) Department of Earth, Atmospheric and Planetary Sciences, Massachusetts Institute of Technology, Cambridge, MA 02139, USA

([27]) Department of Aeronautics and Astronautics, MIT, 77 Massachusetts Avenue, Cambridge, MA 02139, USA

([28]) Department of Astronomy, University of California - Los Angeles, Los Angeles, CA, 90095, USA

([29]) NASA Ames Research Center, Mountain View, CA 94043, USA

([30]) The SETI Institute, 189 Bernardo Ave., Suite 200, Mountain View, CA 94043, USA

([31]) Texas State University, Department of Physics, 601 University Drive, San Marcos, TX 78666, USA

([32]) Max-Planck-Institut für Astronomie, Königstuhl 17, Heidelberg 69117, Germany
([33]) Vatican Observatory Research Group, University of Arizona, 933 N Cherry Avenue, Tucson AZ, 85721-0065, USA
([34]) Graduate Institute of Space Science, National Central University, Taoyuan 32001, Taiwan
([35]) Space Telescope Science Institute, 3700 San Martin Drive, Baltimore, MD 21218, USA
([36]) Department of Physics & Astronomy, Swarthmore College, Swarthmore PA 19081, USA
([37]) George Mason University, 4400 University Drive, Fairfax, VA, 22030 USA
([38]) Patashnick Voorheesville Observatory, Voorheesville, NY 12186, USA
([39]) American Association of Variable Star Observers, 49 Bay State Road, Cambridge, MA 02138, USA
([40]) Tsinghua International School, Beijing 100084, China
([41]) Department of Physics and Astronomy, University of Louisville, Louisville, KY 40292, USA
([42]) National Astronomical Observatories of China, Chinese Academy of Sciences, 20A Datun Road, Beijing, China
([43]) SUPA Physics and Astronomy, University of St. Andrews, Fife, KY16 9SS Scotland, UK
([44]) South African Astronomical Observatory, P.O. Box 9, Observatory, Cape Town 7935, South Africa
([45]) Google LLC, 1600 Amphitheatre Parkway, Mountain View, CA 94043, USA
([46]) NASA Goddard Space Flight Center, 8800 Greenbelt Road, Greenbelt, MD 20771, USA
([47]) University of Maryland, Baltimore County, 1000 Hilltop Circle, Baltimore, MD 21250, USA

This article was submitted to *Nature*.

The main contributions of Merrin Peterson for this article are presented.

- *Spitzer* lightcurve analysis and fitting
- TTV analysis
- Wrote the initial drafts of the paper, which were edited, finalized and submitted by Björn Benneke

ABSTRACT. One main objective of modern astronomy is to identify and characterize temperate Earth-sized exoplanets in order to better understand how the Earth became habitable and whether other planets can develop similarly hospitable conditions. Earth-sized planets around nearby late-type M dwarfs are key in this endeavor [28] because their atmospheres can give rise to detectable transit depth variations even for N_2 and CO_2 atmospheres with their relatively small scale heights. Yet, despite large efforts to search for terrestrial planets orbiting late-type M stars [27], the only low-temperature Earth-sized planets known to orbit late M stars beyond M5 have been the planets in the TRAPPIST-1 system. Here we report the detection of a temperate Earth-sized planet orbiting the cool M6 dwarf LP 791-18. The newly discovered planet, LP 791-18 d, has a radius consistent with that of Earth ($\mathbf{1.03 \pm 0.04\,R_\oplus}$) and an approximate equilibrium temperature of 300–400 K, with the permanent night-side plausibly allowing for water condensation [64]. LP 791-18d is part of a co-planar system with at least two other planets [11], the outermost being a sub-Neptune and providing a to-date unique opportunity to investigate a system with a temperate Earth-sized planet and a sub-Neptune that retained its gas or volatile envelope. Based on observations of transit timing variations, we find a mass of $\mathbf{9.7^{+1.3}_{-1.2}\,M_\oplus}$ for the sub-Neptune LP 791-18c and a mass of $\mathbf{0.9^{+0.5}_{-0.4}\,M_\oplus}$ for the exo-Earth LP 791-18d ($< \mathbf{2.3}\ \mathbf{M_\oplus}$ at 3σ). Intriguingly, the dynamical interactions with the sub-Neptune prevent the complete circularization of LP 791-18d's orbit, resulting in strong continued tidal heating of LP 791-18d's interior similar in magnitude to that of Jupiter's moon Io, the most geologically active body in the solar system [58, 62]. Looking forward, LP 791-18d being a likely highly geologically active Earth-sized planet at the edge of the habitable zone of a late M-dwarf in a system with a sub-Neptune offers multiple unprecedented opportunities for spectroscopic follow-up studies to advance our understanding of Earth-sized planets, including their interiors, volcanic outgassing, and atmospheric retention, as well as the origin of the small-planet radius valley.
Keywords: methods: observational — planets and satellites: atmospheres — planets and satellites: individual (LP 791-18d) — planets and satellites: physical evolution — planets and satellites: terrestrial planets

LP 791-18d was detected through 124 hours of near-continuous *Spitzer* observations of LP 791-18, the third-smallest star known to host planets and the second-smallest star to host transiting planets. LP 791-18 (TOI-736) was previously known to host the hot super-Earth LP 791-18b on a 0.94-day orbit and the sub-Neptune LP 791-18c on a 4.99-day orbit, both discovered in June 2019 by the Transiting Exoplanet Survey Satellite (TESS) [11], but both without radial-velocity confirmation or mass measurements. Thanks to the exceptionally small host star, however, both planets have the potential to be promising targets for transmission spectroscopy with JWST, and the sub-Neptune LP 791-18c is already approved for JWST Guaranteed Time Observations.

Our *Spitzer* observations were undertaken to investigate the possibility of additional terrestrial planets in the system because such planets could be dynamically stable, but could have been missed by TESS. Due to the faintness of LP 791-18 at visible wavelengths, the TESS light-curve lacked the necessary photometric precision to detect planets with radii smaller than approximately 1.2 $R_\oplus$ at periods longer than about 1.5 days. *Spitzer* observed

at 4.5 μm nearly continuously from October 14, 2019 to October 19, 2019, except for a five-hour break for data downlink starting October 17 at 23:30. The observations were timed to also capture two transits of planet c, with at least 2 hours of baseline observations before the first transit and following the second transit.

We extracted the raw photometry using a fixed circular aperture and removed systematics using pixel-level decorrelation [15, 4] (Fig. 3.1). In addition to the known planets, two transits of the previously unknown LP 791-18d are visible in the *Spitzer* light curve. We subsequently confirmed LP 791-18d's ephemeris using ground-based telescopes and discovered that the new planet d opens the system to mass measurements through TTVs. We therefore complemented our *Spitzer* observations of this system with a large, targeted multi-telescope transit campaign using the LCO telescope network, MuSCAT2 [46], MEarth [47, 7], TRAPPIST-N/S [25], ExTrA [8], SPECULOOS [44], and the VATT and Kuiper telescopes of the EDEN network [24]. In total, we observed 67 transits between June 2019 and February 2021 including 42 transits of the Earth-sized planet LP 791-18d (Extended Data Table 3.1, Extended Data Fig. 3.1 and 3.2) and 25 transits of sub-Neptune LP 791-18c (Extended Data Table 3.2, Extended Data Fig. 3.3–3.4). Given the adaptive optics and high-resolution spectra available for the system [11], the probability of any of the LP 791-18 transit events being the product of a bound or background binary system were already small. Our detection of transit timing variations (TTVs), discussed below, confirms the planetary nature of the transit events by evincing the mutual gravitational interaction between planets c and d.

We jointly analyzed all space-based and ground-based transit observations of each planet using ExoTEP [5, 6]. For the newly discovered planet d, we infer a radius consistent with that of the Earth ($1.03 \pm 0.04\,R_\oplus$) and an equilibrium temperature of 395 K for an Earth-like Bond albedo and 305 K for a Venus-like Bond albedo, assuming efficient heat redistribution. The period of the planet d is 2.753 days. In the analysis, we used an updated stellar luminosity ($0.00230 \pm 0.00001\,L_\odot$) and stellar radius ($0.182 \pm 0.007\,R_\odot$), which we determined by constructing an expanded 0.3–17 μm spectral energy distribution from a newly obtained IRTF/SpeX Prism spectrum of LP-791-18 and publicly available broadband measurements [19] (see Methods and Extended Data Table 3.3). We similarly refine the radius estimate of the sub-Neptune LP-791-18c to $2.46 \pm 0.09\,R_\oplus$ (Extended Data Table 3.4). We then derived mass estimates by fitting the 67 mid-transit times of planets c and d using TTVFast transit timing modeling [13] in combination with emcee [21] (see Methods). The transits of planet b (Extended Data Fig. 3.5) were not included in the TTV analysis because it orbits too closely to the host star to exhibit or introduce measurable timing variations for any plausible planetary masses.

Transit timing variations with an amplitude of 5.6 ± 0.7 minutes are detected for planet d consistently in the *Spitzer* and ground-based observations (Fig. 3.2 and Extended Data Fig. 3.6). The TTVs confirm the planetary nature of the LP-791-18 system and constrain

the mass of the sub-Neptune LP 791-18c to $9.7^{+1.3}_{-1.2}\,M_\oplus$ and the mass of the Earth-sized planet LP 791-18d to $0.9^{+0.5}_{-0.4}\,M_\oplus$ (Extended Data Table 3.4). They also constrain the orbital eccentricity of LP 791-18c's orbit to $0.0452^{+0.0070}_{-0.0066}$ and the eccentricity of LP 791-18d's orbit to $0.0345^{+0.0098}_{-0.0092}$, i.e., 6.8σ and 3.7σ away from zero, respectively. Running N-body integrations for the system over 10^9 orbits of planet c, we find that the orbital eccentricities are a direct result of the planets' mutual interaction, and that the system is stable long-term (see Methods). None of our integrations encounter instabilities, even for the highest masses consistent with the TTVs. We further find planets c and d to be near, but not actually in, 9:5 resonance, presenting clear distinction from the resonant planets in the TRAPPIST-1 system. In all N-body simulations, we assumed a circular orbit for planet b, justified by its short tidal circularization timescale.

Comparing the inferred radii and masses to planet interior models, we find that the mass of planet c ($9.7^{+1.3}_{-1.2}\,M_\oplus$) is significantly below the $25\,M_\oplus$ that a purely rocky planet with the measured radius of planet c would have, indicating that planet c retained a significant amount of H_2/He envelope and/or a volatile-rich mantle (Extended Data Fig. 3.7). In interior model grids [66] a best match to the mass and radius is obtained for an Earth-like interior with about 2% of the planet's mass in a H_2/He envelope or, alternatively, interior compositions predominately composed of a much less-dense, ice-rich material. Either way, planet c must have been able to hold onto a substantial amount of volatiles or gas. The newly found planet LP-791-18d, on the other hand, is consistent with a rocky, potentially Earth-like, composition given its radius of $1.03 \pm 0.04\,R_\oplus$ and mass of $0.9^{+0.5}_{-0.4}\,M_\oplus$. Together in the same system, the two planets span the small-planet radius valley and offer a rare opportunity to test planet formation and gas envelope evolution models in the previously poorly explored regime of late M dwarfs. To date, the radius valley is well-established for FGK-type stars, representing a relative lack of planets observed at $1.7-2.0$ $R_\oplus$ [23]. Also, early M stars show a similar dearth of planets between 1.5 and 1.7 Earth radii [9]. Generally, the radius valley is thought to divide the population of small exoplanets into primarily rocky planets and planets hosting thick H/He envelopes, the sub-Neptunes [22]. Multiple theories have been proposed for the existence of the radius valley including photoevaporation [49], core-powered mass-loss [29, 31], impact erosion [55, 63], and a superposition of gaseous planets forming in gas-rich disk environments before disk dissipation and gas-poor planets forming after disk dissipation [40, 39, 41]. In the late M-dwarf regime, little is known to date, but here we find for LP 791-18c and d that our measured mass ($9.7^{+1.3}_{-1.2}\,M_\oplus$ and $0.9^{+0.5}_{-0.4}\,M_\oplus$) are consistent with both the predictions from photoevaporation [48] and the predictions from core-powered mass loss [31, 10].

The discovered planet LP 791-18d itself lies within the range of temperatures and stellar insolations for which a Venus-like runaway greenhouse effect is possible [34]. Meanwhile, LP 791-18d's escape velocity and insolation suggest that it could have held onto an atmosphere,

thereby plausibly resisting runaway atmospheric evaporation (Extended Data Fig. 3.8). As such, the planet offers an opportunity to empirically probe an Earth-sized planet near the inner edge of the habitable zone of a late M-dwarf system. Many elements of the atmospheric evolution of Venus remain insufficiently understood to this date, such as the precise mechanisms and timescales for water loss [34] and whether Venus may briefly have transitioned through a habitable phase. Studying LP 791-18d could help us understand how an Earth-sized planet such as Venus becomes inhabitable, and which terrestrial planets are likely to support Earth-like versus Venus-like atmospheres.

Being tidally locked, however, LP 791-18d could also be different from Venus, with the night side of LP 791-18d likely cold enough for water to condense. 3D GCM simulations of terrestrial planets suggest that the inner edge of the habitable zone is pushed inwards compared to the predictions of 1D models for planets orbiting M dwarfs due to the formation of a thick layer of high-albedo clouds at the substellar point [64]. For a Venus-like Bond albedo of 0.75, for example, the globally-averaged equilibrium temperature would be approximately 300 K, leaving ample possibilities of potentially habitable conditions to exist on LP 791-18d on the night side or at high latitudes. Spectroscopic detections of water, methane, and/or ammonia on LP 791-18d would indicate that some of the key ingredients for life are present on these planets around M stars — all three gases are habitability signatures for Earth, either because they are produced by life (methane and ammonia) or because they are essential for the existence of life on Earth (H_2O).

In addition, we find that the orbital eccentricity of LP 791-18d, resulting from the secular interaction with the ten-times-more-massive planet c, leads to substantial and continued tidal heating of the LP 791-18d's interior (Fig. 3.3). In particular, tidal heating modeling indicates that LP 791-18d's internal tidal heat flux of $0.5 - 5$ W/m^2 is comparable to that of Jupiter's moon Io (1–2 W/m^2), the most volcanically active body in the solar system [58, 62]. In the model, we adopt the Maxwell model of viscoelastic rheology to take into account the feedback between the thermal state of the planet's interior and its response to tidal forcing, as well as the temperature dependency of the viscosity and the shear modulus of the mantle material [20, 43, 32, 17, 3] (see Methods). We then obtain the mantle equilibrium temperature $T_{\rm mantle}$ as the temperature for which the internal tidal heat flux is in equilibrium with the upward convective energy transport towards the surface. We find that LP 791-18d's mantle equilibrium temperature lies above the solidus temperature of rock, indicating that the mantle of LP 791-18d could maintain a permanent liquid magma state over secular timescales (see Methods). For a rocky surface composition, this would result in surface eruptions and volcanic activity, similar to that on Jupiter's moon Io's [58, 62], and would continuously replenish the atmosphere of LP 791-18d with outgassed molecular species.

Looking forward, LP 791-18d, being a likely volcanically highly active, Earth-sized planet at the edge of the habitable zone of a late M-dwarf in a system with a sub-Neptune offers multiple unprecedented opportunities to advance our understanding of Earth-sized planets, the outgassing and atmospheric retention of rocky planets in general, and the origin of the radius valley. Currently, multiple temperate ($< 400\,\mathrm{K}$) Earth-sized planets (TRAPPIST-1b,c,d,e,f, and g) are approved for substantial JWST/GTO and GO observations for spectroscopic follow-up studies; however, there remains a certain possibility that all the TRAPPIST-1 planets have a common formation and evolution history [1], which may have left the system volatile-poor or the planets without an atmosphere. LP 791-18d presents a powerful new opportunity to spectroscopically study a temperate Earth-sized planet outside the TRAPPIST-1 system, thereby broadening our horizon to an Earth-sized planet with an independent evolution history, in particular in a system where at least one planet (LP 791-18c) retained a substantial amount of gas and volatiles. From an observational perspective, LP 791-18's small stellar radius ($0.182 \pm 0.007\,R_\odot$) and extremely low stellar luminosity ($0.00230 \pm 0.00001\,L_\odot$) make LP 791-18d the perfect M star opportunity. The observable transit depth contrast between inside and outside of atmospheric absorption bands should be as high as 30–100 ppm even for the high mean molecular weight terrestrial atmospheres, such as CO_2-dominated, N_2-dominated, or H_2O atmospheres, despite the planet's small size and low temperature (Fig. 3.4). Such transit depth variations across the spectrum are well above the expected systematic noise floor of JWST instruments [14] and its high Transit Spectroscopy Metric (TSM [35]) value allows for efficient observations of LP 791-18d. Other favorable targets with similarly high TSM values such as GJ1132b, GJ357b, L98-59c, LHS 1140c, and LTT 1445Ab are either significantly larger than Earth or substantially more irradiated by their host star (Fig. 3.4). In addition, the smaller host stars of LP 791-18d also results in larger transit depth variations across the transmission spectrum in absolute terms, which enables detections of CO_2-dominated or N_2-dominated atmospheres with their small scale heights without imposing the extremely stringent requirements on the yet unknown systematic noise floor of JWST instruments (see colors in Figure 4). Finally, LP-791-18d is special in its temperature range in that space-based instruments like JWST can observe up to 38 transit of LP 791-18d per year, while other similarly cold planets around stars hotter than M5 would have substantially longer orbital periods and thus much fewer opportunities to observe transits and build up sufficient SNR [6]. The fact that LP 791-18d experiences substantial tidal heating and is likely volcanically highly active furthermore suggests that the atmosphere is continuously replenished by outgassing from the planet's interior, rendering the scenario of a bare rock with a flat transmission spectrum less likely. The outgassed atmosphere would then also enable us to draw conclusions about the interior composition [36].

Beyond the study of Earth-sized planets in isolation, spectroscopic observations of LP 791-18d would simultaneously offers a rare opportunity to empirically probe the origin of the radius valley for a late M dwarf system. This is true, in particular, when observations of LP 791-18d are combined with observations of the sub-Neptune LP 791-18c that appears to have retained its gas- or volatile-rich envelope. Based on our mass measurement, LP 791-18c is similar in bulk properties and temperature to K2-18b (Extended Data Fig. 3.7) and could similarly host a readily detectable H_2-atmosphere [6]. Intriguingly, LP 791-18c would be even more favorable for atmosphere characterization than K2-18b (Fig. 3.4). A comparison between the elemental abundances on LP 791-18c and LP 791-18d could then provide important clues about the origin of the small-planet radius valley. For example, if the radius valley was sculpted by the evaporation of thick primordial atmospheres, heavy molecules on LP 791-18d, such as H_2O, CO, CO_2, and N_2 could have sunk to lower levels and remained shielded from evaporation, leaving behind a thick volatile-rich atmosphere on LP 791-18d, although the volatiles could also have been carried away with the evaporation of H_2 [36]. Alternatively, in the case that LP 791-18d never attained a primordial atmosphere or that such an atmosphere was lost completely, a secondary atmosphere could have formed through the volcanic outgassing of its tidally heated interior and possibly late-disk accretion [37] or impacts with planetesimals. In this context, the presence of LP 791-18c could enable the distinction between volcanic outgassing and late-disk accretion as the primary source of LP 791-18d's atmosphere [36]. Altogether, given the aforementioned special characteristics, LP 791-18d presents a rare opportunity to empirically probe many of the key physical processes driving the evolution of Earth-sized planets, including probing for volcanic activity, analyzing the outgassed molecular species from the interior, constraining escape mechanisms, and, more generally, probing the planet's early formation and accretion history through direct comparison to its companion sub-Neptune.

1. Methods

1.1. Stellar Characterization.

We refine the stellar radius of LP 791-18 reported in the TESS Input Catalog v8 [59, 11] using the same method as used for TRAPPIST-1 and other late M-dwarfs [19]. For that, we construct an expanded 0.3–17 μm spectral energy distribution (SED) by combining a newly obtained IRTF/SpeX Prism spectrum of LP-791-18 at 0.7–2.52 μm taken on 2020-12-23 (Extended Data Fig. 3.9) with publicly available SDSS, PS1, 2MASS, and WISE broadband measurements (Extended Data Table 3.3). Absolute calibration of IRTF/SpeX Prism spectrum is performed using the overlapping photometric measurements, allowing for an offset and linear trend across the spectrum. We then fill any remaining gaps in wavelength space between 0.3 and 17 μm with linear interpolation in logarithm space, and

we use a Rayleigh-Jeans or Wien tail of the appropriate temperature at either ends of the SED. Once the SED is built, we then infer the total bolometric luminosity by scaling the SED using the measured Gaia eDR3 parallax distance of 26.65 ± 0.03 pc and integrating it over all wavelengths. We find a stellar radius of $0.182 \pm 0.007\,R_\odot$ for LP 791-18. Our stellar radius estimate is consistent with that of Ref. [11] for LP 791-18 ($0.171 \pm 0.018\,R_\odot$) albeit with smaller radius uncertainty and inferred based on the empirical reconstruction of the full SED of LP 791-18. Our inferred radius is also consistent with the overall trend in interferometric radii measurements of main-sequence late-M stars [16], where measurements tend to indicate slightly inflated radii versus solar-metallicity models.

1.2. *Spitzer* Photometric Extraction and Systematics Model.

Our near-continuous 124-hour *Spitzer* light curve is divided into six light-curve segments (AORs), which we initially extract and inspect as separate light curves. For that, we first extract the photometry for each segment using a set of fixed circular apertures with sizes ranging from 1.5 to 5 pixels. For each exposure, we estimate and subtract the sky background, calculate the centroid position of the star on the detector array, and then calculate the total flux within the aperture radius [4]. We find an aperture radius of 3 pixels to produce the lowest photometric scatter for all six segments.

Following standard procedure, we detrend our *Spitzer* light-curve segments against a drift in time and intrapixel sensitivity variations using the pixel level decorrelation (PLD) approach [15, 4]. Our systematics model is given by the following equation:

$$S(t_i) = \frac{\sum_{k=1}^{9} w_k D_k(t_i)}{\sum_{k=1}^{9} D_k(t_i)} + m \cdot t_i, \tag{1.1}$$

where D_k represents the raw flux in each of the nine central pixels in the target's point spread function, along with nine simultaneously fitted PLD coefficients w_k and a fitted linear slope m for the sensitivity drift with time. These 10 systematic MCMC parameters are constrained simultaneously with the transit model parameters as described below.

1.3. Initial *Spitzer* Light-Curve Inspection.

We first perform an initial inspection of the *Spitzer* data by detrending each light-curve segment separately. We carefully inspect the resulting detrended photometry for decreases resembling transit-like events. In additional to the predicted transits of LP 791-18b and c, we identify two new transits of planet d at BJD = 2458772.16 and 2458774.9. We double-check that these events do not align with any shift in the background flux or shift in the position of the star's centroid, and find that the transits events of planet d are uncorrelated with any centroid position shifts of the star. We cross-check that these transits persist in the light curve when the flux during these transit events as well as the transits of planets b and c are

masked. The transits of planet d remain in the light curve as marked in purple in Fig. 3.1. We discuss the sensitivity of the light curve to transiting planets more quantitatively below.

1.4. Joint Light-Curve Fitting.

To determine the properties and orbits of each planet, we jointly analyze the TESS, *Spitzer*, and ground-based transit photometry using ExoTEP, a modular tool designed to jointly analyze many transits from different instruments with diverse systematics models [4, 5, 6]. The analysis makes use of the AI-MCMC Ensemble sampler emcee package [21], combined with the batman package for efficient transit light-curve modeling [38]. We jointly fit all observed transits of each planet and derive the joint posterior distribution of the transit light-curve model parameters, the systematics model parameters for the *Spitzer* and ground-based light curves, and a photometric scatter value for each transit light curve. The transit light-curve model for a given planet shares the same impact parameter b and semi-major axis a/R_*, with only the transit depth and the limb darkening coefficients assigned separately for each instrument bandpass.

For *Spitzer*, we simultaneously fit the PLD systematics model parameters described above, while the TESS and ground-based transits are detrended prior to fitting. For the TESS observations, we use the TESS Pre-Search Data Conditioning Simple Aperture Photometry [60, 56, 61] as produced by the TESS Science Processing Operations Center [33], which have been further detrended using quaternions to remove non-astrophysical systematics. To remove any remaining systematics, the TESS light curve was detrended with a Gaussian process with squared exponential kernel and a fixed length scale of 1.0 days. The ground-based transits are detrended against airmass with the exception of the MEarth transits, which show significant systematics possibly caused by water column variation and were therefore detrended using a spline fit that excluded the in-transit data. The first transits of planet b and c in the *Spitzer* data are overlapping and, for this case, we fit the transits of planet b, planet c, and the PLD systematics model simultaneously.

For limb darkening, we use the priors on the quadratic limb darkening coefficients determined in Ref. [11] for the TESS light curves. For the ground-based instruments we use equivalent priors determined with LDTK [50] as listed in Extended Data Table 3.3. For *Spitzer*, we choose to first fit the deep high SNR *Spitzer* transits of planet c in order to empirically determine the 4.5μm quadratic limb darkening coefficients for the star LP 791-18. The resulting *Spitzer* coefficients are then used as priors when fitting planets b and d. The photometric scatter is a free parameter for each transit, except for the TESS data, for which only one scatter parameter is shared by all transits as the overall TESS light curve has a near-constant scatter dominated by photon noise.

The MCMC fit for each planet is performed with four walkers per fitting parameter and run for a total of 16000 steps, much longer than needed for formal convergence. Disregarding

the initial 60% of our chains as burn-in, the resulting transit parameters and calculated properties are recorded for each planet in Extended Data Table 3.4. The resulting transit models for planets b, c and d are shown in Extended Data Figs. 3.1–3.5.

Transits from ExTrA and SPECULOOS (SSO I+z band) are not included in the joint fits, but were used in the TTV analysis. The ExTrA observations were detrended and fit using the package juliet [18] with Gaussian detrending, and with all transit parameters but the timing fixed to the results of our joint fit. The SPECULOOS / SSO (I+z) observations are detrended using polynomials of variable order in airmass, background and position [26].

1.5. Transit Timing Variations.

To determine the masses and orbital parameters of planets c and d, we first infer the mid-transit time from each observed transits of planet c and d. We accomplish this by fitting each transit individually with ExoTEP, while including Gaussian priors on all others parameters based on the best-fit estimate from the joint fit. We do not include planet b in our TTV analysis because the predicted amplitude of the TTVs for planet b are below one second, independent of the masses of planets c and d. With the inferred mid-transit-timing estimates, we then determine the joint posterior distribution of the masses and orbital parameters of planets c and d by modeling and fitting the mid-transit times using TTVFast [13] in combination with emcee [21]. In the analysis, we use all observed complete transits for which no significant systematics in detrended light curves are identified. We excluded a MEarth-N transit of planet d taken 2020-02-08 (ExoFOP tagid 16501) as this transit is partial and disagreed with the timing of the MEarth-S observations taken the same night. We also excluded an LCO observation taken 2020-03-17 (tagid 18144), which is affected by clouds passing during pre-transit, and an ExTrA transit of planet d taken 2020-03-04, which disagreed with the timing of our Mearth-S, TRAPPIST-N and CTIO observations taken the same night. In our TTVFast fit, we fix the inclination to the results from the joint light curve fit and the longitude of the ascending node to $\pi/2$. We parameterize the pair of eccentricity e and argument of periastron ω with the pair of $\sqrt{e}\cos\omega$ and $\sqrt{e}\sin\omega$. We furthermore fit the sum of the mean anomaly and longitude of periastron $M+\omega$ in place of the mean anomaly M itself because $M+\omega$ describes the position of the planet equivalently to M, but is much less correlated with ω, thereby facilitating the convergence substantially. Our set of $\sqrt{e}\cos\omega$, $\sqrt{e}\sin\omega$, and $M+\omega$ is equivalent to the set of e, ω, and M. We use uniform priors for all our fitting parameters except the stellar mass, for which we use a Gaussian prior representing the mass listed in Extended Data Table 3.3. We find a large number of walkers to be necessary to adequately explore the parameter space, and the results reported use 50 walkers per parameter, for a total of 550 walkers run for 12,000 steps. The best-fit results are recorded in Extended Data Table 3.4 and the posterior distribution is shown in Extended Data Fig. 3.10. The transit times corresponding to 68% and 95% confidence intervals from

this fit are shown in Fig. 3.2 and Extended Data Fig. 3.6 and match all observed transit times well.

1.6. System stability analysis.

We perform N-body integrations of the LP 791-18 system using the `Rebound` library [52, 51], choosing the symplectic Wisdom-Holman integrator `WHFast` except where otherwise stated. As a conservative approach, we choose the highest allowed mass and eccentricity within error bars for all the objects. Planet c is initialized as a 11.0 $M_\oplus$ object with eccentricity of 0.052, while planet d is chosen to be a 1.4 $M_\oplus$ object with an eccentricity of 0.044. The eccentricity of planet b is not observationally constrained; however, assuming an effective rigidity $\tilde{\mu} = (10^4 km/R)^2$ and tidal quality factor $Q = 100$ for the planet, we argue that the tidal circulization timescale [45]

$$\tau_e = \frac{4}{63}\frac{\tilde{\mu}Q}{2\pi}\frac{m}{M_*}\left(\frac{a}{R}\right)^5 P \tag{1.2}$$

is only $\tau_e \sim 8.8 \times 10^5$ yr and much shorter than the age of the system. Planet b's eccentricity should therefore be near 0. Here, a is the semi major axis and R the radius of planet b. For the N-body integrations, we furthermore assume zero inclination for all objects. We integrate the system for 10^9 orbits of planet c, with a time step of 0.1 days. This timescale is long enough to allow for secularly driven and chaotic diffusive instabilities to manifest if present. We run 10 simulations with random initial anomalies and argument of periapsis, and find them all to be stable with no extreme eccentricity excitation for any object. An example simulation is shown in Extended Data Fig. 3.11a. To check whether planets d and c are indeed in a 9:5 MMR, we plot in Extended Data Fig. 3.12 the resonant angle $\phi_{9:5} = 9\lambda_d - 5\lambda_c - 4\varpi_d$ as a function of time, which shows that it circulates on a timescale significantly longer than the orbital periods, implying that the system is near, but not in, the MMR.

To assess whether the system can dynamically accommodate a fourth planet, we run an extra suite of N-body integrations with one additional 1 $M_\oplus$ planet introduced on a circular orbit in each simulation. The periods of the hypothetical planets ranges between 0.95 to 5 days with fine spacing. The system stability simulations are performed as before, but using the higher order `IAS15` integrator available in the `Rebound` library. We find that the system can accommodate a 1 $M_\oplus$ planet for periods near 1.8 days (between planets b and d) without triggering dynamical instability. An example is shown in Extended Data Fig. 3.11b. On the other hand, we find that a planet on any shorter or longer orbital between planets d and c will quickly make the system unstable, with either planet d or the fictional planet being ejected. An example is shown in Extended Data Fig. 3.11c.

1.7. Tidal Heating Model.

We use the tidal heating model previously applied to the interior of Io [20, 43, 32, 17] and the TRAPPIST-1 planets [3]. Assuming that the planet is in synchronous rotation, we calculate its tidal energy dissipation as :

$$\dot{E}_{\rm tidal} = -\frac{21}{2}{\rm Im}(k_2)\frac{R^5\omega^5 e^2}{G}, \tag{1.3}$$

where R and e are the planet's radius and orbital eccentricity, ${\rm Im}(k_2)$ is the imaginary part of the planet's Love number, G is the gravitational constant, and ω is equal to $2\pi/P$ with P being the orbital period [54]. Instead of using a fixed tidal quality factor Q to assess the rate of energy dissipation per tidal cycle, we adopt the Maxwell model of viscoelastic rheology to take into account the feedback between the thermal state of the planet's interior and its response to tidal forcing. In the Maxwell model, ${\rm Im}(k_2)$ is evaluated as:

$${\rm Im}(k_2) = -\frac{57\eta\omega}{4\bar{\rho}gR\left[1+\left(1+\frac{19\mu}{2\bar{\rho}gR}\right)^2\frac{\eta^2\omega^2}{\mu^2}\right]} \tag{1.4}$$

where η is the viscosity of the material, μ the shear modulus, $\bar{\rho}$ the average density of the material and g the surface gravity of the planet [32].

We then obtain the mantle equilibrium temperature $T_{\rm mantle}$ as the temperature for which the globally averaged tidal heat flux $F_{\rm tidal} = \dot{E}_{\rm tidal}/4\pi R^2$ is in balance with the rate of radial energy transport towards the surface via solid-state convection $F_{\rm conv}$ [57, 2, 3], i.e., satisfying:

$$\frac{\dot{E}_{\rm tidal}(T_{\rm mantle})}{4\pi R^2} = 0.53\left(\frac{Q^\star}{R_G T_{\rm mantle}^2}\right)^{-4/3}\left(\frac{\rho g\alpha k_{\rm therm}^3}{\kappa_{\rm therm}^3\eta(T_{\rm mantle})}\right)^{1/3}. \tag{1.5}$$

Here, R_G is the universal gas constant, and the properties of rock are used for the activation energy $Q^\star = 333\,{\rm kJ\,mol^{-1}}$, the coefficient of thermal expansion $\alpha = 3\times10^{-5}\,{\rm K^{-1}}$, and the thermal diffusivity $\kappa_{\rm therm} = k_{\rm therm}/(\rho C_p)$ with $k_{\rm therm} = 3.2\,{\rm W\,m^{-1}\,K^{-1}}$ and $C_p = 1200\,{\rm J\,kg^{-1}}$. For the density we use $\rho = 5000\,{\rm kg/m^3}$, appropriate for a pure rock composition [57]. Importantly, $\dot{E}_{\rm tidal}$ depends on $T_{\rm mantle}$ in Eq. 1.5 via the temperature-dependence of the shear modulus μ and the viscosity η. At temperatures below the solidus of rock ($T_s = 1600\,{\rm K}$), we use $\mu = 50$ GPa and $\eta(T) = \eta_0\exp\left(Q^\star/(R_G T)\right)$ with $\eta_0 = 2.13\times10^6\,{\rm Pa\,s}$ [20, 32]. Between the solidus temperature and the "breakdown point" ($T_b = 1800\,{\rm K}$), which marks the transition to a regime in which there is more melted than solid rock [53], we use the shear modulus $\mu(T) = 10^{\frac{\mu_1}{T}+\mu_2}$ where $\mu_1 = 8.2\cdot10^4\,{\rm K}$ and $\mu_2 = -40.6$. The viscosity in this regime is described as $\eta(T) = \eta_0\exp\left(Q^\star/(R_G T)\right)\exp(-Bf)$, where the melt fraction coefficient B describes the dependency of the rock viscosity on the melt fraction f and experimentally constrained to be between 10 and 40 [43]. The melt fraction f, in turn, increases linearly from 0 to 0.5 between T_s and T_b [20, 43].

For LP 791-18d, specifically, we compute the equilibrium mantle temperature and the corresponding tidal flux using the median parameters in Table 3.4 and the experimentally determined values of the melt fraction coefficient B for rock. We explore the full range of eccentricities between 0.01 and 0.05 that result from the secular interactions with planet c in the system (Figure 3.11). We find that equilibrium for LP 791-18d systematically occurs for $T > T_s$, which is a stable equilibrium [43, 17], with corresponding tidal fluxes of $\sim 0.5 - 5$ W/m^2 (Figure 3.3). For LP 791-18d, no equilibrium point exists below the solidus temperature (T_s) and surface volcanic eruptions are a direct consequence of the tidal heating if the rocky mantle reaches up to the planetary surface. The tidal heating thus likely results in the presence of permanent molten magma over secular timescales, with volcanic activity similar to that on Jupiter's volcanically-active moon Io [58, 62].

1.8. Spitzer Sensitivity Tests.

To determine whether additional transiting planet could exist without being detected in the *Spitzer* light curve, we generate 180,000 transit signatures with periods following a log-uniform distribution from 0.5 to 2.4 days, radii randomly distributed between 0.5 and 1.0 Earth radii, and impact parameters randomly distributed between 0 and 0.8. We then inject these simulated transit signatures into the *Spitzer* light curve at 4 random phases, one at a time, and measure the χ^2 improvement of the transit model versus a straight line on the injected light curve. In total, this results in 720,000 injections and χ^2 values. We then randomly selected 6,000 of these injections and run a transit recovery search on them. We model the recovery rate as a function of the χ^2 improvement of the injected signals and use this to calculate a theoretical recovery rate for each signal. These rates are then binned by period and radius to determine which sizes of planets could be missed in the *Spitzer* data at different orbital periods (Extended Data Fig. 3.13). We find that an additional Earth-mass planet could exist between planets b and d without disrupting the dynamical stability of the system, but such a planet would have to have $R < 0.8\,R_\oplus$ to be unseen in our *Spitzer* data. Beyond planet c, any planet with $R > 1.2\,R_\oplus$ transiting within the *Spitzer* observational interval would be detected. The probability of such a planet transiting during our observations is indicated as the solid red curve in Extended Data Fig. 3.14. Any planet smaller than $1.2\,R_\oplus$ on these orbits could plausibly remain undetected in our observations if it transited only once.

Data availability

The raw *Spitzer* data used in this study are publicly available at the *Spitzer* Heritage Archive, `https://sha.ipac.caltech.edu/applications/Spitzer/SHA`. The ground-based telescope observations are uploaded to ExoFOP and are publicly available with our detrended light curves and best fits.

2. Addendum

This work is based principally on observations made with the *Spitzer Space Telescope*, which is operated by the Jet Propulsion Laboratory, California Institute of Technology, under a contract with NASA. The material presented here is based on work supported in part by NASA under contract no. NNX15AI75G. B.B. and M.P. acknowledge financial supported by the Natural Sciences and Engineering Research Council (NSERC) of Canada and the Fond de Recherche Québécois—Nature et Technologie (FRQNT; Québec). This paper includes collected through the TESS mission data was obtained from the MAST data archive at the Space Telescope Science Institute (STScI). Funding for the TESS mission is provided by the NASA Explorer Program. STScI is operated by the Association of Universities for Research in Astronomy, Inc., under NASA contract NAS 5–26555. This work makes use of observations from the LCOGT network. Part of the LCOGT telescope time was granted by NOIRLab through the Mid-Scale Innovations Program (MSIP). MSIP is funded by NSF. This paper includes data taken EDEN telescope network, and we acknowledge support from the Earths in Other Solar Systems Project (EOS) and Alien Earths (grant numbers NNX15AD94G and 80NSSC21K0593) sponsored by NASA. We acknowledge funding from the European Research Council under the ERC Grant Agreement n. 337591-ExTrA. This research has made use of the Exoplanet Follow-up Observing Program (ExoFOP), which is operated by the California Institute of Technology, under contract with the National Aeronautics and Space Administration. RC is supported by a grant from the National Aeronautics and Space Administration in support of the TESS science mission.The MEarth Team gratefully acknowledges funding from the David and Lucile Packard Fellowship for Science and Engineering (awarded to D.C.). This material is based upon work supported by the National Science Foundation under grants AST-0807690, AST-1109468, AST-1004488 (Alan T. Waterman Award), and AST-1616624. This work is made possible by a grant from the John Templeton Foundation. The opinions expressed in this publication are those of the authors and do not necessarily reflect the views of the John Templeton Foundation. This material is based upon work supported by the National Aeronautics and Space Administration under Grant No. 80NSSC18K0476 issued through the XRP Program. M.S.P and C.P. acknowledge support from FRQNT and TEPS Master's scholarships. We acknowledge support from the Earths in Other Solar Systems Project (EOS), grant No. 3013511 sponsored by NASA. The results reported herein benefited from collaborations and/or information exchange within NASA's Nexus for Exoplanet System Science (NExSS) research coordination network sponsored by NASA's Science Mission Directorate. The research leading to these results has received funding from the ARC grant for Concerted Research Actions, financed by the Wallonia-Brussels Federation. TRAPPIST is funded by the Belgian Fund for Scientific Research (Fond National de la Recherche Scientifique, FNRS) under the grant FRFC 2.5.594.09.F. TRAPPIST-North

is a project funded by the University of Liège (Belgium), in collaboration with Cadi Ayyad University of Marrakech (Morocco). MG and EJ are F.R.S.-FNRS Senior Research Associates. Resources supporting this work were provided by the NASA High-End Computing (HEC) Program through the NASA Advanced Supercomputing (NAS) Division at Ames Research Center for the production of the SPOC data products.

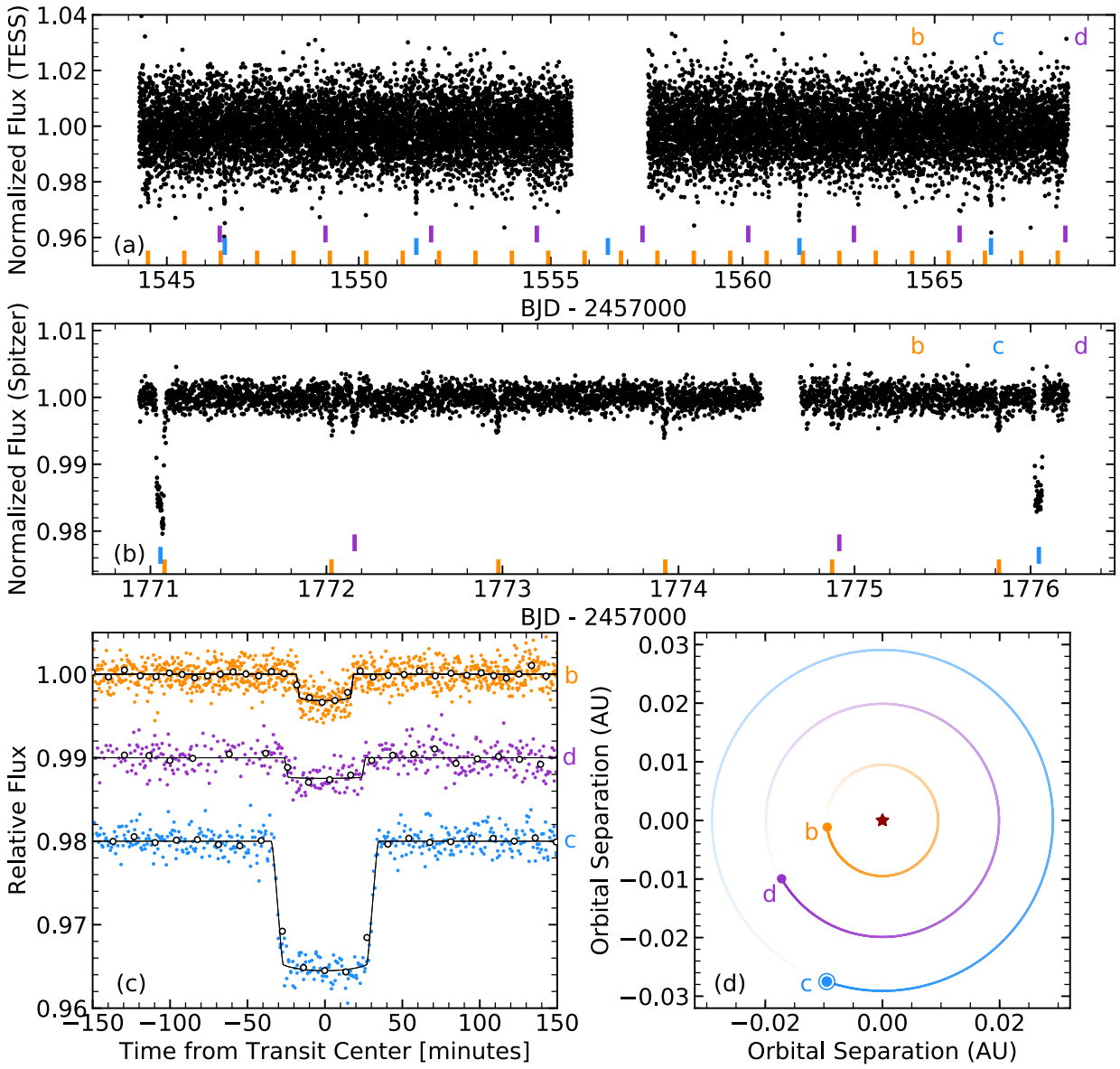

Fig. 3.1. TESS and *Spitzer* light-curves of LP 791-18. **a**, TESS observations of LP 791-18 taken between March 1 and March 25, 2019 detrended using a Gaussian process with a fixed length scale of 1.0 days, with the transit times of planets b, c and d indicated. Only the transits of planet c are visible by eye. **b**, PLD-corrected and detrended *Spitzer* observations deliberately scheduled to capture two transits of planet c, with the first transit appearing much deeper due to overlap with the transit of planet b. The signatures of all three planets are visible by eye in the processed *Spitzer* data, and are also shown phase-folded in Panel **c**. **d**, Snapshot of the orbits of the three planets.

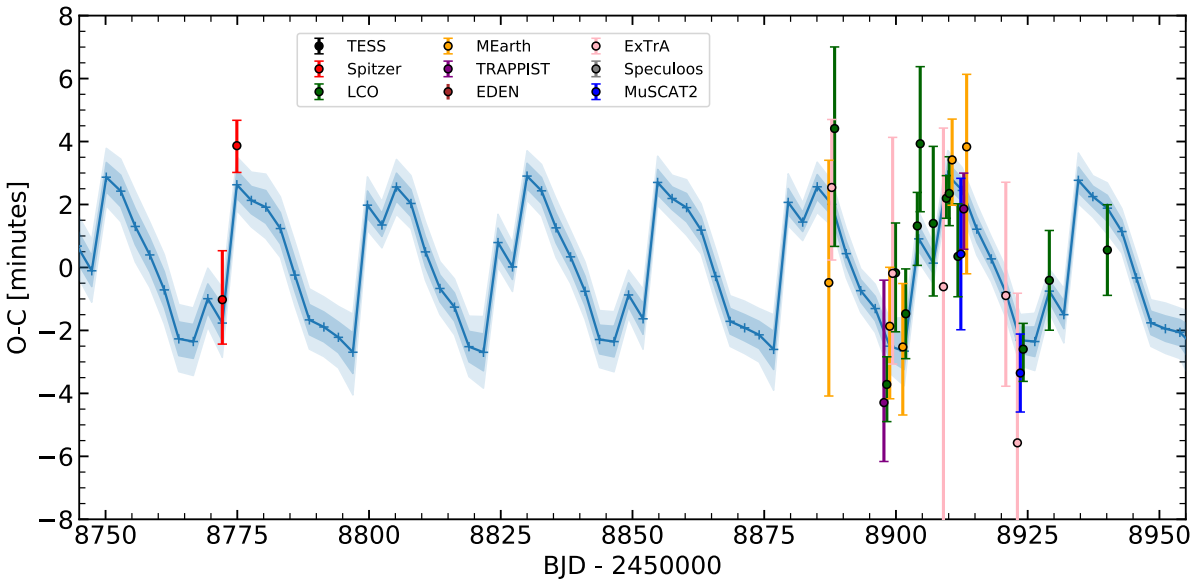

Fig. 3.2. Transit timing variations of LP 791-18d. Colored data points indicate the transit timing measurements obtained with TESS (black), *Spitzer* (red), LCO (green), MuSCAT2 (dark blue), MEarth (yellow), TRAPPIST telescope (purple), EDEN (brown), ExTrA (pink), and SPECULOOS (grey), compared to the best fitting TTVFast model (blue curve). The vertical axis represents the deviation from the best-fitting linear ephemeris and the horizontal axis the Julian Date of the observation. Dark and light shaded regions illustrate the posterior population of models in the MCMC fit corresponding to 68% and 95% confidence, respectively. Transit timing variations with 5.6 ± 0.7 minutes chopping amplitude are consistently detected in both the *Spitzer* and ground-based data, at a phase consistent with the planetary conjunctions of planet c and d. Some transits near $BJD = 2458900$ were observed with up to four telescopes simultaneously, with point slight offset horizontally for clarity. Part of the data set is shown here for clarity, and the full data set is depicted in Extended Data Fig. 3.6

.

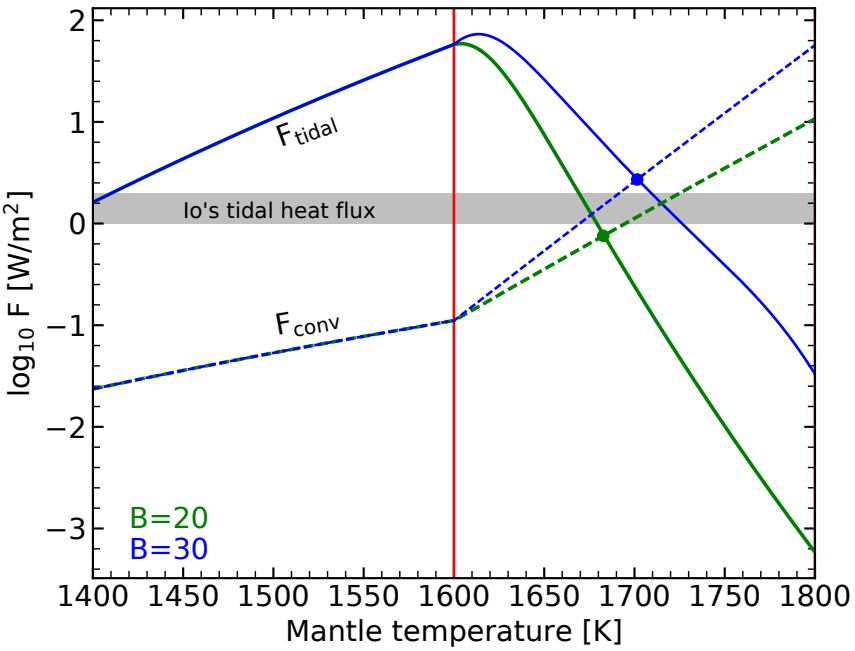

Fig. 3.3. Internal energy balance of LP 791-18d in the presence of tidal heating. Solid and dashed curves trace the tidal heating per unit surface area $F_{\rm tidal} = \dot{E}_{\rm tidal}/4\pi R^2$ and the convective heat transport towards the surface $F_{\rm conv}$ as a function of the mantle temperature. The equilibrium mantle temperature is reached where $F_{\rm tidal} = F_{\rm conv}$ (colored circles). Two sets of curves and equilibrium points (green and blue) are shown for two plausible melt fraction coefficients $B = 20$ and $B = 30$, respectively. In both cases, equilibrium is reached beyond the solidus (vertical red line) indicating that LP 791-18b has a partially molten mantle due to substantial tidal heating. The magnitude of the tidal heating is of the order of 0.5–5 W/m^2 comparable to the tidal heating for Jupiter's moon Io (gray bar), the most geologically-active body in the solar system with strong volcanism, surface eruptions and atmospheric replenishment [58, 62]

.

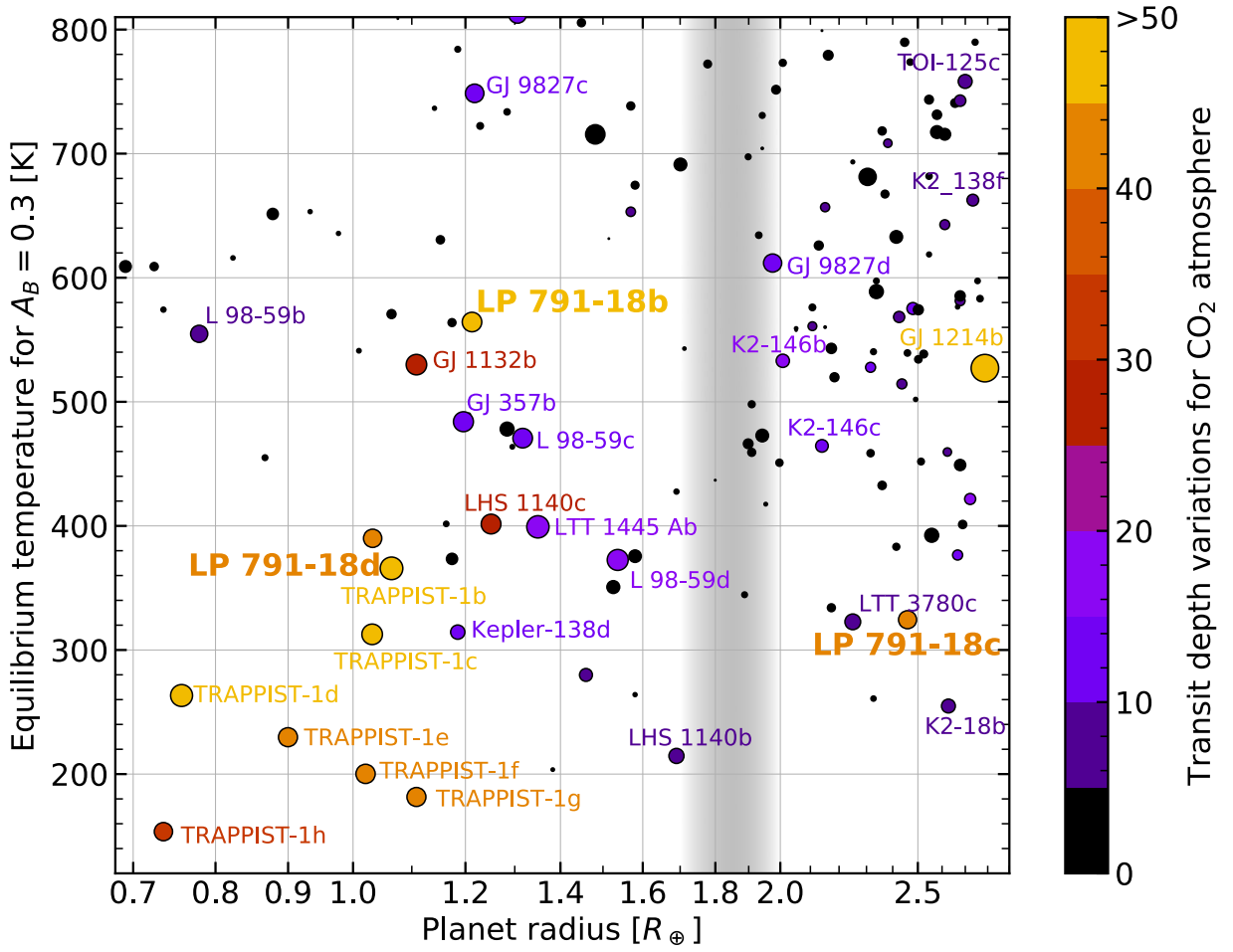

Fig. 3.4. Temperature and radius of small planets amenable to transit spectroscopy. Colors indicate the expected transit depth variations across the spectrum introduced by a CO_2-dominated atmosphere (five scale heights), while point sizes indicate the relative SNR achievable per transit in the photon-noise limit, akin to the TSM [35]. For rocky planets, both quantities (color and marker size) are essential in determining whether a planets is a good target for atmospheric characterization due to the separate limits introduced by photon-noise and the systematic noise floor (e.g., 25 ppm) expected for space-based facilities such as JWST [14, 30, 42]. All planets with expected atmospheric signals greater than 7 ppm for CO_2 atmospheres are labeled by name, albeit many of them would require transit depth precision well below the expected systematic noise floor of JWST (purple labels). Small planets orbiting LP-791-18 and TRAPPIST-1 (yellow, orange) are unique in terms of the scale of their expected atmospheric signatures as well as their number of transits available per year. LP-791-18 and TRAPPIST-1 also represent the only labeled systems that can be observed with the JWST/NIRSPEC prism to simultaneously obtain 0.6–5 μm. The vertical gray stripe highlights the radius valley [22]. Note that the sub-Neptunes to the right side of the radius valley can have extended H_2/He-rich atmospheres [6], which would be detectable much more easily due to the almost 20 times greater atmospheric scale height and signal.

Extended Data Table 3.1. Transit observations of LP 791-18 d

Label	Date	Telescope	Tc	ExoFOP tagid[2]
d0	2019-03-03	TESS	$2458546.38292^{+0.00840}_{-0.00310}$	–
d1	2019-06-22	SSO (I+z)	$2458656.51518^{+0.00110}_{-0.00110}$	–
d2	2019-07-03	SSO (I+z)	$2458667.52903^{+0.00110}_{-0.00110}$	–
d3	2019-10-15	Spitzer (4.5μm)	$2458772.16028^{+0.00108}_{-0.00098}$	–
d4	2019-10-18	Spitzer (4.5μm)	$2458774.91713^{+0.00056}_{-0.00059}$	–
d5	2020-02-08	Mearth-S	$2458887.80550^{+0.00270}_{-0.00250}$	16499
d6	2020-02-08	ExTrA	$2458887.80760^{+0.00150}_{-0.00160}$	–
d7	2020-02-08	McD (Ic)	$2458887.80890^{+0.00180}_{-0.00260}$	16479
d8	2020-02-19	TRAPPIST-S (I+z)	$2458898.81665^{+0.00270}_{-0.00130}$	5781
d9	2020-02-19	CTIO (Ic)	$2458898.81705^{+0.00061}_{-0.00082}$	16793
d10	2020-02-19	MEarth-S	$2458898.81833^{+0.00130}_{-0.00160}$	16796
d11	2020-02-19	ExTrA	$2458898.81950^{+0.00300}_{-0.00200}$	–
d12	2020-02-19	CTIO (Ic)	$2458898.81951^{+0.00110}_{-0.00130}$	16944
d13	2020-02-22	MEarth-S	$2458901.57132^{+0.00140}_{-0.00150}$	16848
d14	2020-02-22	SAAO (I)	$2458901.57206^{+0.00099}_{-0.00099}$	16831
d15	2020-02-24	SAAO (I)	$2458904.32744^{+0.00074}_{-0.00087}$	16854
d16	2020-02-24	SAAO (Ic)	$2458904.32926^{+0.00170}_{-0.00150}$	18878
d17	2020-02-27	SSO (Ic)	$2458907.08095^{+0.00170}_{-0.00160}$	16907
d18	2020-03-01	ExTrA	$2458909.83300^{+0.00350}_{-0.01120}$	–
d19	2020-03-01	CTIO (Ic)	$2458909.83495^{+0.00050}_{-0.00044}$	16939
d20	2020-03-01	CTIO (I)	$2458909.83506^{+0.00081}_{-0.00071}$	16957
d21	2020-03-01	MEarth-S	$2458909.83580^{+0.00090}_{-0.00100}$	16954
d22	2020-03-04	CTIO (Ic)	$2458912.58712^{+0.00116}_{-0.00089}$	17294
d23	2020-03-04	MuSCAT2	$2458912.58717^{+0.00167}_{-0.00167}$	–
d24	2020-03-04	TRAPPIST-N (I+z)	$2458912.58817^{+0.00079}_{-0.00089}$	5781
d25	2020-03-04	Mearth-S	$2458912.58953^{+0.00160}_{-0.00280}$	17299
d26	2020-03-12	ExTrA	$2458920.84660^{+0.00250}_{-0.00200}$	–
d27	2020-03-15	ExTrA	$2458923.59680^{+0.00330}_{-0.00340}$	–
d28	2020-03-15	MuSCAT2	$2458923.59834^{+0.00086}_{-0.00086}$	–
d29	2020-03-15	CTIO (Ic)	$2458923.59887^{+0.00057}_{-0.00071}$	18096
d30	2020-03-20	SSO (Ic)	$2458929.10728^{+0.00110}_{-0.00110}$	18176
d31	2020-03-31	SSO (Ic)	$2458940.12175^{+0.00100}_{-0.00100}$	18886
d32	2020-05-11	MuSCAT2	$2458981.42173^{+0.00175}_{-0.00175}$	–
d33	2020-05-28	SSO (Ic)	$2458997.94503^{+0.00120}_{-0.00100}$	19426
d34	2020-12-15	McD (Ic)	$2459198.94930^{+0.00250}_{-0.00200}$	92622
d35	2021-01-09	CTIO (I)	$2459223.72820^{+0.00310}_{-0.00190}$	93100
d36	2021-01-09	ExTrA	$2459223.72880^{+0.00530}_{-0.01260}$	–
d37	2021-01-11	SAAO (I)	$2459226.47970^{+0.00200}_{-0.00210}$	93141
d38	2021-01-20	MuSCAT2	$2459234.74176^{+0.00055}_{-0.00055}$	–
d39	2021-01-20	CTIO (I)	$2459234.74340^{+0.00190}_{-0.00300}$	93449
d40	2021-02-03	CTIO (I)	$2459248.50750^{+0.00210}_{-0.00210}$	–
d41	2021-02-25	MuSCAT2	$2459270.53282^{+0.00081}_{-0.00081}$	–

Extended Data Table 3.2. Transit observations of LP 791-18 c

Label	Date	Telescope	Tc	ExoFOP tagid[3]
c0	2019-03-04	TESS	$2458546.50925^{+0.00110}_{-0.00110}$	–
c1	2019-03-08	TESS	$2458551.49865^{+0.00120}_{-0.00130}$	–
c2	2019-03-18	TESS	$2458561.47891^{+0.00130}_{-0.00120}$	–
c3	2019-03-23	TESS	$2458566.46935^{+0.00140}_{-0.00130}$	–
c4	2019-06-16	SSO (Ic)	$2458651.29773^{+0.00041}_{-0.00042}$	18731
c5	2019-10-14	Spitzer (4.5μm)	$2458771.05534^{+0.00015}_{-0.00014}$	–
c6	2019-10-19	Spitzer (4.5μm)	$2458776.04497^{+0.00014}_{-0.00015}$	–
c7	2019-12-13	Kuiper 1.5m (I)	$2458830.93368^{+0.00047}_{-0.00047}$	16194
c8	2020-01-27	ExTrA	$2458875.84313^{+0.00048}_{-0.00044}$	–
c9	2020-02-01	ExTrA	$2458880.83303^{+0.00053}_{-0.00056}$	–
c10	2020-02-06	ExTrA	$2458885.82335^{+0.00034}_{-0.00037}$	–
c11	2020-02-11	ExTrA	$2458890.81345^{+0.00036}_{-0.00037}$	–
c12	2020-02-16	VATT 1.8m (I)	$2458895.80312^{+0.00021}_{-0.00022}$	17714
c13	2020-02-21	ExTrA	$2458900.79250^{+0.00042}_{-0.00040}$	–
c14	2020-02-26	ExTrA	$2458905.78238^{+0.00045}_{-0.00041}$	–
c15	2020-03-02	ExTrA	$2458910.77307^{+0.00050}_{-0.00047}$	–
c16	2020-03-07	ExTrA	$2458915.76215^{+0.00058}_{-0.00058}$	–
c17	2020-03-12	SSO (I+z)	$2458920.75273^{+0.00035}_{-0.00035}$	–
c18	2020-03-12	ExTrA	$2458920.75279^{+0.00038}_{-0.00042}$	–
c19	2020-03-17	ExTrA	$2458925.74295^{+0.00044}_{-0.00043}$	–
c20	2020-03-22	ExTrA	$2458930.73283^{+0.00046}_{-0.00039}$	–
c21	2021-01-05	SSO (I)	$2459220.14744^{+0.00084}_{-0.00087}$	92954
c22	2021-01-10	SSO (I)	$2459225.13789^{+0.00042}_{-0.00045}$	93120
c23	2021-01-15	SSO (I)	$2459230.12733^{+0.00044}_{-0.00045}$	93196
c24	2021-01-25	SSO (I)	$2459240.10712^{+0.00057}_{-0.00058}$	93500

3. Supplementary

Extended Data Table 3.4. Planet Parameters

Parameter	Units	b	c	d
ExoTEP Results				
T_0	$BJD_{TBD} - 2457000$	$2458774.86973^{+0.00018}_{-0.00018}$	$2458771.055182^{+0.000091}_{-0.000097}$	$2458772.16211^{+0.00050}_{-0.00082}$
P	day	$0.9479957^{+0.0000027}_{-0.0000027}$	$4.9899093^{+0.0000074}_{-0.0000072}$	$2.7534360^{+0.0000183}_{-0.0000090}$
R_p/R_*	-	$0.0610^{+0.0014}_{-0.0014}$	$0.12364^{+0.00070}_{-0.00069}$	$0.05192^{+0.00090}_{-0.00090}$
R_p	$R_\oplus$	$1.212^{+0.055}_{-0.054}$	$2.458^{+0.096}_{-0.094}$	$1.032^{+0.044}_{-0.043}$
b	-	$0.33^{+0.24}_{-0.22}$	$0.103^{+0.094}_{-0.071}$	$0.27^{+0.17}_{-0.18}$
a/R_*	-	$11.91^{+0.66}_{-1.59}$	$36.94^{+0.28}_{-0.52}$	$25.19^{+1.03}_{-1.63}$
a	AU	$0.0100^{+0.0007}_{-0.0013}$	$0.0312^{+0.0012}_{-0.0013}$	$0.0212^{+0.0013}_{-0.0015}$
T_{14}	minutes	$37.18^{+0.67}_{-0.62}$	$69.25^{+0.38}_{-0.36}$	$50.69^{+1.19}_{-1.06}$
i	degrees	$88.39^{+1.07}_{-1.61}$	$89.84^{+0.11}_{-0.15}$	$89.39^{+0.41}_{-0.44}$
S_{inc}	$S_\oplus$	$24.14^{+0.60}_{-0.58}$	$2.637^{+0.066}_{-0.063}$	$5.83^{+0.15}_{-0.14}$
T_{eq}	K	$564.32^{+3.49}_{-3.39}$	$324.41^{+2.01}_{-1.95}$	$395.52^{+2.45}_{-2.38}$
TTVFast Results				
Mass	$M_\oplus$	-	$9.7^{+1.3}_{-1.2}$	$0.9^{+0.5}_{-0.4}$
e	-	-	$0.0452^{+0.0070}_{-0.0066}$	$0.0345^{+0.0098}_{-0.0092}$
ω	degrees	-	$160.03^{+7.72}_{-7.46}$	$147.4^{+16.2}_{-14.7}$
ω+M	degrees	-	$201.82^{+0.75}_{-0.76}$	$214.63^{+1.10}_{-1.00}$
$K_{RV,predicted}$	m/s	3.4 [3]	$12.96^{+2.09}_{-1.95}$	$1.36^{+0.85}_{-0.68}$

[1] Assuming an Earth-like albedo of A_b=0.3 and uniform heat redistribution. [2] ω+M represents the mean anomaly, as discussed in the Methods. [3] Prediction of RV semi-amplitude of Planet b is based on empirical mass-radius relationship

Extended Data Table 3.3. Stellar Parameters of LP 791-18

Parameter	Value	Source
Identifying Information		
TIC ID	181804752	TIC v8
α R.A. (hh:mm:ss)	11:02:45.709	*Gaia* eDR3
δ Decl. (dd:mm:ss)	−16:24:23.23	*Gaia* eDR3
Epoch (year)	2016.0	*Gaia* eDR3
$\mu_\alpha \cos\delta$ (mas yr^{-1})	-221.29 ± 0.04	*Gaia* eDR3
μ_δ (mas yr^{-1})	-58.84 ± 0.04	*Gaia* eDR3
Distance (pc)	26.65 ± 0.03	*Gaia* eDR3
Photometric Properties		
V (mag)	16.9 ± 0.2	TIC v8
G (mag)	15.0715 ± 0.0013	*Gaia* DR2
G_{BP} (mag)	17.23831 ± 0.072	*Gaia* DR2
G_{RP} (mag)	13.69512 ± 0.0029	*Gaia* DR2
u (mag)	21.28 ± 0.14	SDSS
g (mag)	17.8827 ± 0.0057	SDSS
r (mag)	16.2672 ± 0.0039	SDSS
i (mag)	14.3142 ± 0.0035	SDSS
z (mag)	13.2565 ± 0.0035	SDSS
J (mag)	11.559 ± 0.024	2MASS
H (mag)	10.993 ± 0.022	2MASS
K_S (mag)	10.644 ± 0.023	2MASS
$W1$ (mag)	10.426 ± 0.023	AllWISE
$W2$ (mag)	10.233 ± 0.21	AllWISE
$W3$ (mag)	10.024 ± 0.062	AllWISE
Spectroscopic and Derived Properties		
Spectral Type	M(6.1 ± 0.7)V	[11]
Barycentric RV (km s^{-1})	$+14.1 \pm 0.3$	”
Age (Gyr)	> 0.5	”
[Fe/H]	-0.09 ± 0.19	”
$T_{\rm eff}$	2960 ± 55	”
$\log_{10} g$ (cgs)	5.115 ± 0.094	”
v sin$i$	< 2	”
M_* ($M_\odot$)	0.139 ± 0.005	”
R_* ($R_\odot$)	0.182 ± 0.007	This paper
L_* ($L_\odot$)	0.00230 ± 0.00001	This paper
ld$_0$ TESS	0.26 ± 0.06	[11]
ld$_1$ TESS	0.55 ± 0.07	”
ld$_0$ *Spitzer* 4.5μm	$0.043^{+0.062}_{-0.038}$	This paper
ld$_0$ *Spitzer* 4.5μm	$0.099^{+0.114}_{-0.071}$	”
ld$_0$ LCO	0.34 ± 0.02	”
ld$_1$ LCO	0.40 ± 0.03	”
ld$_0$ MEarth	0.33 ± 0.02	”
ld$_1$ MEarth	0.38 ± 0.03	”
ld$_0$ TRAPPIST	0.26 ± 0.01	”
ld$_1$ TRAPPIST	0.33 ± 0.02	”

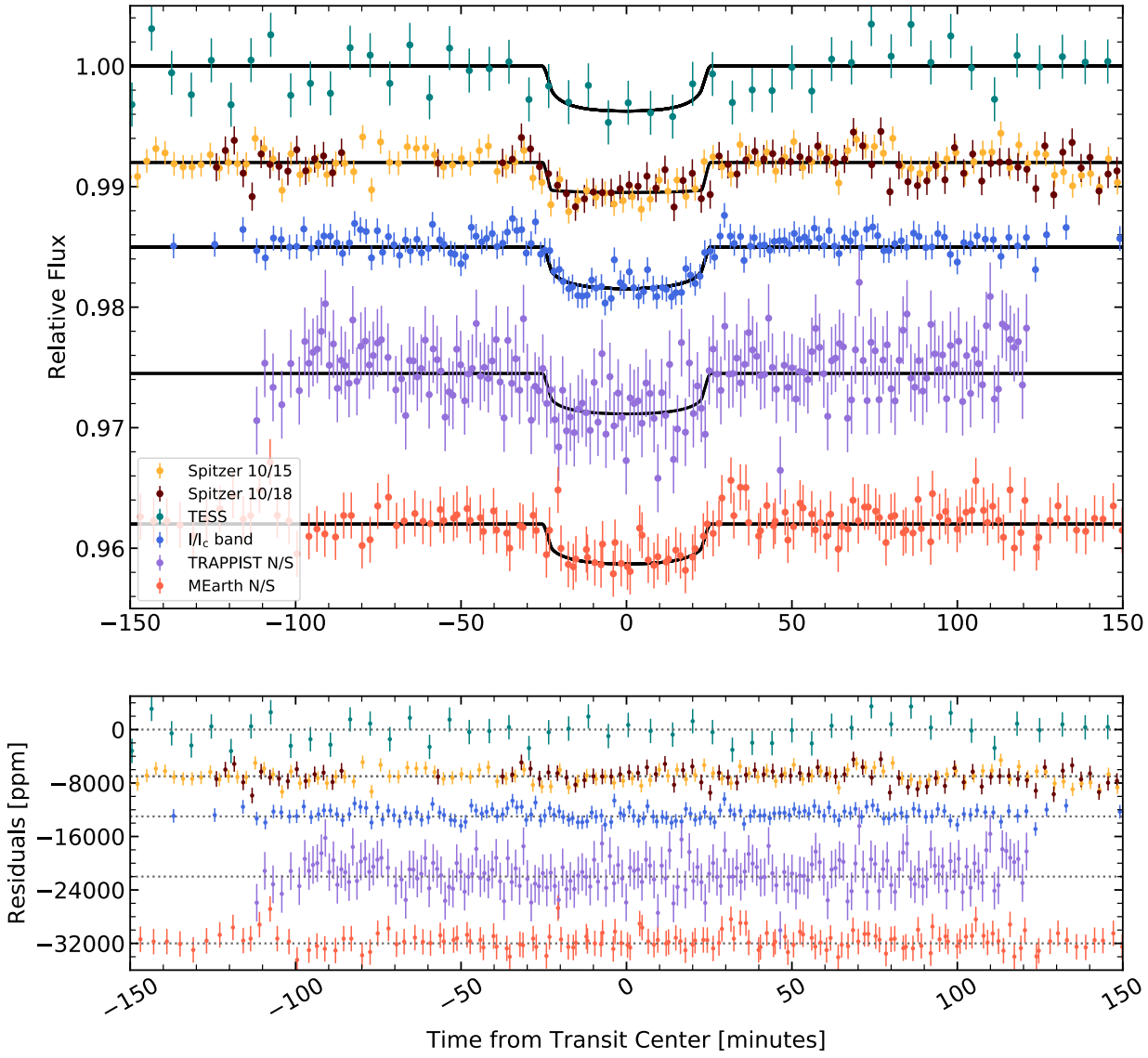

Extended Data Fig. 3.1. Transit observations of LP 791-18d. **a,** From top to bottom, we show the light curves (arbitrarily offset for visual clarity) from TESS, *Spitzer*, I/Ic band, TRAPPIST, and MEarth, in comparison to the transit model in the respective bandpass (black curve). The high signal-to-noise *Spitzer* transits are shown individually while the TESS and ground-based observations are phase-folded and binned by phase. **b,** Residuals to the best-fitting linear ephemeris joint fit (black lines in **a**). The *Spitzer* transits show deviations from the best fit linear ephemeris of approximately ±2.5 minutes caused by transit timing variations, which are visible by eye with the first transit (yellow) slightly early and the second transit (brown) slightly late (see ingress and egress in **a**). The data gap preceding the second *Spitzer* transit is a masked transit of LP 791-18b.

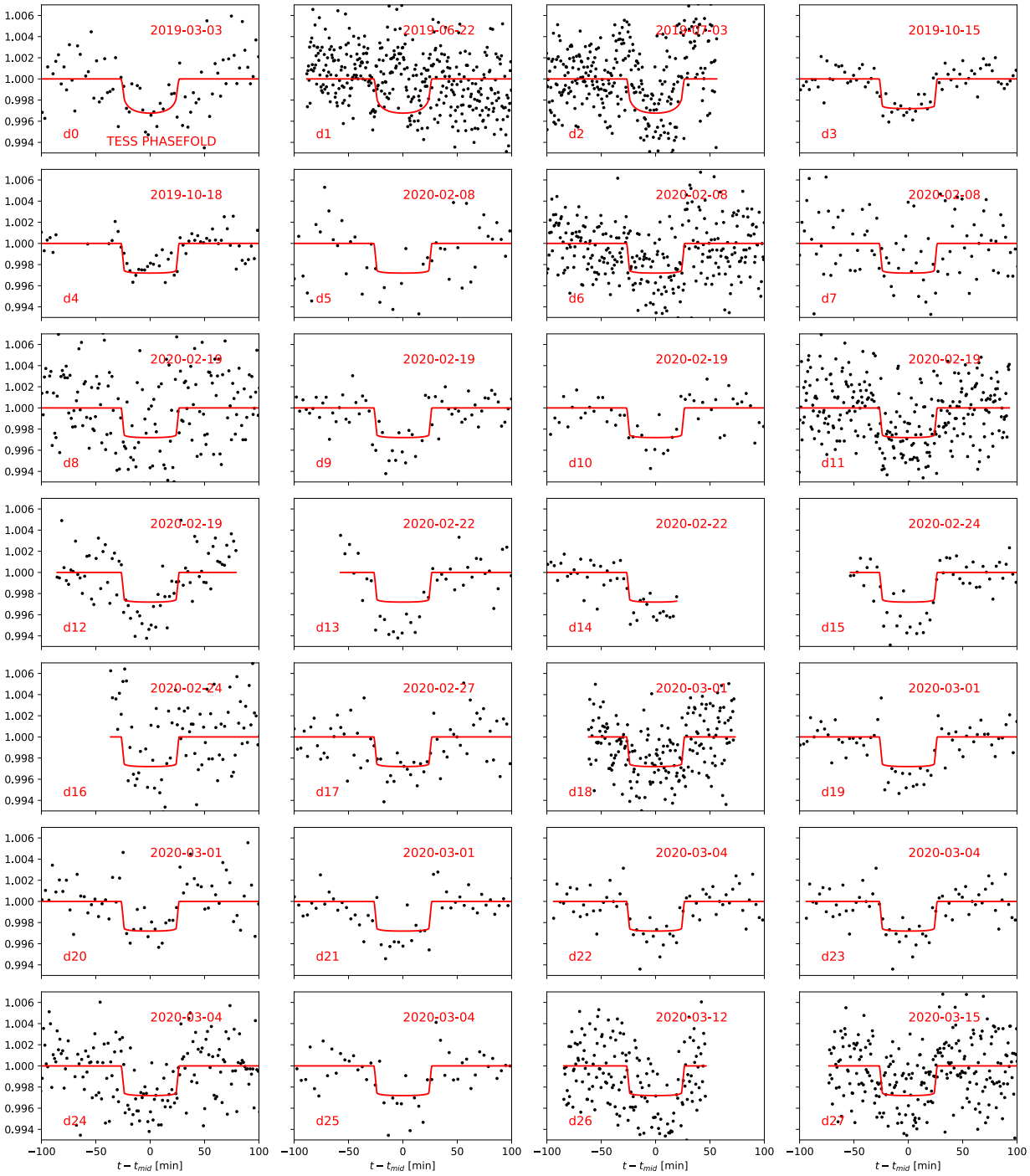

Extended Data Fig. 3.2. Individual transit observations of LP 791-18d. The observational time series of each transit observation (black points) is compared to the corresponding best-fitting transit light curve from the joint fit (red curve). Labels at the bottom left of each panel correspond to the labels listed in Extended Data Table 3.1. Each panel corresponds to an individual transit observation, with only the TESS data (d0) shown phase-folded.

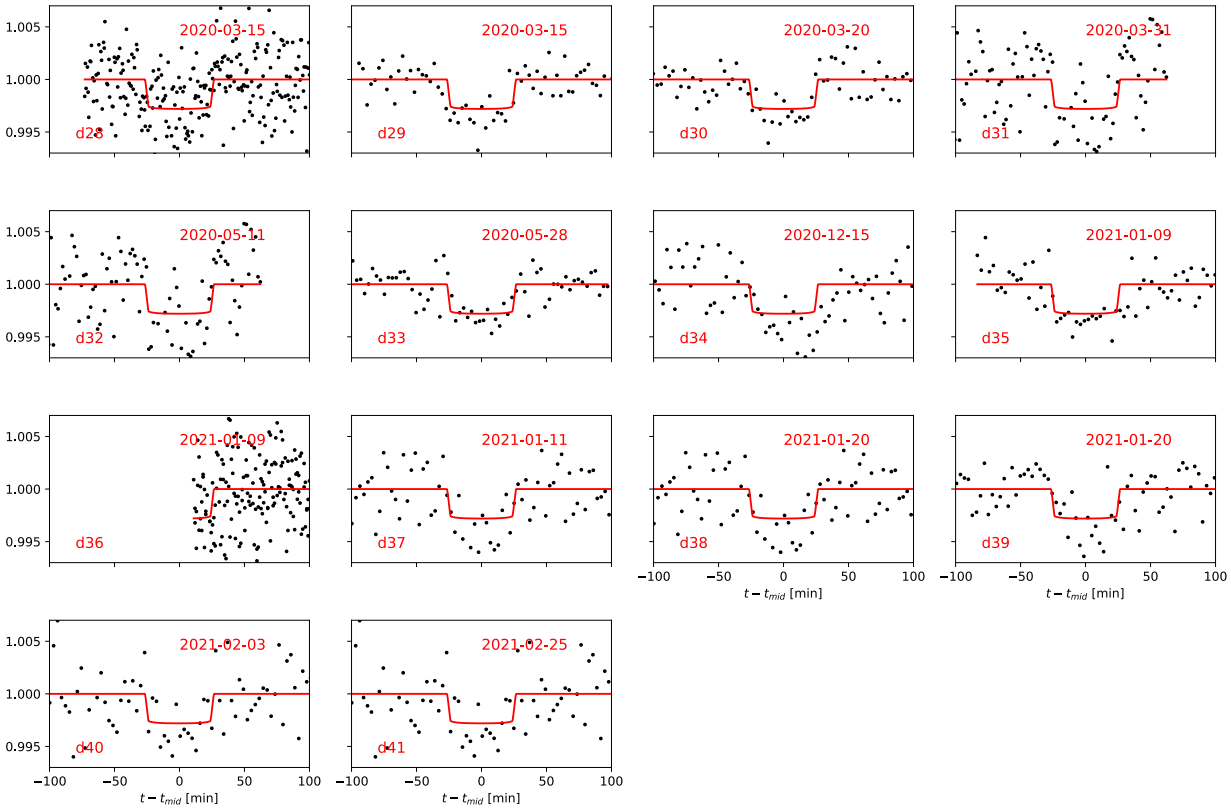

Extended Data Fig. 3.2 (cont.)

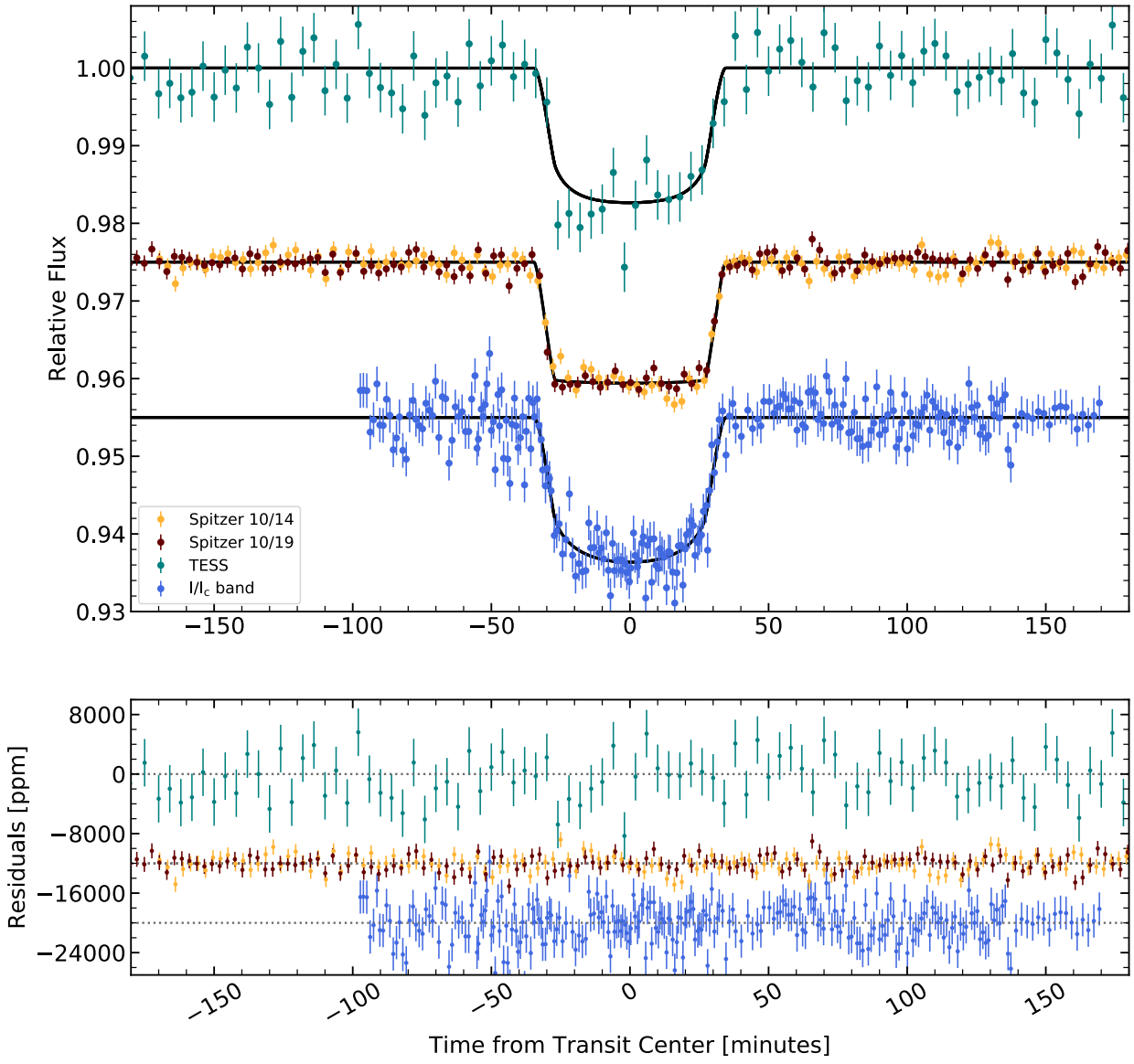

Extended Data Fig. 3.3. Transit observations of LP 791-18c. a, From top to bottom, we show the light curves (arbitrarily offset for visual clarity) from TESS, *Spitzer*, and I/Ic band, compared to the transit model in the respective bandpass (black curve). The high signal-to-noise *Spitzer* and I/Ic-band transits are shown individually while the TESS photometry is shown phase-folded and binned by phase. **b,** Residuals to the best-fitting transit model in the respective bandpass from the joint fit.

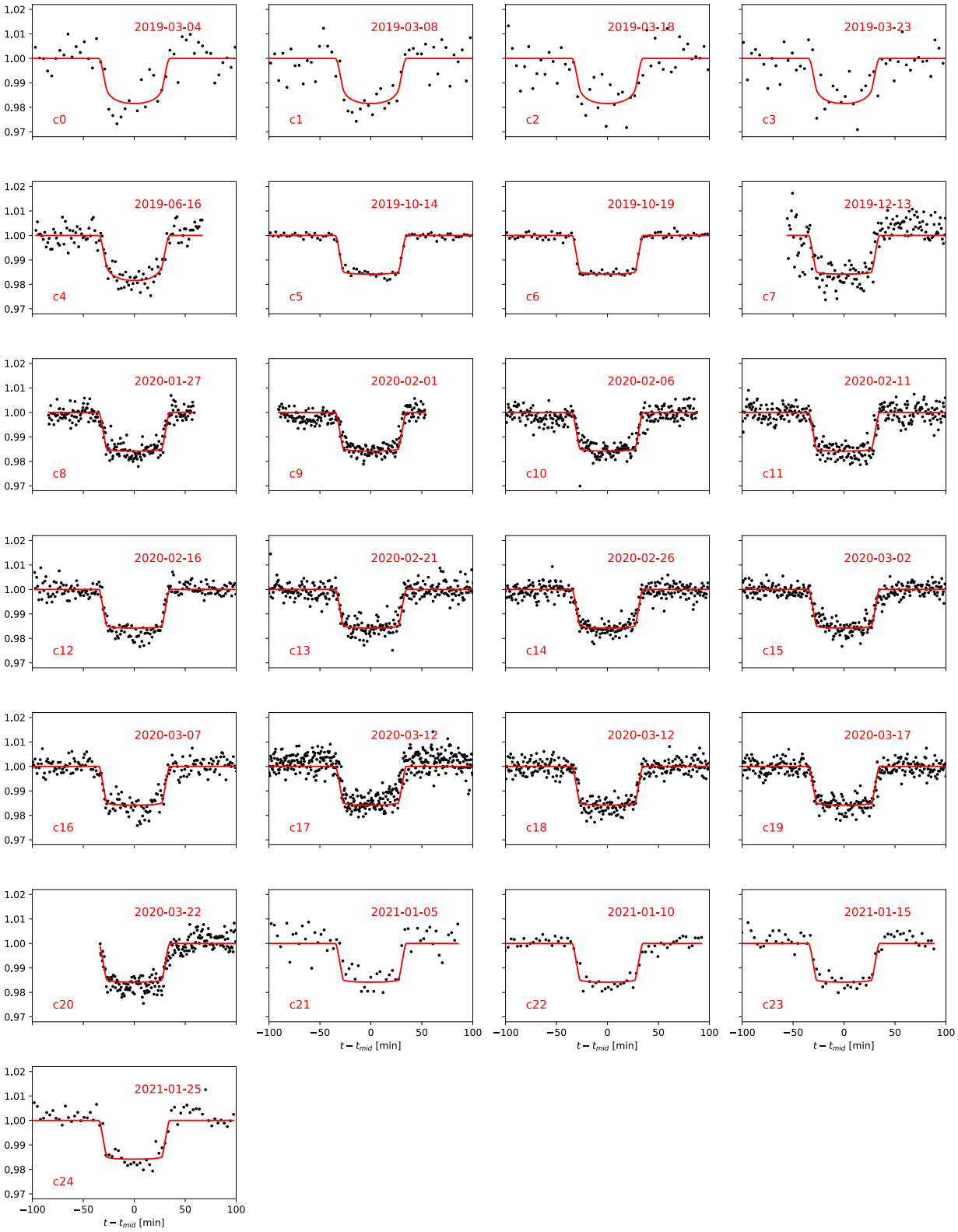

Extended Data Fig. 3.4. Individual transit observations of LP 791-18c. The observational time series of each transit observation (black points) is compared to the corresponding best-fitting transit light curve from the joint fit (red curve). Labels at the bottom left of each panel correspond to the labels listed in Table 3.2.

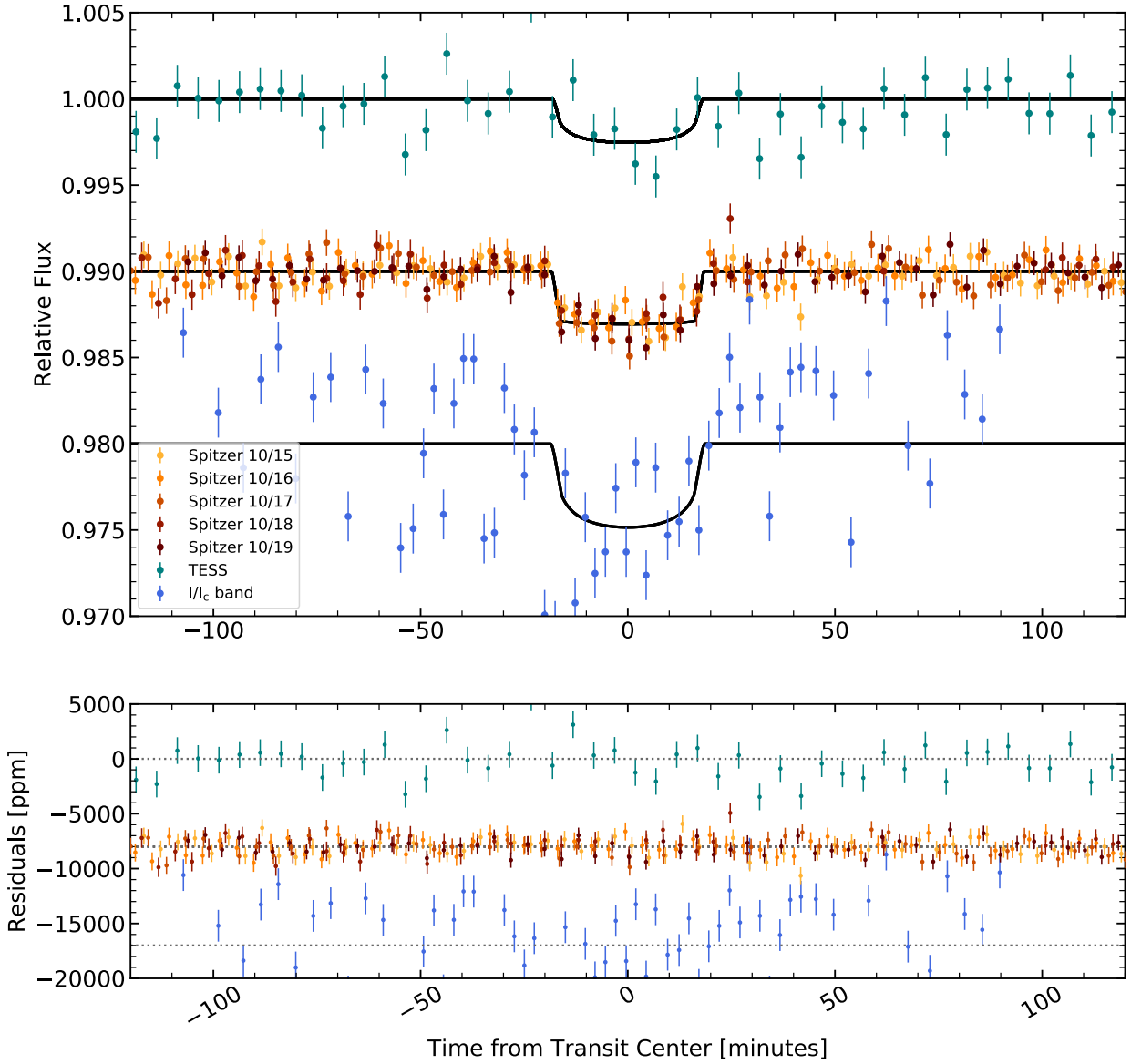

Extended Data Fig. 3.5. Transit observations of LP 791-18b. **a,** From top to bottom, we show the light curves (arbitrarily offset for visual clarity) from TESS, *Spitzer*, and I/Ic band, compared to the transit model in the respective bandpass (black curve). The high signal-to-noise *Spitzer* and I/Ic-band transits are shown individually while the TESS photometry is phase-folded and binned by phase. **b,** Residuals to the best-fitting transit model in the respective bandpass from the joint fit. The timing of the individual transits of planet b are consistent with the linear ephemeris within their 1σ uncertainties.

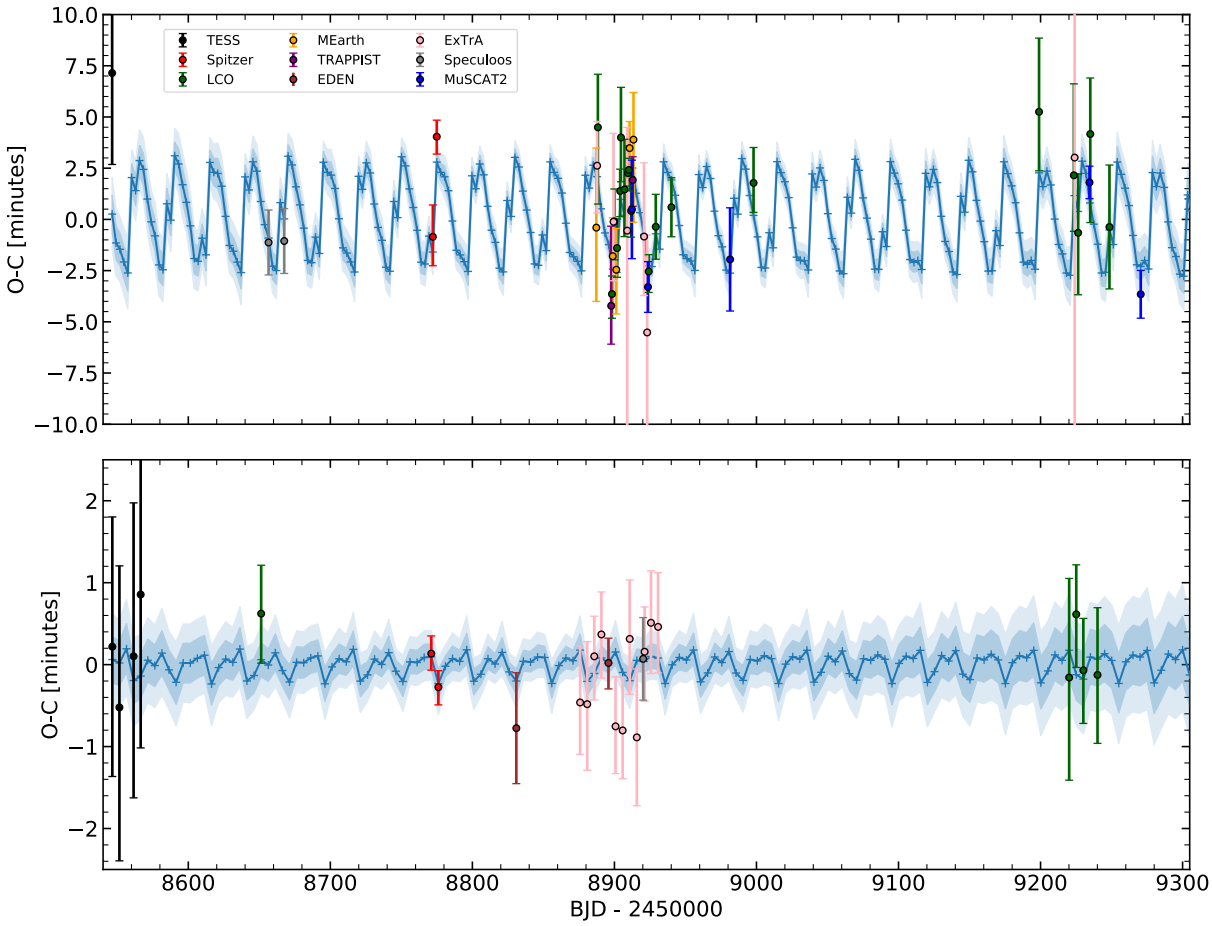

Extended Data Fig. 3.6. Transit timing variations of the Earth-sized planet LP 791-18d (top panel) and the sub-Neptune LP 791-18c (bottom panel). Colored data points indicate the transit timing measurements obtained with TESS (black), *Spitzer* (red), LCO (green), MuSCAT2 (dark blue), MEarth (yellow), TRAPPIST telescope (purple), EDEN (brown), ExTrA (pink), and SPECULOOS (grey), compared to the best-fitting TTVFast model (blue curve). The vertical axis represents the deviation from the best fitting linear ephemeris and the horizontal axis the Julian Date of the observation. Dark and light shaded regions illustrate the posterior population of models in the MCMC fit corresponding to 68% and 95% confidence, respectively.

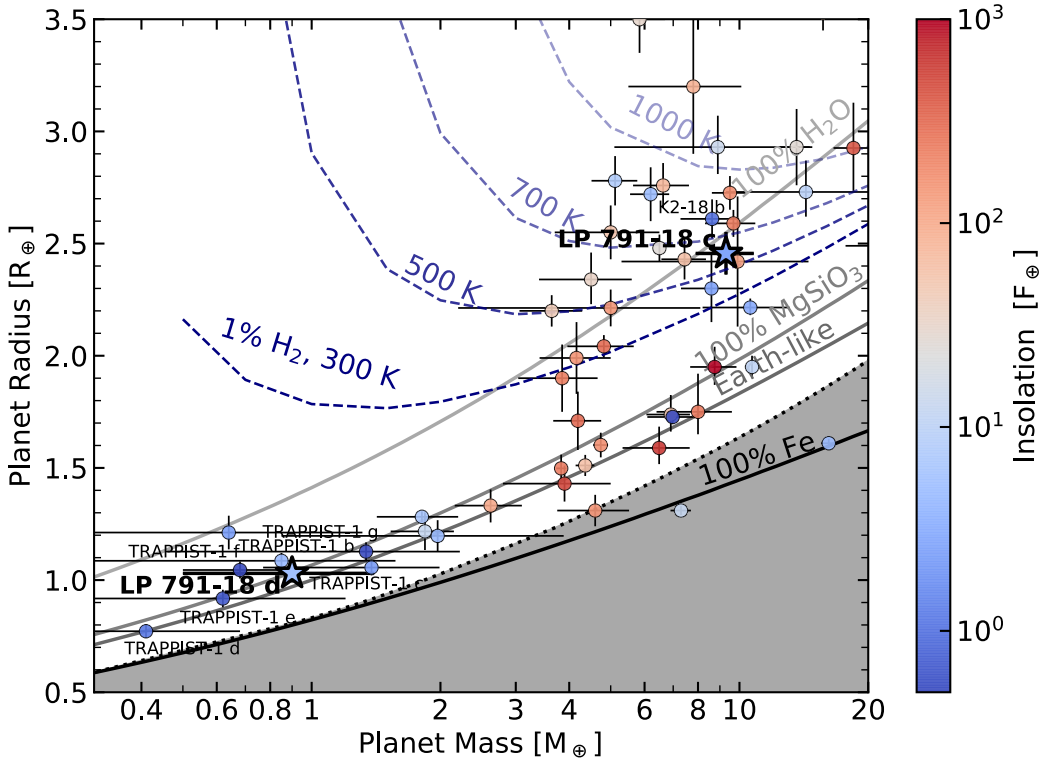

Extended Data Fig. 3.7. Mass-radius diagram of small exoplanets. LP 791-18c and d (bold stars) are shown in comparison to other known small planets with measured masses and radii (circles). Horizontal and vertical error bars represent the 68% confidence intervals of the mass and radius measurements for each planet, and the color indicates the planet's stellar insolation. Mass and radius measurements of LP 791-18c and d are reported in this work, while all other measurements are taken from the Exoplanet Archive. Modeled mass-radius curves are shown for a pure iron composition, an Earth-like composition [65], a pure rocky composition, a pure water composition, as well as an Earth-like core with 1% H_2 envelope at different temperatures [66]. A best match to the mass and radius of LP 791-18c is obtained for Earth-like core with about approximately 2% of the planet's mass in a H_2 envelope or, alternatively, a less-dense, water-rich core with maximum a minuscule H_2 envelope. LP 791-18d's composition is consistent with a rocky, potentially Earth-like composition. The TRAPPIST-1 planets and K2-18b are labeled for comparison to LP 791-18d and LP 791-18c, respectively.

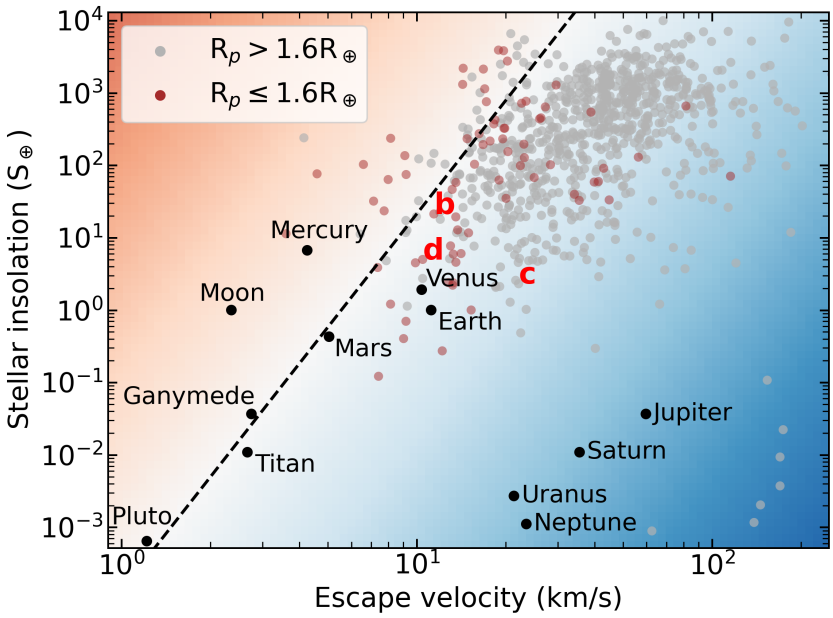

Extended Data Fig. 3.8. Escape velocity and insolation for solar system objects and exoplanets. The empirically determined 'cosmic shoreline' at I$\propto v_{esc}^{5.2}$ divides these objects into those which have and have not retained atmospheres [34]. The "Venus zone" extends from insolations above the one of the Earth to the cosmic shoreline where runaway atmospheric evaporation is expected at approximately 25 $S_\oplus$. In this simplified empirical picture, LP-791-18 d is predicted to have maintained its atmospheres.

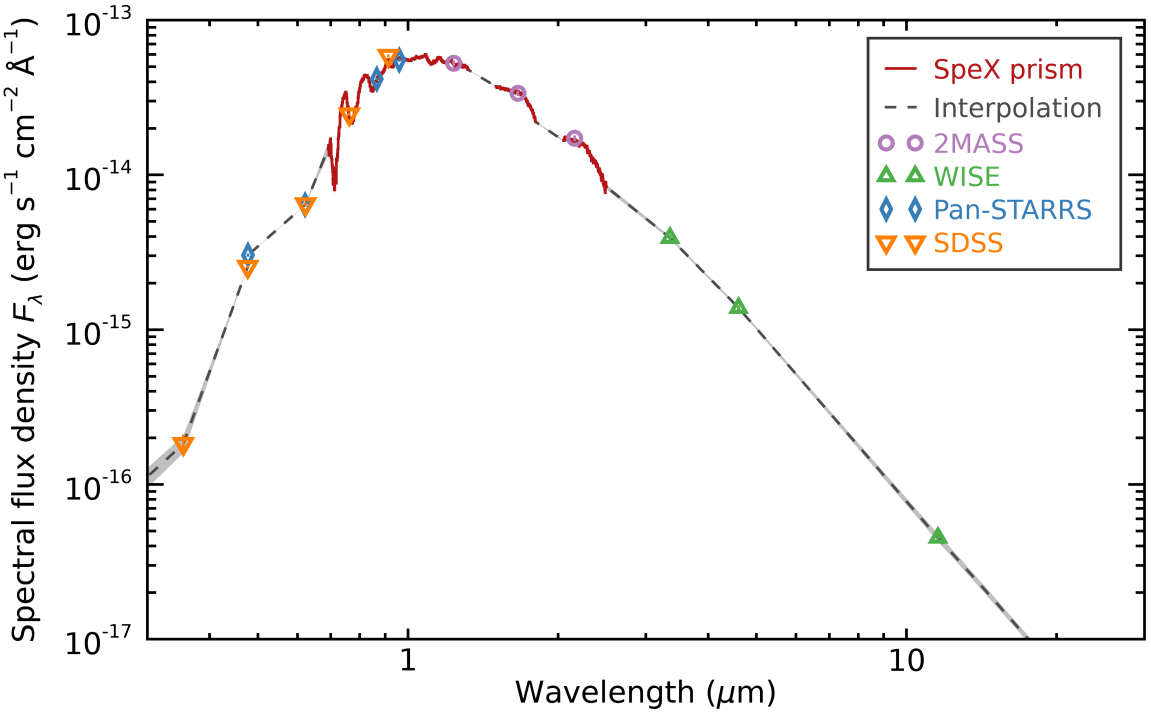

Extended Data Fig. 3.9. Fully empirical SED of the host star LP 791-18. The full empirical SED (dark gray dashed line with pale gray errors) is constructed from our observed IRTF/SpeX spectrum covering the peak of the SED (red line) and publicly available SDSS, PS1, 2MASS, and WISE broadband measurements.

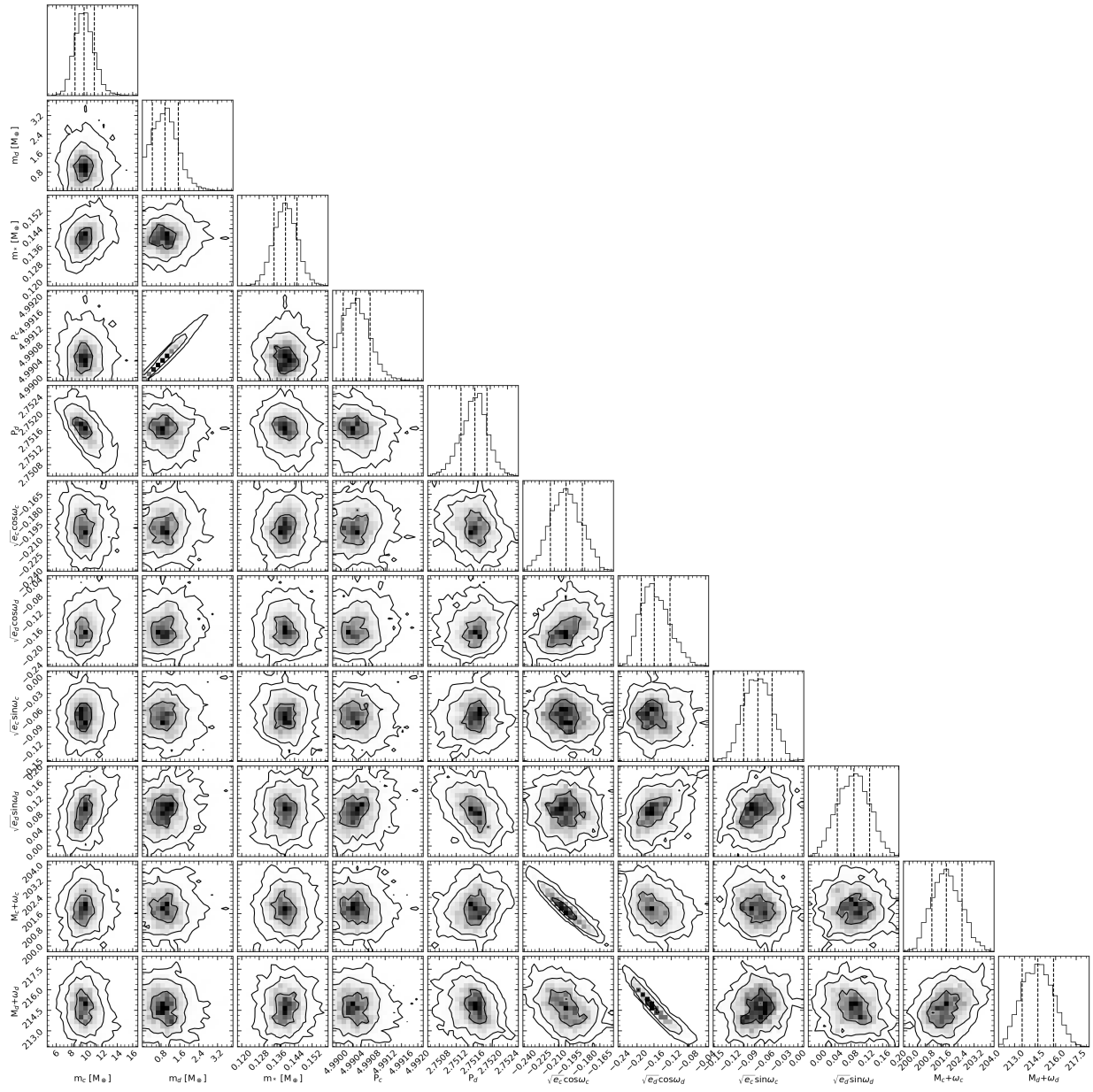

Extended Data Fig. 3.10. Posterior probability distributions of the masses and orbital parameter of LP 791-18c and d. The top panels in each column show the 1D marginalized posterior distributions for each parameter, with dashed vertical lines in the histograms indicating the marginalized 16th, 50th, and 84th percentiles. The 2D panels show the correlations between the parameters, with the light-grey, dark-grey, and black shadings representing the 1σ, 2σ and 3σ credible intervals. The orbital parameters P, $\sqrt{e}\cos\omega$, $\sqrt{e}\sin\omega$, and $M+\omega$ represent the instantaneous values at BJD = 2458763.03, the start time of the TTVFast simulation. Their exact values vary with time due to the planets' mutual gravitational interaction. The period of planet c and mass of planet d are correlated as the amplitude of the chopping in the TTVs are dependent on both the mass of the other planet and how close the two planets are to resonance.[12]

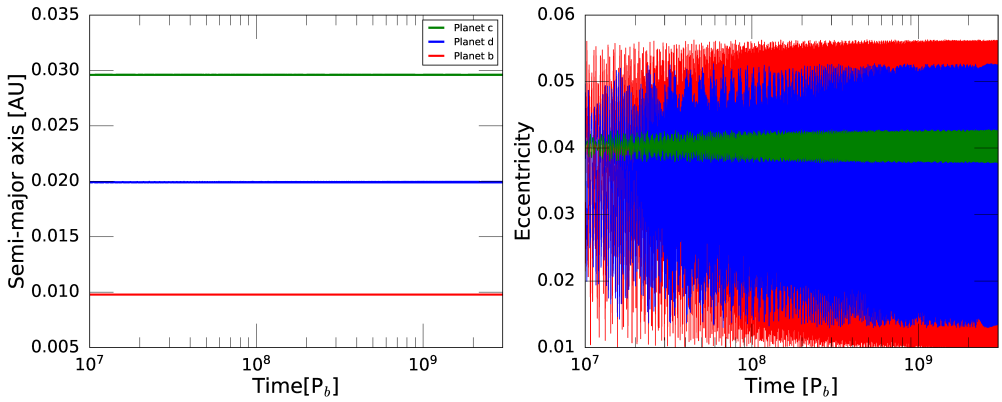

(a)

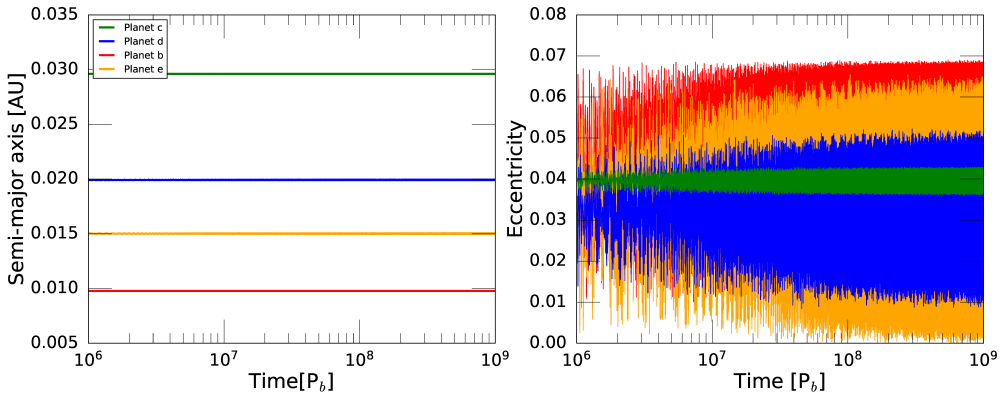

(b)

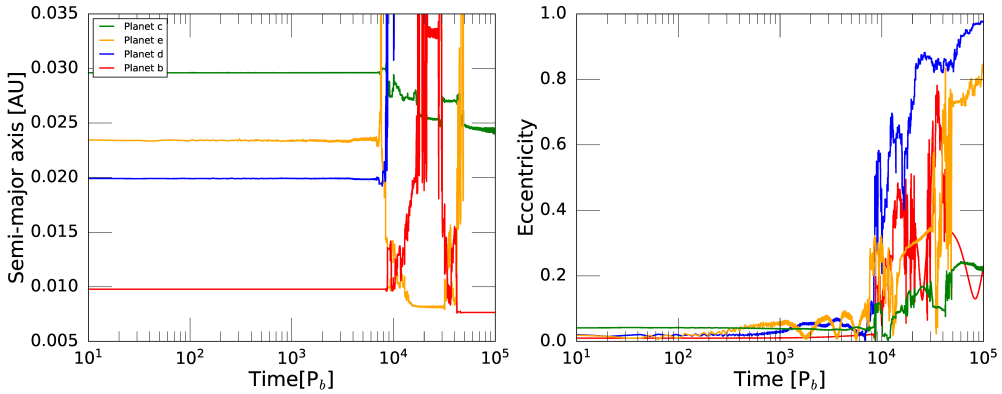

(c)

Extended Data Fig. 3.11. Dynamical stability analysis of LP 791-18 system. a, Long term integration for the observed LP 791-18 system showing that it is stable. **b,** Integration including an additional hypothetical 1 $M_\oplus$ at 0.015 AU. The system remains long term stable with even this hypothetical planet. **c,** Integration including an additional hypothetical 1 $M_\oplus$ at 0.023 AU. The system here becomes quickly unstable.

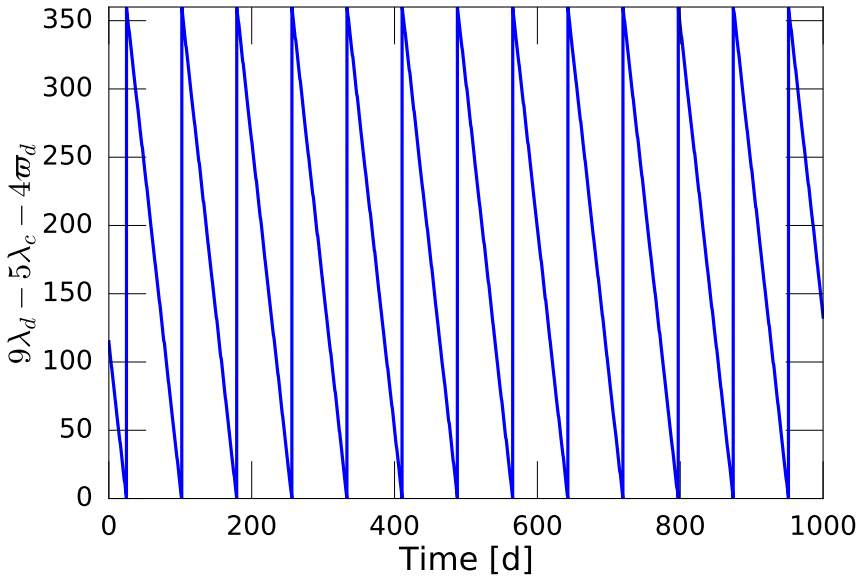

Extended Data Fig. 3.12. Temporal variation of the 9:5 resonant angle between LP 791-18c and d.

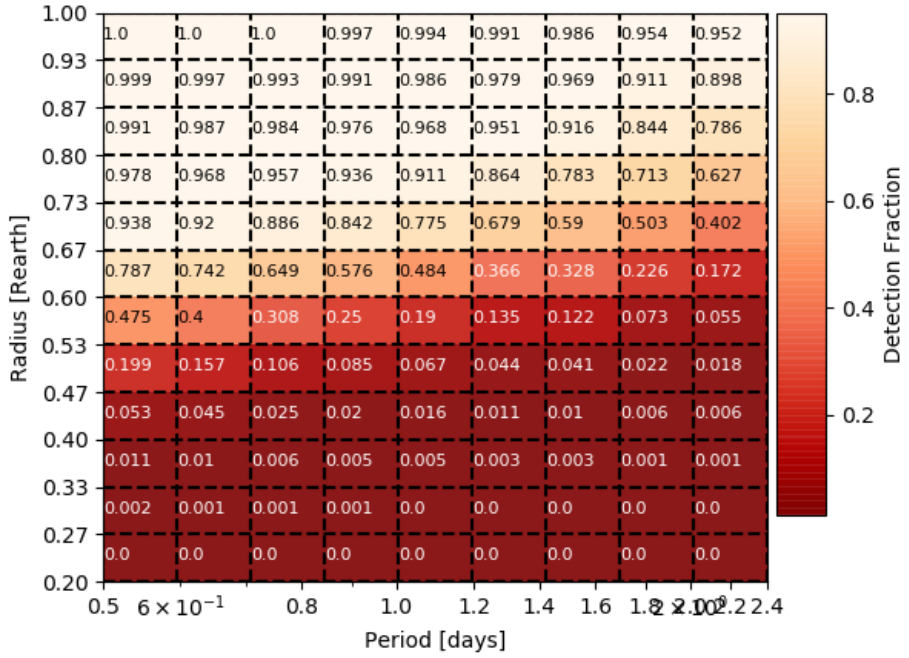

Extended Data Fig. 3.13. Sensitivity of the *Spitzer* light curve to detect additional planets in the system. Colors and numbers indicate the detection fraction of injected planets in a given planet size and orbital period bin from our injection/recovery test on the 124-hour *Spitzer* light curve. If a planet with radii greater than approximately $0.8R_\oplus$ had been present in the LP 791-18 system interior to LP 791-18d, it would have been detected with high probability. Meanwhile, planets smaller than 0.5–$0.6R_\oplus$ would likely have been missed in the *Spitzer* light curve.

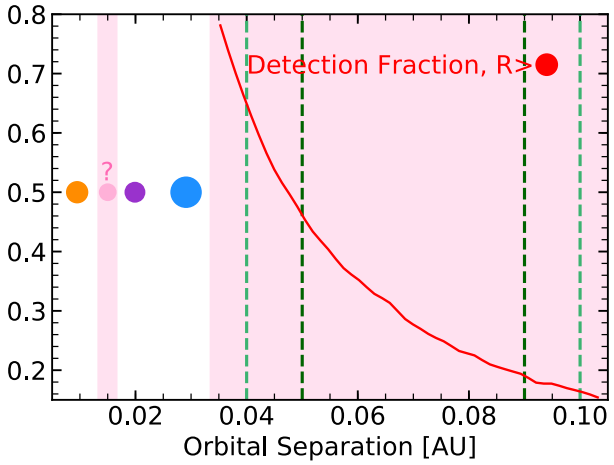

Extended Data Fig. 3.14. Orbits of the LP 791-18 planets with shaded pink regions representing periods at which the system could host additional undetected planets. For period greater than 5 days, the red curve illustrates the detection fraction for planet with radii greater than $1.2\,R_{\oplus}$, which is equivalent to the probability of a random planet with that period transiting during the time interval covered by the *Spitzer* observations.

References

[1] Eric Agol, Caroline Dorn, Simon L. Grimm, Martin Turbet, Elsa Ducrot, Laetitia Delrez, Michaël Gillon, Brice-Olivier Demory, Artem Burdanov, Khalid Barkaoui, Zouhair Benkhaldoun, Emeline Bolmont, Adam Burgasser, Sean Carey, Julien de Wit, Daniel Fabrycky, Daniel Foreman-Mackey, Jonas Haldemann, David M. Hernandez, James Ingalls, Emmanuel Jehin, Zachary Langford, Jérémy Leconte, Susan M. Lederer, Rodrigo Luger, Renu Malhotra, Victoria S. Meadows, Brett M. Morris, Francisco J. Pozuelos, Didier Queloz, Sean N. Raymond, Franck Selsis, Marko Sestovic, Amaury H. M. J. Triaud, and Valerie Van Grootel. Refining the Transit-timing and Photometric Analysis of TRAPPIST-1: Masses, Radii, Densities, Dynamics, and Ephemerides. *Planet. Sci. J.*, 2(1):1, January 2021. ISSN 2632-3338. doi: 10.3847/PSJ/abd022. URL `https://iopscience.iop.org/article/10.3847/PSJ/abd022/meta`. Publisher: IOP Publishing.

[2] Amy C. Barr. Mobile lid convection beneath Enceladus' south polar terrain. *Journal of Geophysical Research (Planets)*, 113:E07009, July 2008. ISSN 0148-0227. doi: 10.1029/2008JE003114. URL `http://adsabs.harvard.edu/abs/2008JGRE..113.7009B`.

[3] Amy C. Barr, Vera Dobos, and László L. Kiss. Interior structures and tidal heating in the TRAPPIST-1 planets. *A&A*, 613:A37, May 2018. ISSN 0004-6361, 1432-0746. doi: 10.1051/0004-6361/201731992. URL `https://www.aanda.org/articles/aa/abs/2018/05/aa31992-17/aa31992-17.html`. Publisher: EDP Sciences.

[4] Björn Benneke, Michael Werner, Erik Petigura, Heather Knutson, Courtney Dressing, Ian J. M. Crossfield, Joshua E. Schlieder, John Livingston, Charles Beichman, Jessie Christiansen, Jessica Krick, Varoujan Gorjian, Andrew W. Howard, Evan Sinukoff, David R. Ciardi, and Rachel L. Akeson. Spitzer Observations Confirm and Rescue the Habitable-zone Super-Earth K2-18b for Future Characterization. *ApJ*, 834 (2):187, 2017. ISSN 0004-637X. doi: 10.3847/1538-4357/834/2/187. URL `http://stacks.iop.org/0004-637X/834/i=2/a=187`.

[5] Björn Benneke, Heather A. Knutson, Joshua Lothringer, Ian J. M. Crossfield, Julianne I. Moses, Caroline Morley, Laura Kreidberg, Benjamin J. Fulton, Diana Dragomir, Andrew W. Howard, Ian Wong, Jean-Michel Désert, Peter R. McCullough, Eliza M.-R. Kempton, Jonathan Fortney, Ronald Gilliland, Drake Deming, and Joshua Kammer. A sub-Neptune exoplanet with a low-metallicity methane-depleted atmosphere and Mie-scattering clouds. *Nature Astronomy*, page 1, July 2019. ISSN 2397-3366. doi: 10.1038/s41550-019-0800-5. URL `https://www.nature.com/articles/s41550-019-0800-5`.

[6] Björn Benneke, Ian Wong, Caroline Piaulet, Heather A. Knutson, Joshua Lothringer, Caroline V. Morley, Ian J. M. Crossfield, Peter Gao, Thomas P. Greene, Courtney Dressing, Diana Dragomir, Andrew W. Howard, Peter R. McCullough, Eliza M.-R. Kempton, Jonathan J. Fortney, and Jonathan Fraine. Water Vapor and Clouds on the Habitable-zone Sub-Neptune Exoplanet K2-18b. *ApJL*, 887(1):L14, December 2019. ISSN 2041-8205. doi: 10.3847/2041-8213/ab59dc. URL https://doi.org/10.3847%2F2041-8213%2Fab59dc.

[7] Zachory K. Berta, Jonathan Irwin, David Charbonneau, Christopher J. Burke, and Emilio E. Falco. TRANSIT DETECTION IN THE MEarth SURVEY OF NEARBY m DWARFS: BRIDGING THE CLEAN-FIRST, SEARCH-LATER DIVIDE. *The Astronomical Journal*, 144(5):145, oct 2012. doi: 10.1088/0004-6256/144/5/145. URL https://doi.org/10.1088%2F0004-6256%2F144%2F5%2F145.

[8] X. Bonfils, J. M. Almenara, L. Jocou, A. Wunsche, P. Kern, A. Delboulbé, X. Delfosse, P. Feautrier, T. Forveille, L. Gluck, S. Lafrasse, Y. Magnard, D. Maurel, T. Moulin, F. Murgas, P. Rabou, S. Rochat, A. Roux, and E. Stadler. ExTrA: Exoplanets in transit and their atmospheres. In *Techniques and Instrumentation for Detection of Exoplanets VII*, volume 9605, page 96051L. International Society for Optics and Photonics, September 2015. doi: 10.1117/12.2186999. URL https://www.spiedigitallibrary.org/conference-proceedings-of-spie/9605/96051L/ExTrA-Exoplanets-in-transit-and-their-atmospheres/10.1117/12.2186999.short.

[9] Ryan Cloutier and Kristen Menou. Evolution of the Radius Valley around Low-mass Stars from Kepler and K2. *AJ*, 159(5):211, April 2020. ISSN 1538-3881. doi: 10.3847/1538-3881/ab8237. URL https://doi.org/10.3847%2F1538-3881%2Fab8237. Publisher: American Astronomical Society.

[10] Ryan Cloutier, Jason D. Eastman, Joseph E. Rodriguez, Nicola Astudillo-Defru, Xavier Bonfils, Annelies Mortier, Christopher A. Watson, Manu Stalport, Matteo Pinamonti, Florian Lienhard, Avet Harutyunyan, Mario Damasso, David W. Latham, Karen A. Collins, Robert Massey, Jonathan Irwin, Jennifer G. Winters, David Charbonneau, Carl Ziegler, Elisabeth Matthews, Ian J. M. Crossfield, Laura Kreidberg, Samuel N. Quinn, George Ricker, Roland Vanderspek, Sara Seager, Joshua Winn, Jon M. Jenkins, Michael Vezie, Stéphane Udry, Joseph D. Twicken, Peter Tenenbaum, Alessandro Sozzetti, Damien Ségransan, Joshua E. Schlieder, Dimitar Sasselov, Nuno C. Santos, Ken Rice, Benjamin V. Rackham, Ennio Poretti, Giampaolo Piotto, David Phillips, Francesco Pepe, Emilio Molinari, Lucile Mignon, Giuseppina Micela, Claudio Melo, José R. de Medeiros, Michel Mayor, Rachel A. Matson, Aldo F. Martinez Fiorenzano, Andrew W. Mann, Antonio Magazzú, Christophe Lovis, Mercedes López-Morales, Eric Lopez, Jack J. Lissauer, Sébastien Lépine, Nicholas Law, John F. Kielkopf, John A.

Johnson, Eric L. N. Jensen, Steve B. Howell, Erica Gonzales, Adriano Ghedina, Thierry Forveille, Pedro Figueira, Xavier Dumusque, Courtney D. Dressing, René Doyon, Rodrigo F. Díaz, Luca Di Fabrizio, Xavier Delfosse, Rosario Cosentino, Dennis M. Conti, Kevin I. Collins, Andrew Collier Cameron, David Ciardi, Douglas A. Caldwell, Christopher Burke, Lars Buchhave, César Briceño, Patricia Boyd, François Bouchy, Charles Beichman, Étienne Artigau, and Jose M. Almenara. A Pair of TESS Planets Spanning the Radius Valley around the Nearby Mid-M Dwarf LTT 3780. AJ, 160(1):3, July 2020. doi: 10.3847/1538-3881/ab91c2.

[11] Ian J. M. Crossfield, William Waalkes, Elisabeth R. Newton, Norio Narita, Philip Muirhead, Kristo Ment, Elisabeth Matthews, Adam Kraus, Veselin Kostov, Molly R. Kosiarek, Stephen R. Kane, Howard Isaacson, Sam Halverson, Erica Gonzales, Mark Everett, Diana Dragomir, Karen A. Collins, Ashley Chontos, David Berardo, Jennifer G. Winters, Joshua N. Winn, Nicholas J. Scott, Barbara Rojas-Ayala, Aaron C. Rizzuto, Erik A. Petigura, Merrin Peterson, Teo Mocnik, Thomas Mikal-Evans, Nicholas Mehrle, Rachel Matson, Masayuki Kuzuhara, Jonathan Irwin, Daniel Huber, Chelsea Huang, Steve Howell, Andrew W. Howard, Teruyuki Hirano, Benjamin J. Fulton, Trent Dupuy, Courtney D. Dressing, Paul A. Dalba, David Charbonneau, Jennifer Burt, Zachory Berta-Thompson, Björn Benneke, Noriharu Watanabe, Joseph D. Twicken, Motohide Tamura, Joshua Schlieder, S. Seager, Mark E. Rose, George Ricker, Elisa Quintana, Sébastien Lépine, David W. Latham, Takayuki Kotani, Jon M. Jenkins, Yasunori Hori, Knicole Colon, and Douglas A. Caldwell. A Super-Earth and Sub-Neptune Transiting the Late-type M Dwarf LP 791-18. *ApJL*, 883(1):L16, September 2019. ISSN 2041-8205. doi: 10.3847/2041-8213/ab3d30. URL `https://iopscience.iop.org/article/10.3847/2041-8213/ab3d30/meta`. Publisher: IOP Publishing.

[12] Katherine M. Deck and Eric Agol. Measurement of Planet Masses with Transit Timing Variations Due to Synodic "Chopping" Effects. *ApJ*, 802(2):116, 2015. ISSN 0004-637X. doi: 10.1088/0004-637X/802/2/116. URL `http://stacks.iop.org/0004-637X/802/i=2/a=116`.

[13] Katherine M. Deck, Eric Agol, Matthew J. Holman, and David Nesvorný. TTVFast: An Efficient and Accurate Code for Transit Timing Inversion Problems. *ApJ*, 787(2):132, 2014. ISSN 0004-637X. doi: 10.1088/0004-637X/787/2/132. URL `http://stacks.iop.org/0004-637X/787/i=2/a=132`.

[14] D. Deming, S. Seager, J. Winn, E. Miller-Ricci, M. Clampin, D. Lindler, T. Greene, D. Charbonneau, G. Laughlin, G. Ricker, D. Latham, and K. Ennico. Discovery and Characterization of Transiting Super Earths Using an All-Sky Transit Survey and Follow-up by the James Webb Space Telescope. *Publications of the Astronomical Society of the Pacific*, 121(883):952–967, September 2009. ISSN 0004-6280. URL `http://www.jstor.org/stable/10.1086/605913`. ArticleType: research-article /

Full publication date: September 2009 / Copyright © 2009 The University of Chicago Press.

[15] Drake Deming, Heather Knutson, Joshua Kammer, Benjamin J. Fulton, James Ingalls, Sean Carey, Adam Burrows, Jonathan J. Fortney, Kamen Todorov, Eric Agol, Nicolas Cowan, Jean-Michel Desert, Jonathan Fraine, Jonathan Langton, Caroline Morley, and Adam P. Showman. SPITZER SECONDARY ECLIPSES OF THE DENSE, MODESTLY-IRRADIATED, GIANT EXOPLANET HAT-P- USING PIXEL-LEVEL DECORRELATION. *ApJ*, 805(2):132, May 2015. ISSN 0004-637X. doi: 10.1088/0004-637X/805/2/132. URL http://iopscience.iop.org/article/10.1088/0004-637X/805/2/132/meta.

[16] B.-O. Demory, D. Ségransan, T. Forveille, D. Queloz, J.-L. Beuzit, X. Delfosse, E. Di Folco, P. Kervella, J.-B. Le Bouquin, C. Perrier, M. Benisty, G. Duvert, K.-H. Hofmann, B. Lopez, and R. Petrov. Mass-radius relation of low and very low-mass stars revisited with the VLTI. *A&A*, 505(1):205–215, October 2009. ISSN 0004-6361, 1432-0746. doi: 10.1051/0004-6361/200911976. URL https://www.aanda.org/articles/aa/abs/2009/37/aa11976-09/aa11976-09.html. Number: 1 Publisher: EDP Sciences.

[17] Vera Dobos and Edwin L. Turner. Viscoelastic Models of Tidally Heated Exomoons. *The Astrophysical Journal*, 804:41, May 2015. ISSN 0004-637X. doi: 10.1088/0004-637X/804/1/41. URL http://adsabs.harvard.edu/abs/2015ApJ...804...41D.

[18] Néstor Espinoza, Diana Kossakowski, and Rafael Brahm. juliet: a versatile modelling tool for transiting and non-transiting exoplanetary systems. *Monthly Notices of the Royal Astronomical Society*, 490(2):2262–2283, December 2019. ISSN 0035-8711. doi: 10.1093/mnras/stz2688. URL https://doi.org/10.1093/mnras/stz2688.

[19] Joseph C. Filippazzo, Emily L. Rice, Jacqueline Faherty, Kelle L. Cruz, Mollie M. Van Gordon, and Dagny L. Looper. FUNDAMENTAL PARAMETERS AND SPECTRAL ENERGY DISTRIBUTIONS OF YOUNG AND FIELD AGE OBJECTS WITH MASSES SPANNING THE STELLAR TO PLANETARY REGIME. *ApJ*, 810(2):158, September 2015. ISSN 0004-637X. doi: 10.1088/0004-637X/810/2/158. URL https://doi.org/10.1088%2F0004-637x%2F810%2F2%2F158. Publisher: IOP Publishing.

[20] H.-J. Fischer and T. Spohn. Thermal-orbital histories of viscoelastic models of Io (J1). *Icarus*, 83:39–65, January 1990. ISSN 0019-1035. doi: 10.1016/0019-1035(90)90005-T. URL http://adsabs.harvard.edu/abs/1990Icar...83...39F.

[21] Daniel Foreman-Mackey, David W. Hogg, Dustin Lang, and Jonathan Goodman. emcee: The MCMC Hammer. *Publications of the Astronomical Society of the Pacific*, 125(925):306–312, March 2013. ISSN 0004-6280. doi: 10.1086/670067. URL http://www.jstor.org/stable/10.1086/670067.

[22] Benjamin J. Fulton and Erik A. Petigura. The California-Kepler Survey. VII. Precise Planet Radii Leveraging Gaia DR2 Reveal the Stellar Mass Dependence of the Planet Radius Gap. *AJ*, 156(6):264, November 2018. ISSN 1538-3881. doi: 10.3847/1538-3881/aae828. URL https://doi.org/10.3847%2F1538-3881%2Faae828.

[23] Benjamin J. Fulton, Erik A. Petigura, Andrew W. Howard, Howard Isaacson, Geoffrey W. Marcy, Phillip A. Cargile, Leslie Hebb, Lauren M. Weiss, John Asher Johnson, Timothy D. Morton, Evan Sinukoff, Ian J. M. Crossfield, and Lea A. Hirsch. The california-KeplerSurvey. III. a gap in the radius distribution of small planets. *The Astronomical Journal*, 154(3):109, aug 2017. doi: 10.3847/1538-3881/aa80eb. URL https://doi.org/10.3847%2F1538-3881%2Faa80eb.

[24] Aidan Gibbs, Alex Bixel, Benjamin V. Rackham, Dániel Apai, Martin Schlecker, Néstor Espinoza, Luigi Mancini, Wen-Ping Chen, Thomas Henning, Paul Gabor, Richard Boyle, Jose Perez Chavez, Allie Mousseau, Jeremy Dietrich, Quentin Jay Socia, Wing Ip, Chow-Choong Ngeow, An-Li Tsai, Asmita Bhandare, Victor Marian, Hans Baehr, Samantha Brown, Maximilian Häberle, Miriam Keppler, Karan Molaverdikhani, and Paula Sarkis. EDEN: Sensitivity Analysis and Transiting Planet Detection Limits for Nearby Late Red Dwarfs. *AJ*, 159(4):169, March 2020. ISSN 1538-3881. doi: 10.3847/1538-3881/ab7926. URL https://doi.org/10.3847/1538-3881/ab7926. Publisher: American Astronomical Society.

[25] M. Gillon, A. H. M. J. Triaud, J. J. Fortney, B.-O. Demory, E. Jehin, M. Lendl, P. Magain, P. Kabath, D. Queloz, R. Alonso, D. R. Anderson, A. Collier Cameron, A. Fumel, L. Hebb, C. Hellier, A. Lanotte, P. F. L. Maxted, N. Mowlavi, and B. Smalley. The TRAPPIST survey of southern transiting planets - I. Thirty eclipses of the ultra-short period planet WASP-43 b. *A&A*, 542:A4, June 2012. ISSN 0004-6361, 1432-0746. doi: 10.1051/0004-6361/201218817. URL http://dx.doi.org/10.1051/0004-6361/201218817.

[26] M. Gillon, A. H. M. J. Triaud, J. J. Fortney, B. O. Demory, E. Jehin, M. Lendl, P. Magain, P. Kabath, D. Queloz, R. Alonso, D. R. Anderson, A. Collier Cameron, A. Fumel, L. Hebb, C. Hellier, A. Lanotte, P. F. L. Maxted, N. Mowlavi, and B. Smalley. The TRAPPIST survey of southern transiting planets. I. Thirty eclipses of the ultra-short period planet WASP-43 b. A&A, 542:A4, June 2012. doi: 10.1051/0004-6361/201218817.

[27] Michaël Gillon. Searching for red worlds. *Nat Astron*, 2(4):344–344, April 2018. ISSN 2397-3366. doi: 10.1038/s41550-018-0443-y. URL https://www.nature.com/articles/s41550-018-0443-y. Number: 4 Publisher: Nature Publishing Group.

[28] Michaël Gillon, Victoria Meadows, Eric Agol, Adam J. Burgasser, Drake Deming, René Doyon, Jonathan Fortney, Laura Kreidberg, James Owen, Franck Selsis, Julien de Wit,

Jacob Lustig-Yaeger, and Benjamin V. Rackham. The TRAPPIST-1 JWST Community Initiative. *Bulletin of the AAS*, 52(2), December 2020. ISSN ,. doi: 10.3847/25c2cfeb.afbf0205. URL https://baas.aas.org/pub/2020i0329/release/1. Publisher: PubPub.

[29] Sivan Ginzburg, Hilke E. Schlichting, and Re'em Sari. Core-powered mass-loss and the radius distribution of small exoplanets. MNRAS, 476(1):759–765, May 2018. doi: 10.1093/mnras/sty290.

[30] Thomas P. Greene, Michael R. Line, Cezar Montero, Jonathan J. Fortney, Jacob Lustig-Yaeger, and Kyle Luther. Characterizing Transiting Exoplanet Atmospheres with JWST. *ApJ*, 817(1):17, 2016. ISSN 0004-637X. doi: 10.3847/0004-637X/817/1/17. URL http://stacks.iop.org/0004-637X/817/i=1/a=17.

[31] Akash Gupta and Hilke E Schlichting. Sculpting the valley in the radius distribution of small exoplanets as a by-product of planet formation: the core-powered mass-loss mechanism. *Monthly Notices of the Royal Astronomical Society*, 487(1):24–33, July 2019. ISSN 0035-8711. doi: 10.1093/mnras/stz1230. URL https://doi.org/10.1093/mnras/stz1230.

[32] Wade G. Henning, Richard J. O'Connell, and Dimitar D. Sasselov. Tidally Heated Terrestrial Exoplanets: Viscoelastic Response Models. *The Astrophysical Journal*, 707: 1000–1015, December 2009. ISSN 0004-637X. doi: 10.1088/0004-637X/707/2/1000. URL http://adsabs.harvard.edu/abs/2009ApJ...707.1000H.

[33] Jon M. Jenkins, Joseph D. Twicken, Sean McCauliff, Jennifer Campbell, Dwight Sanderfer, David Lung, Masoud Mansouri-Samani, Forrest Girouard, Peter Tenenbaum, Todd Klaus, Jeffrey C. Smith, Douglas A. Caldwell, A. Dean Chacon, Christopher Henze, Cory Heiges, David W. Latham, Edward Morgan, Daryl Swade, Stephen Rinehart, and Roland Vanderspek. The TESS science processing operations center. In Gianluca Chiozzi and Juan C. Guzman, editors, *Software and Cyberinfrastructure for Astronomy IV*, volume 9913, pages 1232 – 1251. International Society for Optics and Photonics, SPIE, 2016. doi: 10.1117/12.2233418. URL https://doi.org/10.1117/12.2233418.

[34] Stephen R. Kane, Ravi Kumar Kopparapu, and Shawn D. Domagal-Goldman. On the frequency of potential venus analogs from kepler data. *The Astrophysical Journal*, 794 (1):L5, Sep 2014. ISSN 2041-8213. doi: 10.1088/2041-8205/794/1/l5. URL http://dx.doi.org/10.1088/2041-8205/794/1/L5.

[35] Eliza M.-R. Kempton, Jacob L. Bean, Dana R. Louie, Drake Deming, Daniel D. B. Koll, Megan Mansfield, Jessie L. Christiansen, Mercedes López-Morales, Mark R. Swain, Robert T. Zellem, Sarah Ballard, Thomas Barclay, Joanna K. Barstow, Natasha E. Batalha, Thomas G. Beatty, Zach Berta-Thompson, Jayne Birkby, Lars A. Buchhave, David Charbonneau, Nicolas B. Cowan, Ian Crossfield, Miguel de Val-Borro, René Doyon, Diana Dragomir, Eric Gaidos, Kevin Heng, Renyu Hu, Stephen R.

Kane, Laura Kreidberg, Matthias Mallonn, Caroline V. Morley, Norio Narita, Valerio Nascimbeni, Enric Pallé, Elisa V. Quintana, Emily Rauscher, Sara Seager, Evgenya L. Shkolnik, David K. Sing, Alessandro Sozzetti, Keivan G. Stassun, Jeff A. Valenti, and Carolina von Essen. A Framework for Prioritizing the TESS Planetary Candidates Most Amenable to Atmospheric Characterization. *PASP*, 130(993):114401, September 2018. ISSN 1538-3873. doi: 10.1088/1538-3873/aadf6f. URL https://doi.org/10.1088%2F1538-3873%2Faadf6f. Publisher: IOP Publishing.

[36] Edwin S. Kite and Megan Barnett. Exoplanet secondary atmosphere loss and revival. 2020.

[37] Quentin Kral, Jeanne Davoult, and Benjamin Charnay. Formation of secondary atmospheres on terrestrial planets by late disk accretion. *Nature Astronomy*, 4(8): 769–775, August 2020. ISSN 2397-3366. doi: 10.1038/s41550-020-1050-2. URL https://www.nature.com/articles/s41550-020-1050-2. Number: 8 Publisher: Nature Publishing Group.

[38] Laura Kreidberg. batman: BAsic Transit Model cAlculatioN in Python. *PASP*, 127 (957):1161, November 2015. ISSN 1538-3873. doi: 10.1086/683602. URL http://iopscience.iop.org/article/10.1086/683602/meta.

[39] Eve J. Lee and Eugene Chiang. BREEDING SUPER-EARTHS AND BIRTHING SUPER-PUFFS IN TRANSITIONAL DISKS. *ApJ*, 817(2):90, January 2016. ISSN 0004-637X. doi: 10.3847/0004-637X/817/2/90. URL https://doi.org/10.3847%2F0004-637x%2F817%2F2%2F90.

[40] Eve J. Lee, Eugene Chiang, and Chris W. Ormel. Make Super-Earths, Not Jupiters: Accreting Nebular Gas onto Solid Cores at 0.1 AU and Beyond. *ApJ*, 797(2):95, December 2014. ISSN 0004-637X. doi: 10.1088/0004-637X/797/2/95. URL http://iopscience.iop.org/0004-637X/797/2/95.

[41] Eric D. Lopez and Ken Rice. How formation time-scales affect the period dependence of the transition between rocky super-Earths and gaseous sub-Neptunes and implications for eta_earth. *Mon Not R Astron Soc*, 479(4):5303–5311, October 2018. ISSN 0035-8711. doi: 10.1093/mnras/sty1707. URL https://academic.oup.com/mnras/article/479/4/5303/5049017.

[42] Taro Matsuo, Thomas P. Greene, Roy R. Johnson, Robert E. Mcmurray, Thomas L. Roellig, and Kimberly Ennico. Photometric Precision of a Si:As Impurity Band Conduction Mid-infrared Detector and Application to Transit Spectroscopy. *PASP*, 131 (1006):124502, November 2019. ISSN 1538-3873. doi: 10.1088/1538-3873/ab42f1. URL https://doi.org/10.1088/1538-3873/ab42f1. Publisher: IOP Publishing.

[43] W. B. Moore. Tidal heating and convection in Io. *Journal of Geophysical Research (Planets)*, 108:5096, August 2003. ISSN 0148-0227. doi: 10.1029/2002JE001943. URL http://adsabs.harvard.edu/abs/2003JGRE..108.5096M.

[44] C A Murray, L Delrez, P P Pedersen, D Queloz, M Gillon, A Burdanov, E Ducrot, L J Garcia, F Lienhard, B O Demory, E Jehin, J McCormac, D Sebastian, S Sohy, S J Thompson, A H M J Triaud, V V Grootel, M N Günther, and C X Huang. Photometry and performance of SPECULOOS-South. *Monthly Notices of the Royal Astronomical Society*, 495(2):2446–2457, June 2020. ISSN 0035-8711. doi: 10.1093/mnras/staa1283. URL https://doi.org/10.1093/mnras/staa1283.

[45] Carl D. Murray and S. F. Dermott. *Solar system dynamics*. Cambridge University Press, 2000.

[46] Norio Narita, Akihiko Fukui, Nobuhiko Kusakabe, Noriharu Watanabe, Enric Palle, Hannu Parviainen, Pilar Montañés-Rodríguez, Felipe Murgas, Matteo Monelli, Marta Aguiar, Jorge Andres Perez Prieto, Álex Oscoz, Jerome de Leon, Mayuko Mori, Motohide Tamura, Tomoyasu Yamamuro, Victor J. S. Béjar, Nicolas Crouzet, Diego Hidalgo, Peter Klagyivik, Rafael Luque, and Taku Nishiumi. MuSCAT2: four-color simultaneous camera for the 1.52-m Telescopio Carlos Sánchez. *JATIS*, 5(1):015001, December 2018. ISSN 2329-4124, 2329-4221. doi: 10.1117/1.JATIS.5.1.015001. URL https://www.spiedigitallibrary.org/journals/Journal-of-Astronomical-Telescopes-Instruments-and-Systems/volume-5/issue-1/015001/MuSCAT2--four-color-simultaneous-camera-for-the-10.1117/1.JATIS.5.1.015001.short. Publisher: International Society for Optics and Photonics.

[47] Philip Nutzman and David Charbonneau. Design considerations for a ground-based transit search for habitable planets orbiting m dwarfs. *Publications of the Astronomical Society of the Pacific*, 120(865):317–327, mar 2008. doi: 10.1086/533420. URL https://doi.org/10.1086%2F533420.

[48] James E. Owen and Beatriz Campos Estrada. Testing exoplanet evaporation with multi-transiting systems. MNRAS, 491(4):5287–5297, Feb 2020. doi: 10.1093/mnras/stz3435.

[49] James E. Owen and Yanqin Wu. The Evaporation Valley in the Kepler Planets. *ApJ*, 847(1):29, September 2017. ISSN 0004-637X. doi: 10.3847/1538-4357/aa890a. URL https://doi.org/10.3847%2F1538-4357%2Faa890a.

[50] H. Parviainen and S. Aigrain. ldtk: Limb Darkening Toolkit. *Mon Not R Astron Soc*, 453(4):3821–3826, November 2015. ISSN 0035-8711. doi: 10.1093/mnras/stv1857. URL https://academic.oup.com/mnras/article/453/4/3821/2593683.

[51] Hanno Rein and Daniel Tamayo. whfast: a fast and unbiased implementation of a symplectic Wisdom?Holman integrator for long-term gravitational simulations. *Monthly Notices of the Royal Astronomical Society*, 452(1):376–388, 07 2015. ISSN 0035-8711. doi: 10.1093/mnras/stv1257. URL https://doi.org/10.1093/mnras/stv1257.

[52] Rein, H. and Liu, S.-F. Rebound: an open-source multi-purpose n-body code for collisional dynamics. *A&A*, 537:A128, 2012. doi: 10.1051/0004-6361/201118085. URL

https://doi.org/10.1051/0004-6361/201118085.

[53] Jörg Renner, Brian Evans, and Greg Hirth. On the rheologically critical melt fraction. *Earth and Planetary Science Letters*, 181:585–594, September 2000. ISSN 0012-821X. doi: 10.1016/S0012-821X(00)00222-3. URL http://adsabs.harvard.edu/abs/2000E%26PSL.181..585R.

[54] M. Segatz, T. Spohn, M. N. Ross, and G. Schubert. Tidal dissipation, surface heat flow, and figure of viscoelastic models of Io. *Icarus*, 75:187–206, August 1988. ISSN 0019-1035. doi: 10.1016/0019-1035(88)90001-2. URL http://adsabs.harvard.edu/abs/1988Icar...75..187S.

[55] V. Shuvalov. Atmospheric erosion induced by oblique impacts. *Meteoritics and Planetary Science*, 44(8):1095–1105, August 2009. doi: 10.1111/j.1945-5100.2009.tb01209.x.

[56] Jeffrey C. Smith, Martin C. Stumpe, Jeffrey E. Van Cleve, Jon M. Jenkins, Thomas S. Barclay, Michael N. Fanelli, Forrest R. Girouard, Jeffery J. Kolodziejczak, Sean D. McCauliff, Robert L. Morris, and Joseph D. Twicken. Kepler Presearch Data Conditioning II - A Bayesian Approach to Systematic Error Correction. *PASP*, 124 (919):1000, September 2012. ISSN 1538-3873. doi: 10.1086/667697. URL https://iopscience.iop.org/article/10.1086/667697/meta. Publisher: IOP Publishing.

[57] V. S. Solomatov and L.-N. Moresi. Scaling of time-dependent stagnant lid convection: Application to small-scale convection on Earth and other terrestrial planets. *Journal of Geophysical Research*, 105:21795–21818, September 2000. ISSN 0148-0227. doi: 10.1029/2000JB900197. URL http://adsabs.harvard.edu/abs/2000JGR...10521795S.

[58] John R. Spencer, Julie A. Rathbun, Larry D. Travis, Leslie K. Tamppari, Laura Barnard, Terry Z. Martin, and Alfred S. McEwen. Io's Thermal Emission from the Galileo Photopolarimeter- Radiometer. *Science*, 288:1198–1201, May 2000. ISSN 0036-8075. doi: 10.1126/science.288.5469.1198. URL http://adsabs.harvard.edu/abs/2000Sci...288.1198S.

[59] Keivan G. Stassun, Ryan J. Oelkers, Martin Paegert, Guillermo Torres, Joshua Pepper, Nathan De Lee, Kevin Collins, David W. Latham, Philip S. Muirhead, Jay Chittidi, Bárbara Rojas-Ayala, Scott W. Fleming, Mark E. Rose, Peter Tenenbaum, Eric B. Ting, Stephen R. Kane, Thomas Barclay, Jacob L. Bean, C. E. Brassuer, David Charbonneau, Jian Ge, Jack J. Lissauer, Andrew W. Mann, Brian McLean, Susan Mullally, Norio Narita, Peter Plavchan, George R. Ricker, Dimitar Sasselov, S. Seager, Sanjib Sharma, Bernie Shiao, Alessandro Sozzetti, Dennis Stello, Roland Vanderspek, Geoff Wallace, and Joshua N. Winn. The Revised TESS Input Catalog and Candidate Target List. *AJ*, 158(4):138, September 2019. ISSN 1538-3881. doi: 10.3847/1538-3881/ab3467. URL

https://doi.org/10.3847/1538-3881/ab3467. Publisher: American Astronomical Society.

[60] Martin C. Stumpe, Jeffrey C. Smith, Jeffrey E. Van Cleve, Joseph D. Twicken, Thomas S. Barclay, Michael N. Fanelli, Forrest R. Girouard, Jon M. Jenkins, Jeffery J. Kolodziejczak, Sean D. McCauliff, and Robert L. Morris. Kepler Presearch Data Conditioning I—Architecture and Algorithms for Error Correction in Kepler Light Curves. *PASP*, 124(919):985, August 2012. ISSN 1538-3873. doi: 10.1086/667698. URL https://iopscience.iop.org/article/10.1086/667698/meta. Publisher: IOP Publishing.

[61] Martin C. Stumpe, Jeffrey C. Smith, Joseph H. Catanzarite, Jeffrey E. Van Cleve, Jon M. Jenkins, Joseph D. Twicken, and Forrest R. Girouard. Multiscale systematic error correction via wavelet-based bandsplitting inKeplerData. *Publications of the Astronomical Society of the Pacific*, 126(935):100–114, jan 2014. doi: 10.1086/674989. URL https://doi.org/10.1086%2F674989.

[62] Glenn J. Veeder, Dennis L. Matson, Torrence V. Johnson, Ashley G. Davies, and Diana L. Blaney. The polar contribution to the heat flow of Io. *Icarus*, 169:264–270, May 2004. ISSN 0019-1035. doi: 10.1016/j.icarus.2003.11.016. URL http://adsabs.harvard.edu/abs/2004Icar..169..264V.

[63] M. C. Wyatt, Q. Kral, and C. A. Sinclair. Susceptibility of planetary atmospheres to mass-loss and growth by planetesimal impacts: the impact shoreline. MNRAS, 491(1): 782–802, January 2020. doi: 10.1093/mnras/stz3052.

[64] Jun Yang, Yonggang Liu, Yongyun Hu, and Dorian S. Abbot. WATER TRAPPING ON TIDALLY LOCKED TERRESTRIAL PLANETS REQUIRES SPECIAL CONDITIONS. *ApJL*, 796(2):L22, November 2014. ISSN 2041-8205. doi: 10.1088/2041-8205/796/2/L22. URL https://iopscience.iop.org/article/10.1088/2041-8205/796/2/L22/meta. Publisher: IOP Publishing.

[65] Li Zeng, Dimitar D. Sasselov, and Stein B. Jacobsen. Mass–Radius Relation for Rocky Planets Based on PREM. *ApJ*, 819(2):127, 2016. ISSN 0004-637X. doi: 10.3847/0004-637X/819/2/127. URL http://stacks.iop.org/0004-637X/819/i=2/a=127.

[66] Li Zeng, Stein B. Jacobsen, Dimitar D. Sasselov, Michail I. Petaev, Andrew Vanderburg, Mercedes Lopez-Morales, Juan Perez-Mercader, Thomas R. Mattsson, Gongjie Li, Matthew Z. Heising, Aldo S. Bonomo, Mario Damasso, Travis A. Berger, Hao Cao, Amit Levi, and Robin D. Wordsworth. Growth model interpretation of planet size distribution. *PNAS*, 116(20):9723–9728, May 2019. ISSN 0027-8424, 1091-6490. doi: 10.1073/pnas.1812905116. URL https://www.pnas.org/content/116/20/9723.

Summary and Conclusion

With the expansion of our catalogue of exoplanets from a few dozen to a few thousand in only the past two decades, our understanding of planetary systems has changed dramatically. To build a complete picture of how these systems, including our own, are formed, we must identify those rare, fortuitous targets which can be studied in detail through mass measurements and transit spectroscopy. This is most important for the super-Earths and sub-Neptunes, the preferred outcomes of planet formation, which don't exist in our solar system and yet are abundant in the Universe. Furthermore, we must find these planets across a range of radii, insolations and temperatures, around a variety of stars and in systems of varying architecture to reveal the changes in planet formation under unique circumstances. In this work, we've introduced two extremely useful cards to this growing deck of exoplanets: Wolf 503 b and LP 791-18 d.

At 2 Earth radii, Wolf 503 b is intriguing because it is exactly the rare class planet along the boundary between super-Earths and sub-Neptunes for which it is difficult to predict whether the planet should retain a thick atmosphere. As shown in Fig. 4.1, Wolf 503 b lies at a radius and insolation for which essentially no planets have been determined to be either unambiguously gaseous or rocky. Depending on the planet's bulk composition, the planet's gravitational influence on the star should result in an easily measured radial velocity signature of at least 2.5 m/s. At its radius, a mass of roughly 10 $M_\oplus$ or larger would indicate that the planet must be rocky, whereas a small gas envelope of only 0.01% H/He by mass would suggest a mass of 8 $M_\oplus$ (with larger envelopes resulting in smaller masses), and a sufficient number of measurements could reveal the planet to be unambiguously rocky or gaseous. Either composition will help to resolve the nature and boundaries of the radius gap. It's more likely that, like other planets near the radius gap and with a limited precision on the mass, its mass could be explained by a rocky core low in iron with little to no atmosphere or a dense iron-rich core enveloped in a thick atmosphere both could account for its' mass. In this case, transit spectroscopy, ideally with the JWST, could be used to break this degeneracy.

In the gas-empty scenario, Wolf 503 b should actually have formed at a location in the stellar disk with enough gases to support the accretion of a significant H/He atmosphere and

is unambiguously a sub-Neptune. In both the gas-poor and gas-rich formation pathways for the small planet distribution, Wolf 503 b should be in the centre of the radius gap and is interpreted to have an intermediate atmosphere, smaller than those of most sub-Neptunes but large enough to account for a fraction of the planet's radius. For the gas-poor scenario, the planet would have maintained this thin envelope from creation, having not had enough material to accrete a thicker envelope, and in the gas-rich scenario, Wolf 503 b would have initially accreted a thick primordial atmosphere which was only partially evaporated, either because it exists at an insolation for which photoevaporation did not completely strip the planet's atmosphere, or because core-powered mass loss was not efficient enough to remove the planet's entire atmosphere. Estimates of the envelope mass fractions of several planets like Wolf 503 b near the radius gap will determine whether gas-empty formation is responsible for the radius gap around M dwarfs or Sun-like stars.

To shed light on the formation of smaller, Earth-like secondary atmospheres, uniquely observable terrestrial planets such as LP 791-18 d are needed. While the TRAPPIST-1 planets orbit an even smaller star and are theoretically more amenable to transit spectroscopy with JWST, this can only be done if the planets have atmospheres to observe. Recent modeling of transiting timing variations in this system has revealed that all of the TRAPPIST-1 planets are consistent with bare rocky compositions [1], suggesting that either no sub-Neptune atmospheres were ever initially created in the system, or these atmospheres didn't survive the planets' early cooling stages and heavy XUV stellar output. The LP 791-18 system on the other hand supports a sub-Neptune on a 5-day orbit, a mere 0.01 AU from the orbit of LP 791-18 d, suggesting that the system is a much more hospitable environment in which to grow atmospheres. With a highly similar radius and insolation to Venus, the presence of a Venus-like secondary atmosphere on LP 791-18 d would help to inform whether a Venus-Earth dichotomy exists for late M dwarfs. The heavy tidal heating caused by the planet's elliptical orbit also provides a promising mechanism for LP 791-18 d to replenish a secondary atmosphere through volcanic outgassing even if it is depleted through photoevaporation. No secondary atmosphere has ever been detected on a terrestrial exoplanet, and LP 791-18 d may well be one of few targets for which this is ever possible.

The discovery of LP 791-18 d also has implications on the frequency of planets around the very smallest stars. The frequency of multiple systems appears to increase dramatically for the coolest known stellar systems, and LP 791-18 d only adds to this effect. Although TESS has not yet discovered a significant population of planets around the latest M dwarfs, LP 791-18 d wasn't found in the initial TESS lightcurve. The planet was only revealed through 5 days of continuous *Spitzer* observations, and the system still hasn't been effectively searched for planets on longer periods. The discovery of LP 791-18 d suggests that monitoring these late M dwarfs for a longer period of time (and ideally with more precise photometry), could still reveal many of the best targets in the night sky. With TESS revisiting these sectors in

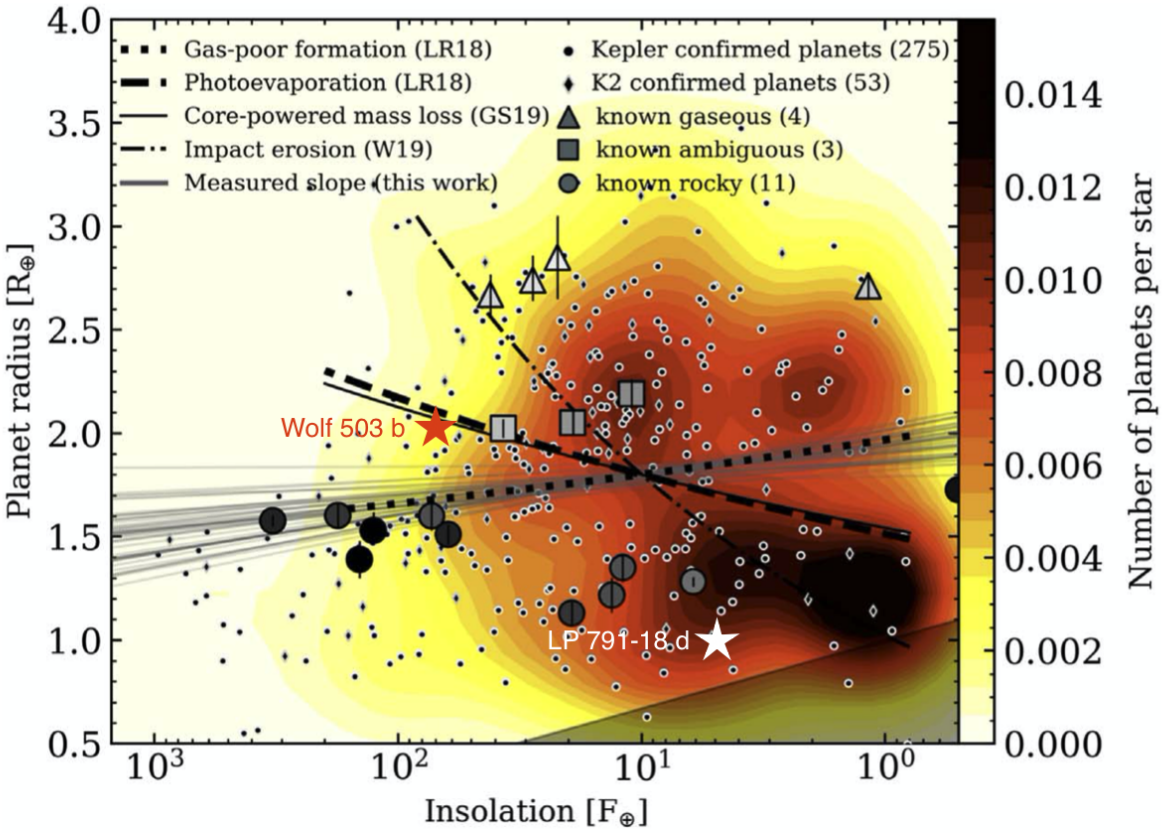

Extended Data Fig. 4.1. Radius gap for cool dwarfs based on confirmed planets from Kepler and K2 [2], with Wolf 503 b and LP 791-18 d shown. LP 791-18 d is at a radius and insolation that indicates it is terrestrial, regardless of the assumed planet formation theory, whereas Wolf 503 b is at a more critical location in period-radius space where thermal mass-loss suggests the planet should be a bare rock, whereas gas-empty formation would suggest the planet is in the sub-Neptune population. Note: in this figure, "Gas-poor formation (LR18)" represents what I have called gas-empty formation. The gas-poor relation quoted in the introduction is not shown in this figure but is effectively the same as that of photoevaporation.

the coming years, hopefully LP 791-18 d will not remain unique for long, and can be studied in detail as one in a collection of similarly observable, but richly varied, terrestrial exoplanets neighbouring Earth.

One ultimate goal in studying exoplanets is to prove that life exists somewhere in the Universe other than Earth, and with the discovery that planets are a ubiquitous consequence of star formation, it seems unlikely that Earth's inhabitants could be alone. This question has motivated the search for "Earth analogue" planets, to see Earth's evolution recreated in another solar system in hopes of detecting life there as well. Unfortunately, with any current or upcoming instrumentation, we can't study the atmospheres of true Earth analogues with the precision required to make such a detection. We must instead find small planets orbiting

small, nearby stars on which to test our theories of planetary and atmospheric evolution, such as those introduced here. These are the planets which will, in time, inform us what kinds of planets can host life and under what conditions.

References

[1] Eric Agol, Caroline Dorn, Simon L. Grimm, Martin Turbet, Elsa Ducrot, Laetitia Delrez, Michaël Gillon, Brice-Olivier Demory, Artem Burdanov, Khalid Barkaoui, Zouhair Benkhaldoun, Emeline Bolmont, Adam Burgasser, Sean Carey, Julien de Wit, Daniel Fabrycky, Daniel Foreman-Mackey, Jonas Haldemann, David M. Hernandez, James Ingalls, Emmanuel Jehin, Zachary Langford, Jérémy Leconte, Susan M. Lederer, Rodrigo Luger, Renu Malhotra, Victoria S. Meadows, Brett M. Morris, Francisco J. Pozuelos, Didier Queloz, Sean N. Raymond, Franck Selsis, Marko Sestovic, Amaury H. M. J. Triaud, and Valerie Van Grootel. Refining the Transit-timing and Photometric Analysis of TRAPPIST-1: Masses, Radii, Densities, Dynamics, and Ephemerides. *The Planetary Science Journal*, 2(1):1, February 2021.

[2] Ryan Cloutier and Kristen Menou. Evolution of the radius valley around low-mass stars from kepler and k2. *The Astronomical Journal*, 159(5):211, apr 2020.